UNIVERSITÀ
DEGLI STUDI
DI PADOVA

Head Office: Università degli Studi di Padova

Department: Geoscienze

Ph.D. COURSE IN: Geosciences
SERIES: XXXIV

GROUND MOTION SEISMIC MONITORING BY THE USE OF DISTRIBUTED LOW-COST SENSORS

Coordinator: Prof. Claudia Agnini
Supervisor: Prof. Jacopo Boaga
Supervisor: Prof. Lapo Boschi

Ph.D. student : Valeria Cascone

To Riccardo

"Seismology would be a very different science without instruments"
Jens Havskov and Gerardo Alguacil

Acknowledgments

I would like to express my sincere gratitude to my supervisor, Prof. Jacopo Boaga, for his continued guidance and supply of fascinating and interesting projects. He always gave me the motivation and the enthusiasm to improve my work. It is a fulfilling pleasure to conclude my PhD studies and I hope to carry on this research in the future. I am grateful to my co-supervisor, Prof. Lapo Boschi, who expertly guided me through the noise interferometry and introduced me to Prof. Kees Weemstra, giving me the opportunity to spend one month abroad in a prestigious University, the TU Delft. In this context, I would like to thank Prof. Kees Weemstra for the hospitality (difficult pandemic period notwithstanding), for the patience, and for his suggestions to improve my work. I thank also his PhD Student, Amin Rahimi Dalkhani, for his help. I gratefully recognize the help of Prof. Giorgio Cassiani and Dr. Ilaria Barone, with whom I worked together on several projects.
I would like to thanks my roommate Giorgia, for her continuous supports on work and daily life. Many other university colleagues are not directly included in this list, but I thank them for the beautiful moment spent together.
I thank my friends Alessia, Francesca and Eleonora. I am grateful to my mother Daniela, for passing on her passion for science to me. I thank my father Claudio who is an example of tenacity. My deep gratitude goes to my sister Arianna, for carrying the weight of the world on her shoulders. I thank Perla, for her fluffy support. Finally, I thank Riccardo: if I am the Earth, he is my starry Sky.

Acknowledgment to Reviewers

I am grateful to the reviewers of this thesis, Fabio Romanelli and Kees Weemstra, for their precious time and dedication. They have provided many constructive comments and valuable suggestions which improve the quality of the work.

Abstract

This thesis has three different aims with the common final task of seismic risk reduction. The first aim consists in the evaluation of the seismicity detection efficiency of a novel accelerometer prototype adopting the Micro-Electro-Mechanical-System (MEMS) technology, named ASX1000. The cost of this miniaturized device is 2 order of magnitude less than the traditional high-sensitive seismic stations. Six prototypes are installed in Northern Italy to monitor the seismicity in the Venetian Plain that is a large and deep alluvial basin. Ten prototypes are installed in Central Italy. We demonstrate that, for the first time, the ASX1000 MEMS is able to record small local earthquakes with a threshold of $M_L = 1.5$. It provides also an efficient estimate of strong motion parameters. The second aim is related to seismic hazard scenarios of the Venetian Plain. Here, deeper velocity structures, fundamental for seismic site response, are often unknown. Thus, we quantify the effects of different shear-wave velocity gradients' equations, finding variation on the estimated ground motion parameters. This result has an important impact on a-seismic design. The third aim involves ambient noise analysis. Firstly, the Coronavirus outbreak gave the unique opportunity to discriminate the cultural noise from the natural one. Then, we consider the possibility to use the ASX1000 for seismic noise interferometry. This method is important to retrieve subsoil structures in absence of seismic events. The ASX1000 MEMS is a promising geophysical tool, but at the moment it is not suitable for passive analysis. So, we perform noise interferometry with a different dataset, belonging to the high-quality seismic stations of the national seismic network, and we show some interesting preliminary results.

Sommario

Questa tesi affronta tre tematiche finalizzate alla riduzione del rischio sismico. La prima riguarda lo studio della performance di un nuovo prototipo di accelerometro che utilizza la tecnologia MEMS (Micro-Electro-Mechanical-System), l'ASX1000. Il costo di questi dispositivi miniaturizzati è inferiore di almeno 2 ordini di grandezza rispetto ai tradizionali sensori sismici ad alta risoluzione. Sei ASX1000 sono installati nel nord Italia per caratterizzare la sismicità della Pianura Veneta, un bacino alluvionale profondo ed esteso. Dieci sono installati nell'Italia Centrale. In questo lavoro dimostriamo che il prototipo può registrare microsismi fino ad una Magnitudo Locale pari a 1.5. Inoltre, il MEMS ASX1000 può stimare accuratamente i parametri di scuotimento del suolo. Il secondo argomento riguarda la realizzazione di scenari di pericolosità sismica della Pianura Veneta. Abbiamo effettuato uno studio sull'influenza di gradienti di velocità delle onde di taglio sulla risposta sismica in superficie. Questo risultato è fondamentale per il design anti-sismico. Il terzo argomento riguarda l'analisi del rumore ambientale. Abbiamo analizzato il rumore registrato durante il lockdown imposto dal governo italiano per mitigare la diffusione del Coronavirus, in modo da caratterizzare il rumore antropico. Abbiamo poi valutato la possibilita' di utilizzare l'ASX1000 per studi di interferometria sismica come metodo utile per ottenere strutture di velocità sismiche. I risultati suggeriscono che questi dispositivi, al momento, non sono idonei ad analisi di sismica passiva. Abbiamo allora applicato l'interferometria sismica alle sequenze di rumore registrate dalle stazioni sismiche ad alta risoluzione della rete sismica nazionale. In questo lavoro mostriamo i risultati preliminari.

Contents

Chapter 1

Introduction

1.1 Background and motivations

Earthquake ground motion represents the shaking associated with a sudden release of energy due to a fault rupture. The physical properties of the ground motion are closely related to the source process, the medium and the local site condition, according to local geological and geophysical features (Mai [2009], Atik et al. [2010]). Sampling of seismic ground motion is crucial for a detailed characterization of the seismic excitation in proximity of an epicentral area (useful for emergency operation in the immediate post-earthquake phase) (D'Alessandro et al. [2014]) and earthquake engineering purposes (the estimate of the effects on the buildings and infrastructures, urban planning and rehabilitation actions in active seismic zones, microzonation studies) (Ansal et al. [2009]; Romanelli and Vaccari [1999]). The technical advancement throughout the 20th century made possible to realize reliable and sensitive seismic sensors, able to characterize the strong motion with great accuracy and a over a wide range of frequencies. Of course, larger the accuracy of the observations, the more reliable the knowledge of the seismic phenomena and any following consideration about the seismic hazard

(D'Alessandro et al. [2014]). At the same time, the improvement of the performance capabilities may cause an increase of the prize of the instrument. Because of the high costs of advanced commercial seismometers (considering also the installation, maintenance and surveillance expenses), the number of the sensors generally deployed in the national seismic networks is relatively low, leading to a limited spatial sampling. The sparse sampling of the ground motion parameters, coupled with the large spatial variability of local geophysical and geological parameters (even within small distances), complicate the correct characterization of earthquake effects (Cochran et al. [2011], D'Alessandro et al. [2019]; Lawrence et al. [2014]). To mitigate the high cost of installing standard seismic arrays using conventional seismometers, inexpensive sensors such as MEMS (Micro-Electro-Mechanical System) accelerometers could be adopted (Evans et al. [2014]). MEMS accelerometers are devices with a very small footprint (micrometers to a few millimeters in size) and with low power consumption. These sensors are usually silicon devices composed of a free mass anchored to a chip by means of flexible silicon threads forming a mass-spring mechanical system (Evans et al. [2014]). The mass acceleration is converted in an electric signal using a capacitive circuit. MEMS accelerometers are extremely popular and inexpensive products, adopted in a variety of fields (monitoring of machine and vehicle, space exploration, game controllers, etc.) (Evans et al. [2014], D'Alessandro et al. [2014]). In the last decades they became even more lightweight and sensitive, and suitable for the requirements of earthquake monitoring (Boaga et al. [2019]; Lawrence et al. [2014]). Because of their low price, low power demand and small size, a large number of devices can be efficiently deployed. Recently, several attempts were made to include low-cost MEMS accelerometers in seismological investigations by the use of dense networks of sensors (Clayton et al.

[2011]). The individual instruments can be attached to "volunteers" computer (e.g. Cochran et al. [2009]) or they can be installed as independent instruments at individual hosts (e.g.Clayton et al. [2011]), or in public buildings such as schools, hospitals etc (D'Alessandro et al. [2014]). Another approach is to exploit a network of built-in MEMS sensors in smartphones (Kong et al. [2016]). However, their full potential when it comes to recording ground motion has not been explored. In particular, the major limitation of using MEMS sensors for seismological purposes is the high instrumental noise and low sensitivity of the currently available devices. That is, MEMS sensors are able to record only large or moderate earthquakes at short distances (Boaga et al. [2019], Cenni et al. [2019], Lawrence et al. [2014]). Thus, the low quality of the current device limits the magnitude detection threshold (Evans et al. [2014]) In this Thesis we introduce a promising prototype of a new MEMS sensors, named ASX1000, which is a tri-axial capacitive accelerometer. This device is designed to be easily installed in local telecommunication infrastructures: it can be fixed with screws and plug at the basement of the server rooms and connected to a miniaturized data logger connected via cable or other streaming devices. In this way, the recorded waveforms can be processed in real-time in order to infer ground motion parameters such as PGAs and Spectral Accelerations.

The ASX1000 prototypes were installed in two different zones of Italy (North-east and Central Italy), one of the most seismically active countries in the Mediterranean, being the site of several large and extremely damaging earthquakes since historical times. The recent seismic history of Italy proves that the effects of moderate and large earthquakes are often destructive in the high vulnerable areas. Those are the case of Umbria and Marche seismic sequences in 1997-1998 (Deschamps et al. [2000]), L'Aquila

in 2009 (Lucente et al. [2010]), Emilia-Romagna in 2012 (Bignami et al. [2012]) and the Amatrice-Visso-Norcia in 2016-2017 (Michele et al. [2016]). On November 2019 we installed six of these sensors in north-east Italy regions (Veneto and Friuli Venezia Giulia), a mid-to-high seismic hazard area, with documented historical events. This region is characterized by the presence of the Venetian Po Plain, a large and deep sedimentary basin which represents the foreland basin of the Southern Alps (Doglioni [1993]). It is well known that the geological configuration of soft sedimentary layers overlying bedrock-like formations leads to seismic amplification effects (Rathje et al. [2010]). A denser seismic network could characterize in more detail the seismic ground motion, enhancing the knowledge of local seismic amplification effects due to different geological conditions. In this work we present an experimental network built with few ASX1000 MEMS sensor prototypes, aimed to evaluate their seismic detection efficiency. In addition, on January 2020, 10 of these MEMS sensor prototypes were installed in the inner part of the Umbria Valley (Central Italy), replacing a pre-existing MEMS network, already installed since 2016 and detailed described in the works of Boaga et al. [2019] and Cenni et al. [2019]). This area of Central Apennines is characterized by a continuous release of seismic energy, which is frequent but relatively moderate, and can be considered a sort of natural laboratory for seismological study (e.g., TABOO, The Alto Tiberina Near Fault Observatory; Chiaraluce et al. [2014]). This work analyzes in detail the preliminary and experimental data obtained with these prototype networks, in order to promote a project regarding the installation of hundreds of ASX1000 MEMS sensors in the Veneto Region (expected to start in 2022).

1.2 Objectives of the thesis

This thesis has three different objectives.

The main objective of this work consists of exploring the capabilities and the performance of a MEMS sensors prototype, the ASX1000, for earthquake engineering and seismological studies. We evaluate the seismicity detection efficiency and the use for ground motion characterization of this new MEMS accelerometer (Cascone et al. [2021]a). The first study case is the Venetian Po Plain, a densely populated deep alluvial basin, where a detailed ground motion recording is fundamental for the evaluation of local seismic effects. Although strong seismic events didn't occur recently, this area was of interest because of the effect of strong earthquakes occurring in the neighbor territories, such as the Friuli (1976) and Emilia seismic sequences (2012) (Poli et al. [2008], Bignami et al. [2012]). The second study case is the seismologically active central Italy area, located in Umbria region, where we substituted the older sensors with the new prototype ASX1000. We test the suitability of the MEMS sensor ASX1000 prototype to record earthquakes, recovering the combination of minimum local magnitude and epicentral distances detectable. Performance validation is achieved through a comparison of the MEMS sensors' records with the national strong-motion network data (RAN Rete Accelerometrica Nazionale), built with high-quality and high-sensitive instruments. This study showcases for the first time, the ability to monitor small local earthquakes ($1.5 \geq M_L \geq 2.5$) with MEMS sensors (see APPENDIX A, section A.1). The performance of the new MEMS accelerometers enables monitoring not only local seismic events (with epicentral distances in the order of 50 km), but also strong teleseismic events (with epicentral distances in the order of 300 km), nucleating outside the Italian territories, for example in Slovenia and Croatia.

The second objective of this Thesis focuses on the detailed seismic site analysis of the Venetian Po Plain, which involves the use of shear-waves velocity gradients. This area, characterized by a mid-to-high seismic risk, lacks a geophysical characterization below the tens meters of subsoils (e.g., shear-wave velocity profiles)(Cascone et al. [2022]). Generally, the ground motion records of the most recent destructive earthquakes provide new opportunities to revise, and improve the procedure for seismic hazard assessment. It is well known that the Veneto Region was stuck by strong historical seismic events (e.g. Verona Earthquake, $M_L = 6.8$, 1117) (Guidoboni et al. [2005]). As previously said, this sector didn't release energetic seismic events in recent times, so, the recorded ground motion is limited in distribution and size. The seismic site characterization of geological setting of deep alluvial basins is fundamental: the amplification of seismic waves caused by alluvial deposits can strengthen the incident motion and increase the effects of earthquakes on structures and buildings (Boore et al. [1993], Martin et al. [1994]). Moreover, deep alluvial basins are often the most densely populated part of a country, enhancing the exposure to the risk. In this case, a neodeterministic approach, such as synthetic ground motions, can be good supplement for analysis of site characterization and regional seismic hazard assessment(Anderson et al. [2000]; Panza et al. [2002], Panza et al. [2003], Romanelli et al. [2010], Zuccolo et al. [2008]). This method allows to define a set of earthquake scenarios without having to wait for strong events to occurs and it is possible to assess the impact of future earthquakes on a defined area of exposure (Romanelli et al. [2010]). The final results of this study is the estimate of the amplified response of soil layer under earthquakes excitation and thus the variation of strong motion parameters (such as PGAs and Spectral Accelerations). Seismic site amplification can be described as the motion modification

due to soft soil during the wave propagation through the stratigraphic column, from the basement bedrock upward to the ground surface (Boore et al. [1993]). The distribution of shear wave velocities of the shallow subsoil (the first tens or hundred meters depth) is then fundamental to quantify amplification effects (Martin et al. [1994], Mascandola et al. [2019]). Unfortunately, in big alluvial basins deep shear-wave velocity profiles are rare, and often generic velocity gradients models are adopted. This implies a relevant uncertainty in the computation of seismic response analysis for these important territories. For this objective we perform a comparative study which, for the first time, evaluates the effect of different shear-wave velocity gradients on stochastic analysis of seismic site response in deep alluvial basins.

The Third objective of this work involves the evaluation of the use of ASX1000 prototype for noise interferometric technique (Boschi and Weemstra [2015],Boschi et al. [2016],Shapiro and Campillo [2004]; Shapiro et al. [2005],Weemstra et al. [2016],Weemstra et al. [2017]). This approach is fundamental for obtaining shear wave velocity profiles adopted for seismic response studies (Boaga et al. [2007]), particularly where classical controlled source explorations are challenging, as in deep alluvial basins. In these environments, such our study area (the Venetian Po Plain), the deeper structures are often unknown, and this technique could be rather useful to improve the modelling of ground motion. Ambient noise, or the seismic signal recorded in absence of earthquakes, consists of microseisms resulting from the coupling between oceans and solid earth at frequencies mostly below 1 Hz (Longuet-Higgins [1950]), while at higher frequencies it includes the "anthropogenic" or "cultural" noise associated with human activities at or near the surface of the Earth (Bungum et al. [1985], Halliday et al. [2017]; Zhang et al. [2009]). One of the most used method involves the extraction of

Green's Function from ambient noise field (Shapiro and Campillo [2004], Boschi and Weemstra [2015]): the resultant function from the cross-correlation of random noisy waves recorded at two different stations corresponds to the Green's function, i.e., as if an impulse force is applied at one station and recorded at other station. The low-frequency content of noise allows to map the deep structures of the Earth lithosphere (Shapiro et al. [2005], Weemstra et al. [2016]). Anthropogenic noise can be used for relatively small scales, for instance in characterizing the shallower subsoils (Louie [2001], Boaga et al. [2007]). The application of noise interferometric technique in geophysics can be useful to evaluate the surface wave dispersion in a passive way, without controlled sources (Campillo and Paul [2003],Roux et al. [2005], Boschi and Weemstra [2015]). This method can furnish relevant tools for seismic hazard scenario modelling, especially for the case of deep alluvial basins such as the Venetian Plain, where shear waves velocity profiles reaching relevant depth are required (e.g. 100 - 200 m) (Boaga et al. [2007]). And although the estimation of the fundamental mode Rayleigh wave through cross-correlation is a well known technique, the innovative aspect of this part of the thesis consists in the possibility to perform this technique with inexpensive MEMS sensors. In order to retrieve subsoil models of the Veneto region, extending our small prototype network, we started considering the continuous noise recording of the high-quality seismometers of the Italian Seismic Network managed by the INGV (Istituto Nazionale di Geofisica e Vulcanologia, Italy). These seismic data is public and distributed through the Orfeus European Integrated Data Archive (EIDA). In this context, the unexpected situation of the COVID-19 outbreak and the consequent lock-down measures between March and May 2020, allow us to quantify the anthropogenic impact on seismic ambient noise. On March 2020, the government of Italy imposed

a national lockdown, restricting the movement of the population and closed all non-essential industries, in response to the growing pandemic of COVID-19 in the country. While earlier studies have attempted to characterize high-frequency seismic noise, the Italian lockdown of industrial activities and reduction in road and train traffic represents an unprecedented opportunity to discriminate the anthropogenic noise from the natural noise. The seismic signature of the containment measures is evident from the analysis of continuous recording at INGV stations in time and frequency domains (Poli et al. [2020], see APPENDIX A, section A.2). The observation that the most of energy loss occurs at frequency between 1-10 Hz can be useful for future studies of noise cross-correlation to characterize the upper subsoil. To summarize, the three different studies proposed in this work have in common the final objective of the earthquake risk reduction, with a focus on seismic local response of deep alluvial basins (see figure 1.1).

To evaluate in denser way the seismic ground motion, new MEMS based network can be adopted. High sensitive MEMS sensors can be even be adopted for seismic noise analysis, inferring models which can be adopted in ground motion scenarios. These approaches aim to obtain more accurate information on ground shaking and represent essential tools needed for city planning, disaster preparedness, hazard mitigation decisions and risk reduction in earthquakes prone areas.

1.3 Thesis Outline

In this section we report the outline of the thesis. The three objectives of the thesis listed in Section 1.2 are discussed in three different chapters. Each chapter has its own Introduction-Method-Results-Discussions and Conclusions sections. In order to avoid

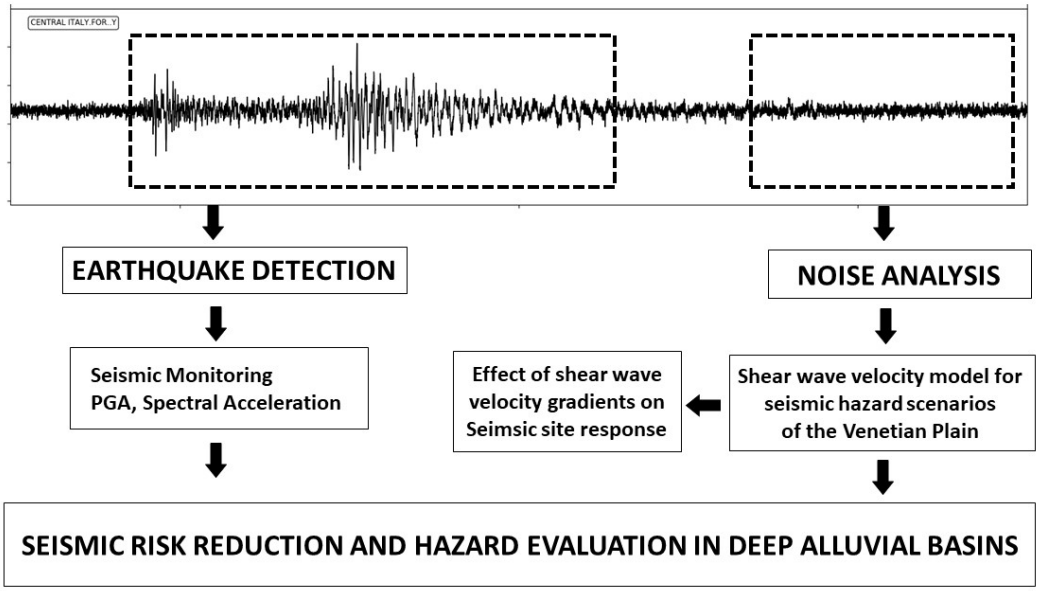

Figure 1.1: Summary of the three main aims of the Thesis.

repetition, some of the results contained in published papers, are shown directly in APPENDIX A.

Chapter 2 explores the literature review of MEMS sensors and introduces the ASX1000 prototype, showing its technical features. We show the performance of our prototype on a certified shake table apparatus belonging to the Seismological Research Center of the OGS (Istituto di Oceanografia e Geofisica Sperimentale, Italy). We introduce the MEMS prototype arrays installed in Northern and Central Italy and we discuss the general criteria to identify seismic events from the continuous data recorded by the ASX1000 prototype. A catalog of earthquakes recorded by our MEMS sensor prototype, collected since January 2020, is then reported. Finally, we present the results of the comparison between the MEMS sensors and RAN high-quality stations in terms of PGAs and Spectral Accelerations. The results related to the microsesimcity monitor-

ing is reported in APPENDIX A (section A.1).

Chapter 3 discusses the analysis of seismic local effects of the Venetian Plain. We introduce this chapter with the geodynamical and geological setting of the study area. Here we discuss the importance of shear-waves velocity gradients for accurate seismic scenarios in deep alluvial basins. In this case, the chapter has the same structure of a manuscript submitted on "The Journal of Geophysics and Engeenering" (see APPENDIX A, section A.3).

Chapter 4 is related to the analysis of ambient noise and the cross-correlation technique. The basic idea is the future use of MEMS sensors as passive arrays. Nowadays, their high level of instrumental noise and their poor performance at lower frequencies limit the noise cross-correlation of seismic ambient noise, even if promising improvements are coming from recent study on a new prototype. In the meanwhile we focus on the characterization of the velocity model of the Venetian Plain, performing the cross-correlation of ambient noise as recorded by the broad-band forced balanced seismometers belonging to the INGV IV network. A section of this chapter is dedicated to the cross-correlation processing computational routine. The results related to effect of anthropogenic activities on seismic noise during the coronavirus lock-down in Italy are shown in APPENDIX A (section A.2).

Finally, Chapter 5 presents the main conclusions of this work and recommends future research directions.

Chapter 2

Earthquake detection with MEMS sensors

2.1 Introduction

Seismology is a recent field of the Earth Sciences that has only been studied quantitatively since around 1900, when seismic instruments started to be available. The first time-recording seismograph, based on undamped pendulums was built by the Italian physicist Filippo Cecchi in 1875 (Shearer [2019]). Soon after this, higher quality instruments were developed. Nowadays, the sensitivity of seismic instruments allows earthquakes location, the accurate measurement of the true ground motion and many other applications.[1]

During the last decades, the instrumentation for earthquake observation greatly

[1]DECLARATION: The part of this chapter related to small earthquake detection has been published as "Small local earthquake detection with low-cost MEMS accelerometers" in *The Seismic Records, vol. 1, pp. 20-26, 2021*
CONTRIBUTION: Design of the work, Data Collection and Interpretation

improved in term of sensitivity and reliability of the seismic data Scudero et al. [2018]. The most diffused seismic sensors, based on a spring-mass principle, have reached very high precision and sensitivity. However, these devices are usually expensive, and the heavy proof masses make this device bulky, difficult to transport and manage. For this reason, one of the problem in seismology is the efficient wave-field recording, due to the limited number of installed sensors (D'Alessandro et al. [2014]). One key factor to improve seismic monitoring is the implementation of a seismic sensor network, which requires the widespread deployment of seismic instruments. However, the cost and complexity of installing numerous traditional seismic instruments are too high. A dense coverage of stations is fundamental for many reasons, first of all the effectiveness of rescue operations in the immediate post-earthquake phase when a destructive earthquake occurs. The possibility to map the distribution of earthquake intensity with adequate resolution depends on the availability and on the spatial distribution of monitoring stations. The limitations of the traditional instruments were overcome and significant improvements were boosted by MEMS (Micro-Electro-Mechanical-System) technology (D'Alessandro et al. [2019]). MEMS sensors have low costs, small size, low power, and high bandwidth devices enabling a wide range of applications in term of scales and typology of recorded signals. The dimension of a MEMS device is in the order of the microns: the electromechanical system are highly miniaturized devices integrated onto an unique silicon substrate (Crone and Sharpe [2008]). These devices are considered as one among the most promising technology for this century, capable to revolutionize the industrial world and the commercial product market (Scudero et al. [2018]). These inertial sensors, in particular, have seen widespread application in the consumer and automotive electronic industries, game controllers, smartphones, space missions and so

on. Further applications include geotechnical surveying and the monitoring of natural hazards, such as earthquakes. The progresses achieved in MEMS technology, coupled with the progress reached also in wireless data transmission, enabled the extension of the sensing capability and, consequently, opened the door for their use in a wide field on applications (D'Alessandro et al. [2014], Scudero et al. [2018]). These sensors could be integrated in the existent seismic networks and increase the number of sensors, to have a quick parameterization of an earthquake (such as shake maps), as well as to investigate seismic site effects caused by local geological condition. In this Chapter we introduce a new MEMS sensor prototype named ASX1000. We explore its physical functioning principles, its sensitivity and its use for earthquake observation. For this purpose we present two experimental arrays deployed with MEMS based accelerometers, located in Northern and Central Italy. In particular, we investigate whether the advances in MEMS sensors enable us to create a dense distributed sensor network in a high-risk area.

2.2 Methods

2.2.1 Seismic Sensors

A seismic sensor is an instrument used to measure the ground motion when it is shaken by a perturbation. Ground motion can be measured in terms of displacement, velocity, and acceleration. Ground displacement represents how far the surface has been moved. Ground acceleration is how fast the ground velocity is changing with respect to time. Traditionally, seismometers, or weak-motion sensors, are very sensitive to small and distant events and are thus too sensitive for strong-motion signals. So, dur-

ing most damaging earthquakes, seismometers which are installed close to the epicenter are clipped (a signal clips and is distorted when it exceeds the threshold of the sensor's dynamic range). The accelerometers, or strong motion sensors, are designed to record the strongest events at small hypocentral distances. Their maximum on scale acceleration is usually expressed as g, a fraction of the Earth's gravity (1g = 9.81 m/s^2, the average of Earth's gravity between the equator and the poles). In high seismic risk areas where the main goal of networks is future seismic risk mitigation, strong-motion recordings play an important role, and two sets of sensors will have to be installed so that the system never clips. Italy, which is one of the country in Mediterranean with the highest seismic risk, has two fundamental seismic networks: (1) the RSN (National Seismometric Network -Rete Sismometrica Nazionale) managed by the National Institute of Geophysics and Volcanolgy; (2) the RAN (National Accelerometric Network - Rete Accelerometrica Nazionale) managed by Civil Protection Authorities. Generally, seismologists prefer recording weak motion (displacement or velocity), for easy interpretation of seismic phases, while engineers consider strong motion acceleration, whose peak values are directly related to structures seismic load: ground acceleration is the most important factor in determining the stress induced to structures during earthquakes. This Thesis focuses on strong-motion sensors category or accelerometers.

Accelerometers: Basic Physical Theory

Accelerometers are inertial sensors designed to detect velocity variations, typically in the medium-to-high range of frequency. The measurements are done in a moving reference frame (the Earth surface), so the sensing system of an accelerometer is designed for the detection of inertial forces on the base of a damped spring-mass structure.

The relative motion between the suspended mass and the ground is a function of the ground motion. The sensor mass displacement is linearly proportional to the external acceleration. The system can be described by the equation of motion for a rigid body, expressed with the Newton's second law:

$$\vec{F} = m\vec{a} \tag{2.1}$$

Considering a single direction (the x-direction, for example), the vector equation is reduced to a scalar expression:

$$F_x = ma_x \tag{2.2}$$

It is possible to use Newton equations even in a no-inertial system, replacing the reference system. The origin point of the new reference system must be fixed on the device (coordinates of the moving body, Figure 2.1). It turns out that acceleration a_x, calculated in global coordinates, is replaced with acceleration $\ddot{x}$, calculated in body coordinates. Equation (2.1) can be re-written considering the new reference system. The equation of motion for the mass proof in the body coordinate system $x = X_m - X_0$ is:

$$m(\ddot{X}_m - \ddot{X}_0) + b(\dot{X}_m - \dot{X}_0) + k(X_m - X_0) = -m\ddot{X}_0 \tag{2.3}$$

On the left-hand side are the contributions related to the inertial motion of the proof mass (m), to the damping (b, expressed in N/(m/s)), and to the linear force of the spring (k, expressed in N/m). On the right-hand side is the initial external force, which is often referred to as the apparent force. The Capacitive electrodes shown in

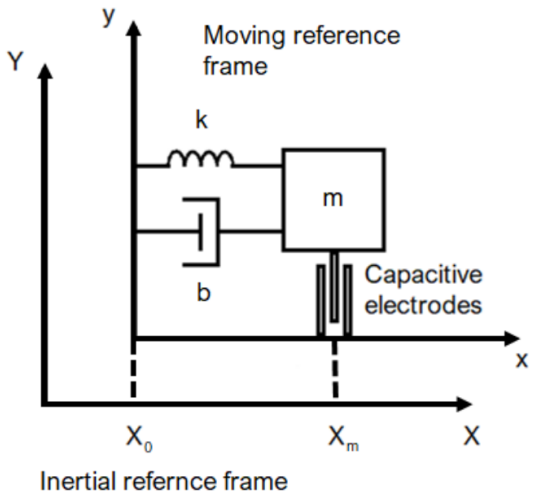

Figure 2.1: Simple scheme of an accelerometer

Figure 2.1 are characterized by a capacitance which varies with the displacement of the mass.

Mems sensors

Several works demonstrate that MEMS (Micro-Electro-Mechanical System) sensors can efficiently integrate the use of common accelerometers and their use for seismology related applications has been emerging considerably in the last decades. Among the various typologies of MEMS accelerometers (such as piezoelectric, piezoresistive or strain gauge), the electro-mechanical piezoresistive or capacitive sensors are the most widely employed (Shaeffer [2013]). Capacitive accelerometers are based on a spring-mass like system placed on a silicon substrate. The capacitor consists of two parallel metal plates separated by an insulating material. When the device goes under an

acceleration, the inertial map shifts, causing a change of the configuration of the capacitor plates and causing, in turn, a change in the capacitance. The displacement is proportional to the capacitance difference, such difference is measured by an integrated electronic system and the value of the acceleration in then calculated with a conversion factor (Figure 2.2). The advantage of these capacitive instruments is the miniaturized dimensions and the very low-cost of production.

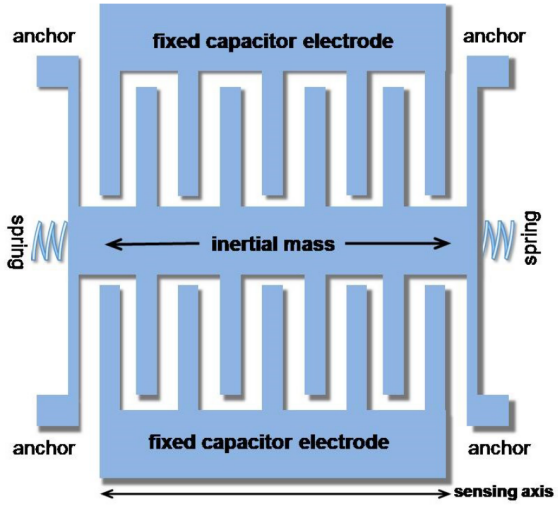

Figure 2.2: Scheme of a capacitor which characterizes the capacitive MEMS accelerometers

In a MEMS accelerometer each sensor has a lot of capacitor sets. The dimension of a single sensor is in the order of few hundreds of micrometers and thickness in the order of few tens of micrometers. Since these sensors are directional device, they can detect accelerations along a single axis. To measure accelerations on the three dimensions, three sensors are oriented along the axes of orthogonal triad. This task could be challenging in the microscopic scale where the flat base of silicon wafer sets the manufacturing limits. If it could be relatively easy to create two identical structures

on the plane, it is harder to extend the structure perpendicularly off plane. This lead to a different sensitivity on the vertical axes. The final packing of a triaxial sensor could be as small as few millimeters each side. The basic production process involves the "printing" of the pattern of the circuit on the crystalline silicon wafer, creating a three-dimensional structure D'Alessandro et al. [2019]. (Figure 2.3)

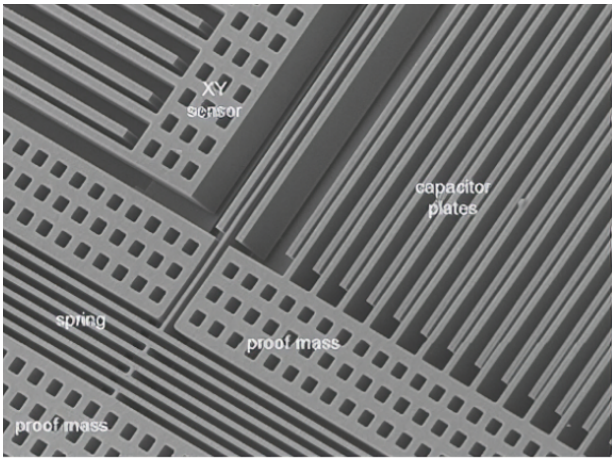

Figure 2.3: The crystalline silicon wafer typical of the MEMS capacitive sensors

Because of the constructive constraints of a MEMS device, first of all the small dimension, the inertial mass has a very limited weight but it must be in condition to induce detectable electrical outputs. Consequently, MEMS devices are naturally sensitive to the strong motion in the higher part of the earthquake frequency range. Several studies demonstrates that these sensors can reach an efficient performance for moderate ($5.0 > M_w > 5.9$) to large ($M_w > 6$) earthquakes detection at distances in the order of tens of kilometers. (Boaga et al. [2019], Lawrence et al. [2014])

2.2.2 ASX1000 Accelerometer Prototype Design

In this Thesis we present a new MEMS based accelerometer prototype named ASX1000. It is a low noise density triaxial-multirange accelerometer, characterized by low-power consumption. It has an internal circuit of transduction, providing digital output. It is designed and produced by ADEL srl, an Italian based company specialized in technology and telecommunications. This accelerometer prototype is thought to be a platform for the data acquisition and recording for long period measurements. The device adopted in this study is shown in Figure 2.4. The circuit is inserted in a fixed metal plate and the cover is completely hermetic and dust/water proof (Figure 2.4a). Figure 2.4b shows the internal circuit batch; the MEMS sensor parts are marked by the yellow square.

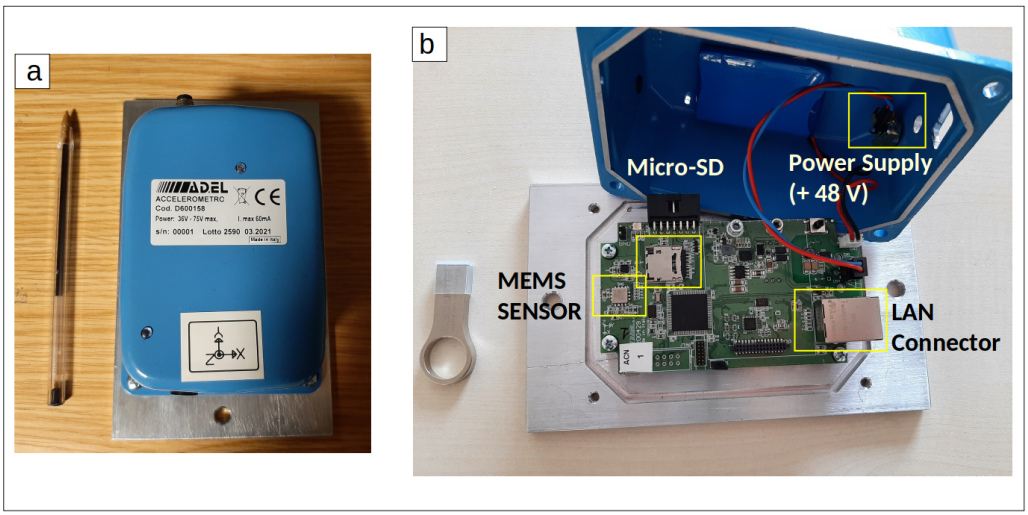

Figure 2.4: (a): ASX1000 MEMS sensor prototype; (b) its internal circuit batch

The system is equipped with three communication channels for remote control and data transmission (Figure 2.4). These channels are:

1) 10/100Mbit LAN with TCP/IP protocol.

2) Multi-standard serial RS422, RS485 and RS232 with a maximum speed of 115200 baud.
3) USB 2.0 type.

The MEMS device has a low power consumption. Power can be supplied in three ways:
1) +48Vdc, the typical DC power which supply the telecommunication infrastructures.
2) +5V from USB
3) +5V from external power supply, through the multistandard serial connectors.

This sensor operates in high sensitivity mode for an acceleration range of $\pm 2g$, but it supports the and $\pm 4g$ full scale (the full scale is the maximum signal amplitude that can be measured). In these ranges, the sensor provides a linear output signal. This value guarantees that the sensor can record even very strong accelerations, such as those induced by a catastrophic earthquake, remaining in linear regime. The bandwidth (which is the frequency band in which the system has linear response), was designed in the range 0 - 62.5 Hz, since the frequencies generated by an earthquake are at most of the order of tens of Hz. Earthquake engineering frequencies of interest, i.e. those that can create more damage to buildings triggering resonance phenomena, are included in a more narrow range (approximately 0.1-20 Hz) and therefore largely contained in the frequency band of this MEMS accelerometer D'Alessandro et al. [2014]. The ASX1000 accelerometers prototype is designed with a sampling rate of 250 Hz (but it is an adjustable parameter). To completely characterize the earth's movement, the motion must be measured in three perpendicular directions: the sensors have three sensing elements (X-Y-Z), oriented along mutually orthogonal axes. The micromachined elements are fully differential, comprising the lateral x-axis and y-axis and the

vertical z-axis sensors. In particular, the three axes go through separate signal paths that minimize offset drift and noise. Devoted software for the acquisition samples the data at frequency of 250 Hz. The waveform files are written in three different formats: Comma-separated-values (csv); Binary (bn); The Standard for the Exchange of Earthquake Data (mseed). The ASX1000 MEMS prototype has a built-in digitizer to eliminate the unnecessary noise, where the measured data can be processed with digital filters, which can be set remotely. The acquired data are recorded by the accelerometers in a continuous mode and are stored locally in a micro-SD memory card (visible in Figure 2.4b), with storage up to 64 Gbyte (the maximum storage is up to four months, then the memory card is reset). The data transmission, through the three communication channels mentioned above, involve near real-time data transfer from the remote stations to the central processing site, managed by ADEL computer room. At the moment, the available software, processed the waveforms automatically but is not equipped with a triggering detector useful to identify the seismic event. So the ASX1000 MEMS prototypes cannot be adopted for the identification of automatic seismic events. In order to perform seismic monitoring, several processing implementations (such as a ring-server, a central trigger and selected time-window) are needed.

2.2.3 MEMS Sensors' Seismic Arrays in Italy

In order to test the performance while detecting earthquakes, 16 ASX1000 prototypes are installed at two seismic active areas in Italy. In this Thesis we present two experimental MEMS sensors-based networks deployed in North-East Italy (with 6 sensors) and Central Italy (with 10 sensors). The geographic coordinates are reported in Table 2.1 The networks' configuration is shown in Figure 2.5a and Figure 2.5b (red triangles).

When possible, the ASX1000 MEMS sensor prototype were compared to the national strong motion high quality sensors (Kinematics Episensor ES-T sensors) belonging to RAN (green triangles).

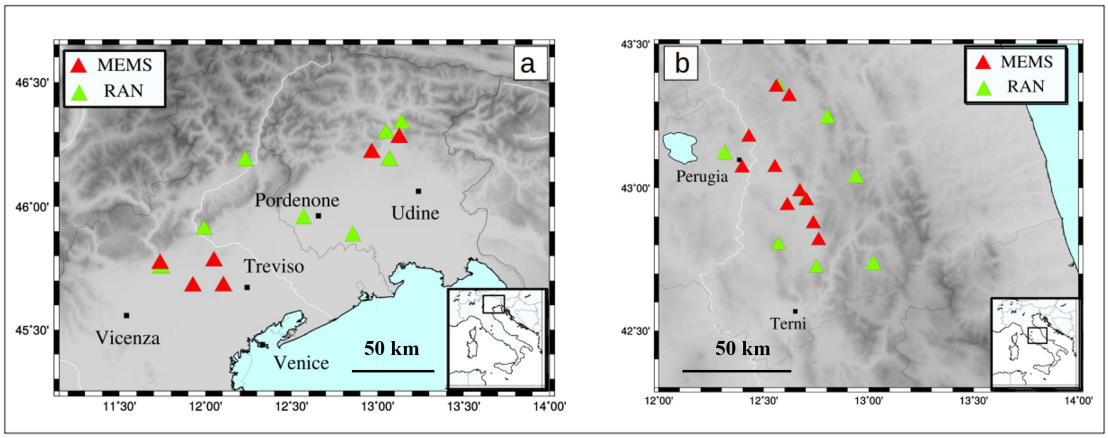

Figure 2.5: MEMS-based network in (a) Northern Italy and (b) Central Italy

The urban networks have been designed and installed in agreement with the italian telecommunication company TIM spa. The MEMS sensors were installed inside the TIM telecommunication infrastructures at the base of local server rooms, and the sensors were firmly coupled to the building with screws and plugs with a two-sided tape (Figure 2.6a). Each sensor is connected to a wall outlet for power and the azimuth is measured after the installation, using a compass (Figure 2.6b).

Seismological Framework of the study areas

The ASX1000 MEMS sensors prototype are installed in the Italian regions characterized by a high seismic risk. The Northern-East Italy (Veneto and Friuli Venezia Giulia Regions) is frequently shaken by earthquakes.The seismicity in this sector is often attributed to the active thrusts of Southern-East Alpine Front. Nowadays, the

Figure 2.6: (a)ASX1000 prototype installed in a local telecommunication infrastructure.(b) Azimuth measurement

INGV National Seismic Network in Veneto and Friuli Regions is integrated by local networks, managed by the Seismological Research Center of the OGS (Istituto Nazionale di Oceanografia e Geofisica Sperimentale). In the Veneto Region the instrumental seismicity of the last decades is moderate (Romano et al., [2009]): only 3 earthquakes have exceeded the M_L >4.4 (Priolo, [2008]). But earthquakes' occurrence in this area has been historically documented since the fifteenth century (Poli et al. [2008]), where The most destructive historical earthquakes are characterized by M_w >5.5. The Friuli Region is also characterized by a high level of seismic activity. The last destructive seismic events occurred from May to September 1976, where four seismic events with $M_w \geq 5.9$ destroyed several villages causing hundreds of casualties.

The second study area is the inner Part of the Umbria Valley. Here, the intra-Apennines active extension produces a broad and complex system of normal seismo-

genic faults, as indicated by the strong earthquakes that recently occurred (Gubbio 1984, M_w= 5.6; Colfiorito 1997, M_w=6.0; Norcia 1979, M_w= 5.9; L'Aquila 2009, M_w= 6.1; Amatrice 2016, M_w= 6.1; Norcia M_w= 6.5).

2.2.4 From the Earth to the computer desktop

In this section we illustrate the general criteria to retrieve seismic events detected by the ASX1000 MEMS sensor prototypes installed in Italy. As shown previously, all the installed MEMS sensors have real time communications and data is available typically within minutes of real-time. A private (at the moment) website platform designed and programmed by ADEL, accessible with a user account, is available to download the data acquired by the MEMS sensor prototypes. The Graphic-User-Interface (GUI) programmed by ADEL is shown in Figure 2.7. It allows to select manually the seismic sensors belonging to the two experimental arrays in Italy. The first column reports the name of the hosting telecommunication infrastructure. The second column displays the identifier code of each MEMS sensor installed, where the network code is "0080E100". The third and forth column report the date and the time of the last acquisition. For each seismic sensor it is possible to select the start time of the downloaded data. In the drop-down menu it is possible to select the time window, with a maximum of 60 minutes. On January 2020 it was possible to download the data in .csv format (Figure 2.7). Starting from May 2021, the mseed and binary formats were available too.

The CSV file is organized in this way:

- First column: Date
- Second column: Time

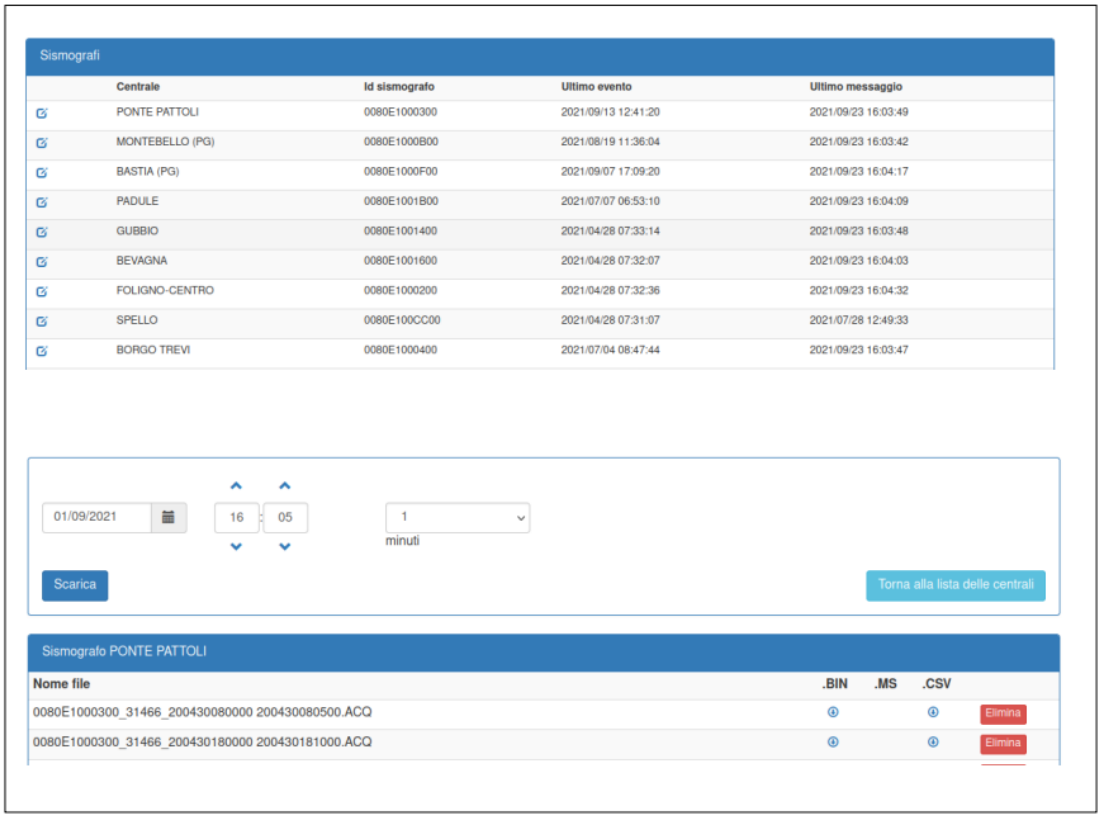

Figure 2.7: The platform developed by ADEL in order to download the raw data acquired by the installed MEMS sensors.

- Third column: Millisecond

- Forth column: Voltage output values of the X component

- Fifth column: Voltage output values of the Y component

- Sixth column: Voltage output values of the Z component

As shown previously, the dataflow is not processed in order to identify seismic events. This means that the user, who knows a priori the origin time, location and magnitude of a seismic event, download the time window which may contains the earthquake and download it from the ADEL website.

Since the first available format was the ".csv", I programmed python and shell-based scripts in order to convert the voltage to acceleration and to infer an immediate visualization of the seismic waveforms. As mentioned in paragraph 2.2.2, the waveforms are not processed with a triggering detector, so the ASX1000 prototype is not capable of identifying seismic events. The seismic events are retrieved from the INGV database. The routine to infer the earthquake waveforms (schematize in Figure 2.8) is the following: 1) A Weekly check on the INGV (Istituto Nazionale di Geofisica e Vulcanologia) website or INGV smartphone app, in order to make a list of the seismic events occurred in proximity of the two experimental networks. The website and the app display several earthquake information such as the origin time, the ipocenter and the local or moment magnitude.

2) I log in the ADEL platform, I select the considered station, I select a time window centered on the origin time reported on the INGV database and then I download the raw data.

3) I run a shell-based script which converts the output voltage in acceleration. The Azimuth correction is performed, considering the ASX1000 prototype Azimuth, measured during their installation (Figure 2.4). I remove the trend and the mean. I apply a bandpass using a Butterworth filter, generally at 1-10 Hz. Then convert the column in the binary SAC (Seismic Analysis Code) A header of the SAC file is created too, considering the information contained in the csv format such as the date and time. These operations are performed on the three components.

4) I run a python-based script, with obspy package (CITAZ), plots the waveforms of the three components and infer the maximum values of acceleration (the peak ground accelerations, PGAs)).

When the mseed format started to be available, the step 3 and 4 wasn't necessary anymore.

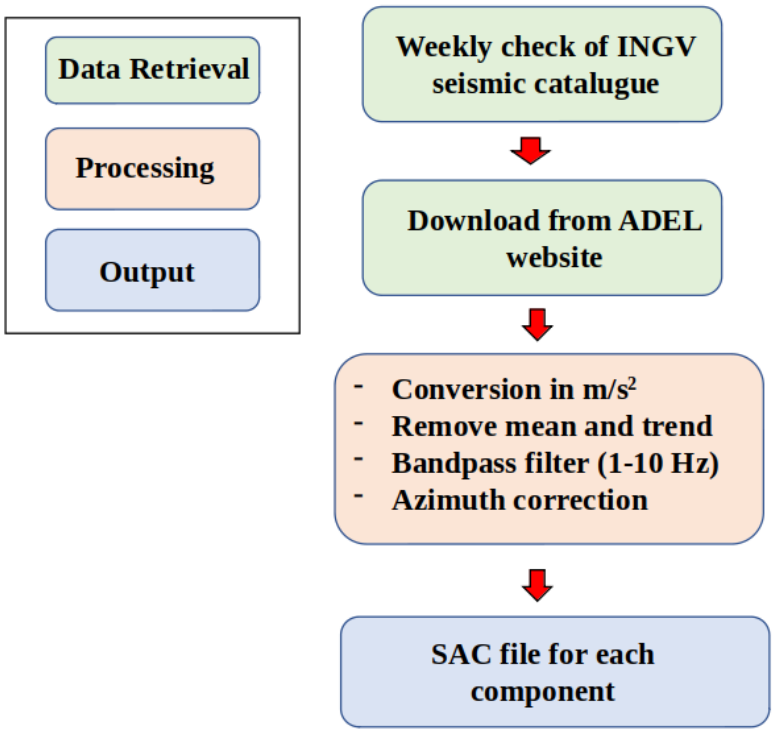

Figure 2.8: Workflow adopted in this work to retrieve seismic waveforms recorded by the ASX1000 MEMS sensor prototype

2.2.5 Shake Table Test

The ASX1000 MEMS sensor prototype was calibrated in the laboratory on a certified shake table, in order to evaluate its suitability in strong motion related studies. In fact, the determination of instrument response is fundamental to reconstruct the true earthquake ground motion.

The shake table apparatus built and used at the Seismological Research Centre of OGS (Istituto Nazionale di Oceanografia e Geofisica Sperimentale) in Udine (Italy), is

able to generate controlled frequency signals.

The system hardware features a shaking table, a laser interferometer and an interface board that allows for A/D conversion between the laser interferometer and a personal computer. The instrument is shown in Figure 2.9a. The system software automatically determines the response of curves of the sensors after the shake table has been driven with the target frequency range. For the horizontal components' calibration, a laser sensor LDS-3000 is adopted. It is a displacement sensor which allows accurate measures in a range of 400 mm and a resolution of 2.54 nm. For the vertical component a laser sensor LM-300 is used, a displacement sensor which allows accurate measures in a range of 3 mm and a resolution of 200 nm, in a frequencies up to 400 Hz. During the experiment on the shake table, the ASX1000 prototype was excited with a sweeping signal characterized by a frequency range between 0 and 100 Hz, a duration of 60 seconds, and a maximum and minimum amplitude of ± 0.2 m/s^2 (Figure 2.9b). In the time domain, the acceleration time histories of the sweeping waves recorded by the MEMS sensor prototype and the laser are in good agreement.

The analysis in the frequency domain involves the estimate of the ratio between the FFT (Fast Fourier Transform) of the acquired signals. Thus, a plot of both Amplitude and Phase are produced during the experiment (Figure 2.10). The prototype proves to be in a very good agreement with the laser motion reference also for the frequency response up to 80 Hz. These results suggest that our MEMS sensor prototype gives a reasonable response in the frequency range of interest for earthquake engineering. Thus, it can be installed and acquire seismic data.

A noise analysis was performed, leaving the MEMS sensor prototype in the shake table laboratory, which is isolated from source of anthropic noise, for 30 minutes. This

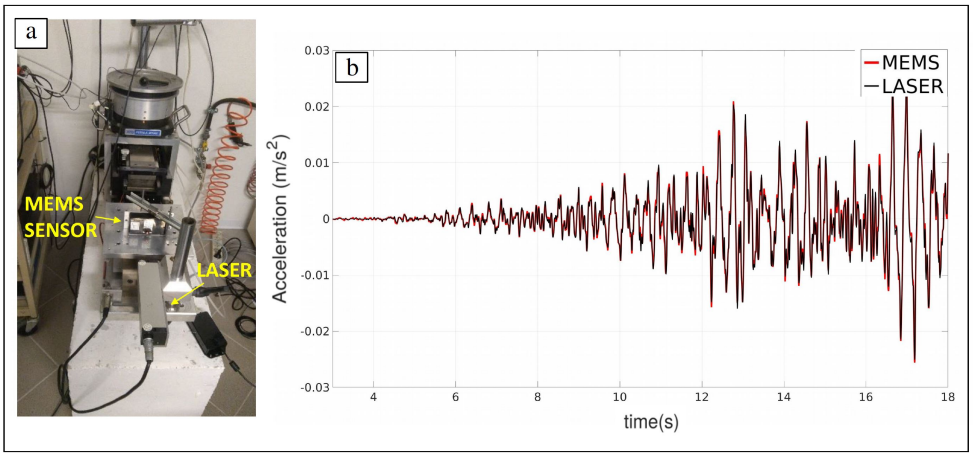

Figure 2.9: Shake table with the co-mounted lasers and the ASX1000 prototype. (b) Time series of the sweeping waves (18 seconds window) recorded by the X component of the ASX1000 MEMS sensor prototype (red line) and laser (black line).

test is useful to evaluate the noise floor of the MEMS sensor: the recorded signal in the absence of any external perturbations. This non-null output corresponds to the noise produced by the sensor itself. We estimate the Power Spectrum Density (PSD) of the 30 minutes signal (expressed in Volt, V) for each component. The plots of the PSD is shown in Figure 2.11. The PSD shows a general downward trend between -80 dBV^2 and -120 dBV^2 in the 0.1-250 Hz frequency range. This result is fundamental in order to evaluate the detectable magnitude of the ASX1000 MEMS sensor prototype (Cascone et al. [2021])(see the Figure 1 in the APPENDIX A, section A.1).

2.3 Results

2.3.1 Earthquake detection

Starting from the first January 2020 to December 2021, the MEMS-based networks in Italy detect 44 Earthquakes with 1.5 <M <6.3. Their epicentral and hypocentral

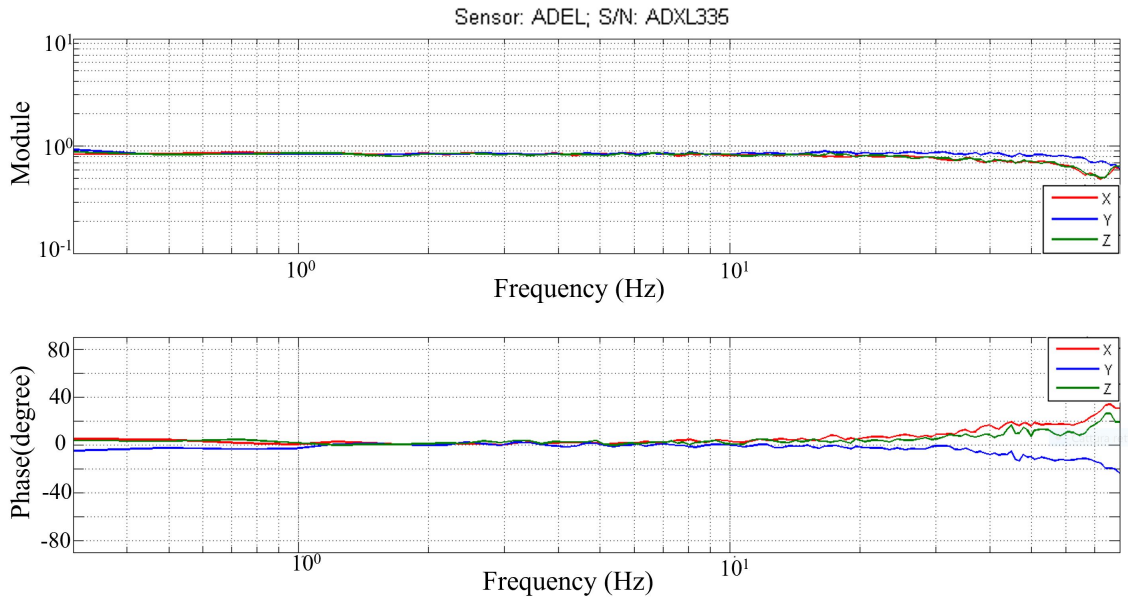

Figure 2.10: Modules and phases estimated during the experiment on the shake table

distribution are shown in Figure 2.12 and 2.13.

The earthquakes parameters, visible on the INGV website, are reported in Table 2.1. Here, we report the recorded seismic event in a chronological order. We assign an ID for each seismic event: "CI" and "NI" for the seismic events recorded in Central and Northern Italy, respectively (see Table 2.1). Then we report the information inferred from the INGV website: the date and origin time; the location expressed in decimal coordinates; the moment or local magnitude. The nucleation depth of the seismic events varies typically between 6 and 16 km. With the exception of the seismic event "NI_8", which has nucleated at 31 km depth. On the basis of the distance between epicenters and the MEMS senor's networks, we arbitrary classify the events in Small Seismic Events (1.5 $<M_L$ <2.5), Small-to-Moderate Seismic Events (2.5 $<M_L$ <5), and Moderate seismic (M_L >5) events.

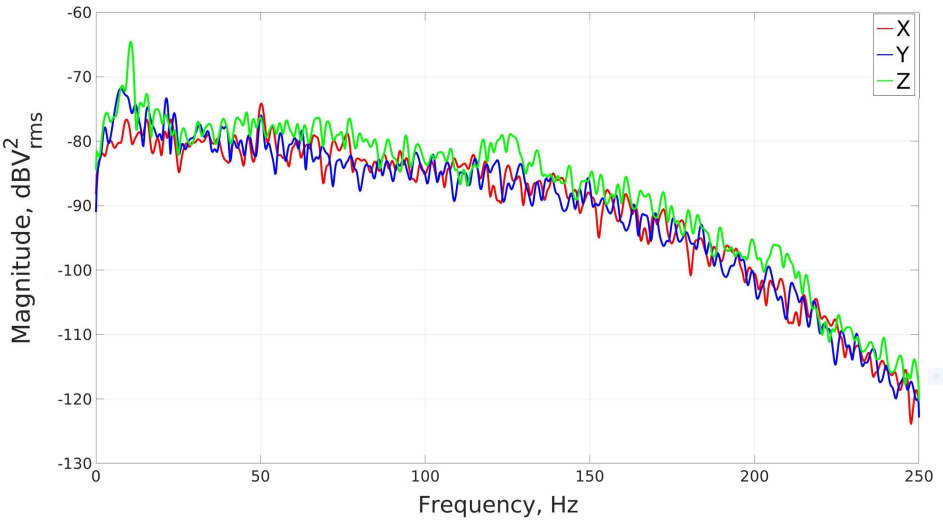

Figure 2.11: PSD of the self-noise which characterize the ASX1000 MEMS sensor prototype

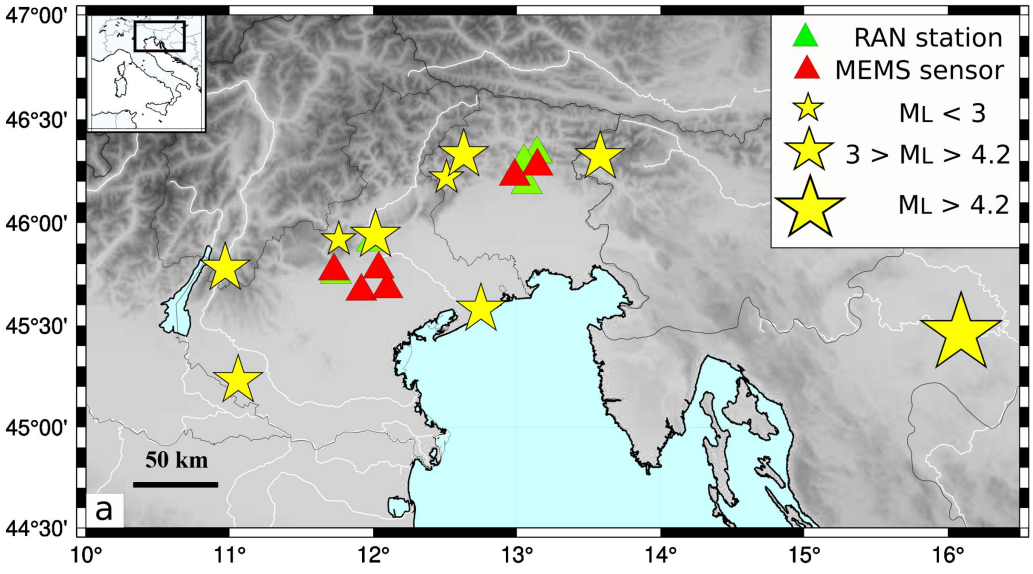

Figure 2.12: Epicenters distribution of the seismic events recorded by the ASX1000 MEMS sensor prototypes in Northern Italy.

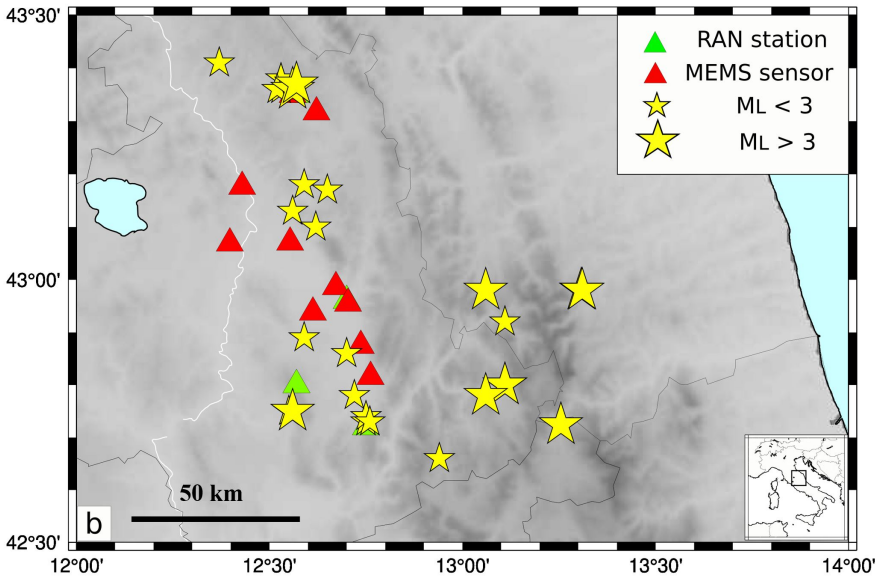

Figure 2.13: Epicenters distribution of the seismic events recorded by the ASX1000 MEMS sensor prototypes in Central Italy.

Small Seismic Events detection

The ASX1000 MEMS sensor prototype recorded a total of 24 small seismic events The lowest M_L recorded is equal to 1.5. (Figure 2.14)

The Earthquake occurred on 28th November 2021 (see CI_32 in Table 2.1) The distance between the epicenter and the MEMS sensor that has recorded the event is equal to 4 km. The waveforms of the three components are plotted in Figure 2.14. It is worth notice that the vertical component (blue signal in Figure 2.14) is characterized by a higher level of instrumental noise with respect the horizontal components. The reason of the noisy vertical component is explained in section 2.2.1. The analysis of the other small seismic events, reported in Table 2.1 are described in detail in a paper published in The Seismic Record, available online from 13th May 2021, (APPENDIX A, section A.1).

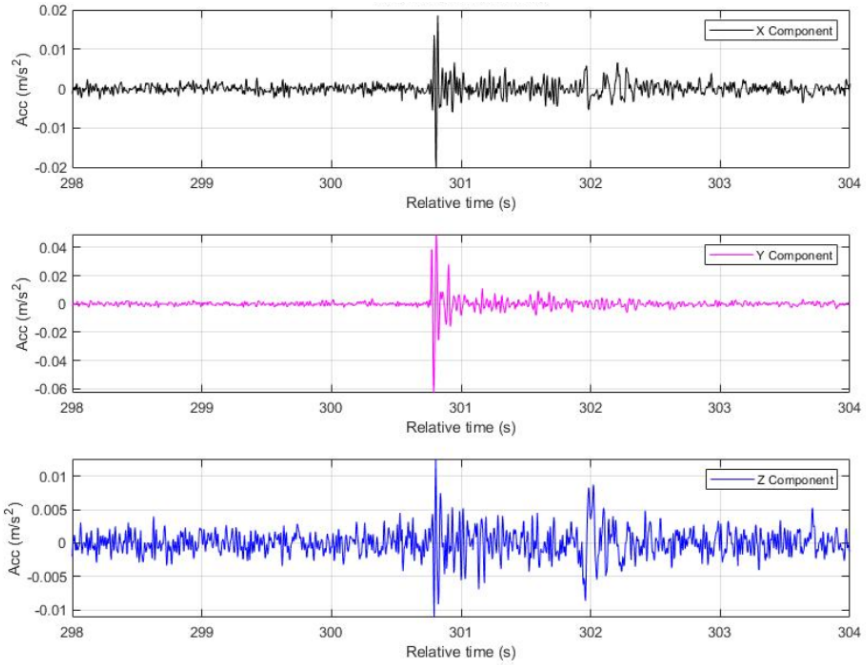

Figure 2.14: The smallest seismic event recorded by the ASX1000 MEMS sensor prototype ($M_L = 1.5$)

Small-to-Moderate and Moderate Seismic Events detection

The ASX1000 MEMS sensor prototype recorded a total of 19 Small-to-Moderate seismic events. For seismic events with $M_L \geq 2.5$ a comparison with the signals inferred from the RAN stations can be made. The data, in terms of waveform and strong motion parameters can be download under request on RAN website (ran.protezionecivile.it.). The comparison can be made in terms of waveforms, PGA (Peak Ground Acceleration) and 5 percent damped Spectral Acceleration (Sa). The PGA quantify the maximum acceleration experienced by a particle on the ground. The Sa is a fundamental strong motion parameter which represents approximately what is experienced by a building, which is modeled by a particle mass on a mass-less vertical rod having the same natural period of vibration as the building. The PGA is easily inferred considering the absolute value of the seismic waveform. The Spectral Acceleration are inferred considering the Newmark linear method. This method allows to obtain pseudo-velocity and pseudo-acceleration on the basis of the maximum displacement captured for each period (T) The ASX1000 MEMS sensor prototype recorded a total of four moderate seismic events. One located in Italy, near the town of Salizzole; three located outside the Italian territories, in Slovenia and Croatia (Figure 2.12).

Here we show the comparison of strong motion parameters of the Salizzole Earthquake and and Slovenia Earthquake (Figure 2.15 and 2.16). It is worth notice that the signal recorded by the MEMS ASX1000 during the Slovenia earthquake shows clearly the S-waves and surface waves arrivals.

The most energetic seismic event(NI_5 in Table 2.1), nucleated near the Petrinja City (Croatia), has a $M_w = 6.3$. This earthquake is recorded by all the ASX1000 MEMS sensor installed in Italy: this means that these new prototypes are capable of

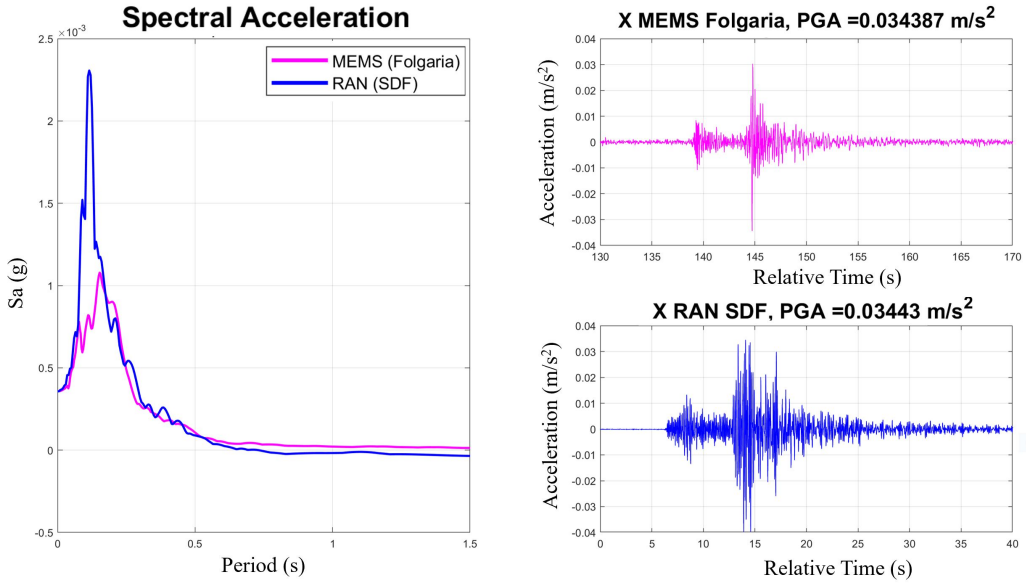

Figure 2.15: Strong motion parameters comparison of Salizzole Earthquake

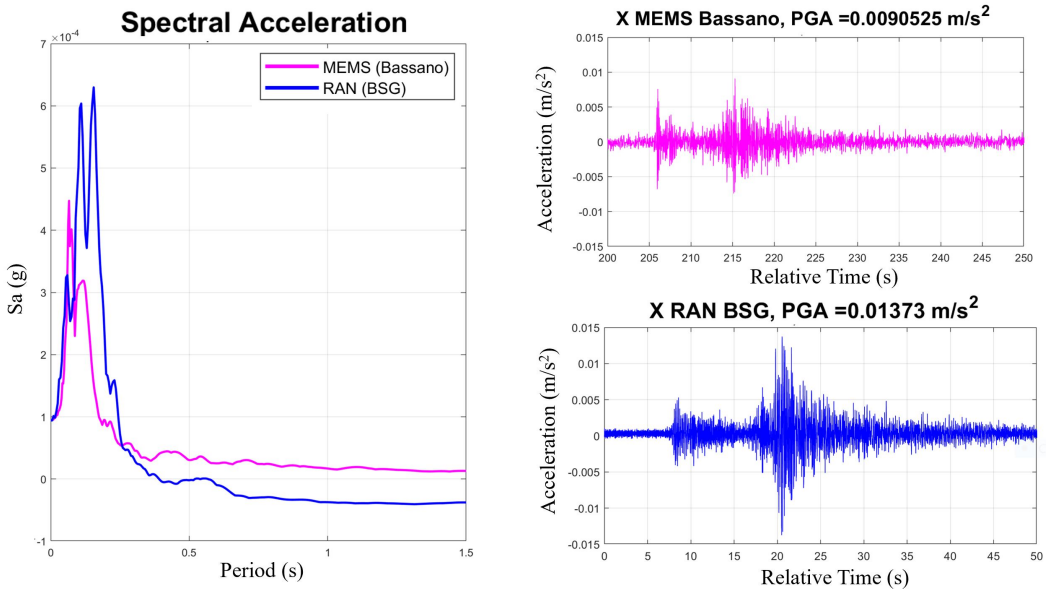

Figure 2.16: Strong motion parameters comparison of Slovenia Earthquake

recording energetic telesismic events, also at distances greater than 300 km.

2.3.2 Multi-sensor TEST

On 5th of March 2021 an experiment with an active seismic source was made in order to evaluate the possibility to design a multi-sensor accelerometer and improve the sensor sensitivity. Each device includes four MEMS sensors instead on one, to improve the Signal to Noise Ratio (SNR) of the recording signal. The experiment is performed outside the Geoscience Department at University of Padova. The experimental set-up consists of a falling weight mass (35 Kg) as an active seismic source and the acquisition system composed by four MEMS ASX1000 sensors (ACN1, ACN3, ACN4, ACN5)(Figure 2.17).

Figure 2.17: Multi-sensors' experimental set-up

The raw X-component acquisitions are shown in Figure 2.18a. It is possible to recognize the recording of the elastic waves generated by the seismic source. In order to perform the stacking, the raw signals are aligned considering the lag time inferred

from the cross-correlation technique, which is detailed explained in Chapter 4. The ACN1 trace is considered as the master signal, and it is marked in magenta (Figure 2.18b). The aligned signals are then stacked: all recordings are summed to produce one stacked record (Figure 2.18c).

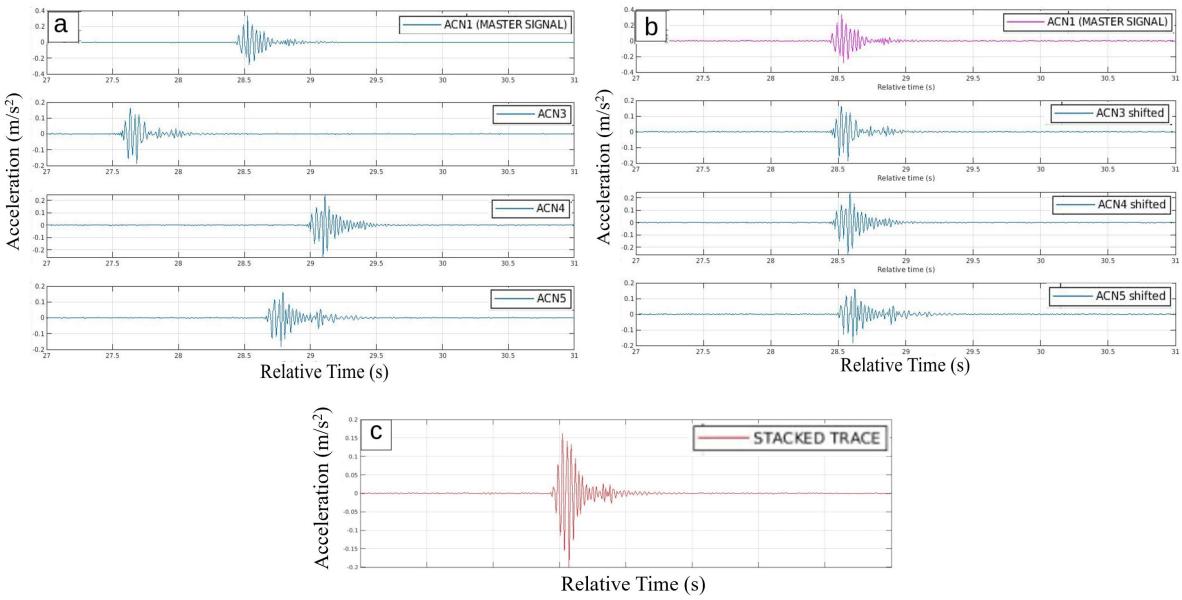

Figure 2.18: (a) Raw Traces; (b) Shifted traces considering the Lag time obtained from the cross-correlation and the magenta signal represents the master trace; (c) Stacked Trace

We show the Power spectrum of the four traces (marked in cyan) and the stacked trace (marked in red) (Figure 2.19). It is worth notice that in the frequency band interesting for earthquake engineering (the first tens Hz), the spectrum estimated on the stacked trace is shifted on lowest values of decibels (dB), demonstrating a noise level reduction and suggesting a promising approach for the design of new prototypes based on multiple MEMS sensors.

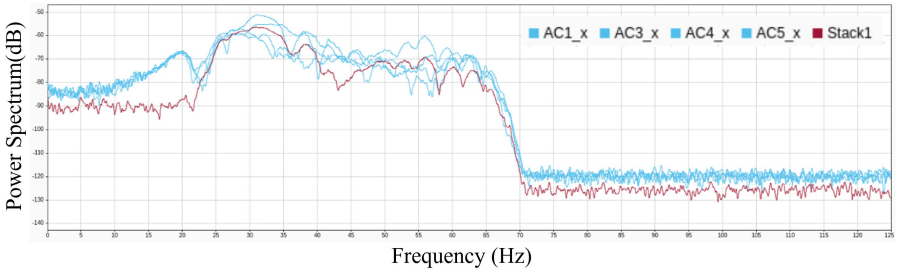

Figure 2.19: Power spectrum of the four acquired traces (cyan spectra) and the stacked traces (red spectrum)

2.4 Discussions and Conclusions

In this chapter we evaluate the suitability of a new prototype of inexpensive MEMS sensor, named ASX1000, to detect seismicity. The sensor shows a good performance on a calibration experiment on a shake table apparatus. The two experimental networks of MEMS accelerometers installed in Northern and Central Italy are able to record local earthquakes and distant seismic events. In particular, these sensors are capable of recording small magnitude seismic events (see APPENDIX A, section A.1). We demonstrate that this new MEMS sensor prototype can reach efficient performance for the detection of local seismicity with M_L >1.5 at epicentral distances lower than 10 km. These miniaturized devices are able to record also earthquakes with a M_L of 3.0 at epicentral distances in the order of 30 km. The fundamental strong motion parameters (PGA and Spectral Acceleration) inferred from the accelerograms recorded by MEMS sensors, are comparable with the ones inferred from the broad-band seismic stations (the seismic data of the RAN network can be downloaded only for seismic events with M_L >2.5). These parameters represent practical indexes to describe, at a particular site, the degree of shaking. They are critical also for seismic design of engineering

structures. Thus, a denser seismic network built with low-cost MEMS sensors, can improve the seismic wavefield recording. We remark that networks based on MEMS sensors cannot substitute the broad-band seismometers, especially for weaker events. On the other hand, considering the quick industrial development of MEMS technology, in the near future these sensors could integrate the existing strong-motion networks.

Table 2.1: In the Table are reported the ID, epicenter, date (dd/mm/yy), origin time (hh/mm/ss), coordinates, and local magnitude of the recorded seismic event. The magnitudes marked with * refer to the moment magnitude

ID	Epicenter	Date	Time	Lat	Lon	Z (km)	M
CI_1	Accumoli (PG)	28-01-2020	16:37:34	42.722	13.2	8	3.3
CI_2	Mt Cavallo (MC)	20-03-2020	04:49:43	42.97	13.05	9	3.3
CI_3	Gubbio(PG)	05-04-2020	14:33:48	43.37	12.52	9	2.4
NI_1	Claut(PN)	08-04-2020	15:10:46	46.22	12.50	8	2.9
CI_4	Amandola (FM)	05-05-2020	02:05:38	42.98	13.29	11	3.4
CI_5	Norcia(PG)	04-05-2021	20:05:06	42.8	13.11	9	3.0
CI_6	Norcia (PG)	18-05-2020	02:18:30	42.77	13.16	9	3.0
NI_2	Forni Di Sotto(UD)	13-07-2020	12:06:53	46.33	12.63	10	3.5
CI_7	Valfabbrica(PG)	10-09-2020	07:45:13	43.17	12.65	9	2.5
NI_3	Slovenia	17-07-2020	02:50:57	46.31	13.57	11	3.8*
NI_4	Cismon D.G.(VI)	29-07-2020	20:26:34	45.93	11.73	11	2.7
NI_5	Croatia	29-12-2020	11:19:54	45.4	16.2	9	6.3*
NI_6	Salizzole(VR)	29-12-2020	14:36:57	45.23	11.06	15	3.9*
CI_8	Gualdo C.	10-02-2021	00:49:57	42.89	12.59	8	2.0
CI_9	Spoleto(PG)	14-02-2021	23:59:14	42.74	12.76	8	2.4
CI_10	Spoleto(PG)	15-02-2021	04:39:31	42.73	12.75	8	2.4
CI_11	Pietralunga(PG)	19-02-2021	22:42:45	43.41	12.45	8	2.6
NI_7	Ala(TN)	22-02-2021	12:04:06	45.78	10.97	12	3.5
CI_12	Pietralunga(PG)	25-02-2021	20:34:10	43.39	12.48	9	2.7
CI_13	Montone(PG)	26-03-2021	05:32:27	43.41	12.37	6	2.8
CI_14	Norcia(PG)	05-04-2021	20:05:06	42.80	13.11	9	3.0
CI_15	Valfabbrica(PG)	09-04-2021	04:12:10	43.13	12.56	9	2.6
CI_16	Trevi(PG)	11-04-2021	17:41:15	42.86	12.70	7	2.5
CI_17	Gubbio (PG)	15-05-2021	07:56:01	43.36	12.56	8.6	3.9
CI_18	Gubbio (PG)	15-05-2021	08:07:20	43.37	12.57	7	3.1
CI_19	Gubbio (PG)	15-05-2021	12:08:28	43.37	12.55	8	2.0
CI_20	Gubbio (PG)	23-05-2021	20:51:23	43.36	12.55	8	3.0
CI_21	Gubbio(PG)	09-06-2021	10:36:56	43.36	12.53	8	2.1
CI_22	Gubbio(PG)	10-06-2021	01:39:31	43.38	12.53	7	2.4
CI_23	Assisi (PG)	12-06-2021	05:17:59	43.10	12.62	7.5	2.9
NI_8	Eraclea(VE)	14-06-2021	06:31:19	45.58	12.75	31	3
CI_24	Gubbio (PG)	27-06-2021	10:38:13	43.36	12.52	6	2.9
CI_25	Gubbio (PG)	27-06-2021	13:27:16	43.36	12.55	6	2.9
CI_26	Massa Martana (PG)	22-07-2021	14:06:22	42.75	12.55	7	3.5
CI_27	Massa Martana (PG)	22-07-2021	15:52:33	42.75	12.56	8	2.7
CI_28	Spoleto(PG)	21-09-2021	14:40:40	42.77	12.74	10	2.8
CI_29	Norcia(PG)	16-07-2021	08:00:49	42.78	13.06	9	3.3*
NI_9	Valdobbiadene	28-09-2021	00:46:44	45.94	12.01	10	3.6
NI_10	Valdobbiadene	28-09-2021	01:32:21	45.94	12.01	10	2.7
NI_11	Valdobbiadene	29-09-2021	14:20:38	45.94	12.01	11	3.3
CI_30	Visso(MC)	18-10-2021	12:54:17	42.92	13.11	9	3.7*
CI_31	Campello (PG)	08-11-2021	16:20:02	42.78	12.72	7	2.6
CI_33	Gubbio (PG)	28-11-2021	20:00:22	43.37	12.53	8	1.5
CI_34	Gubbio (PG)	23-12-2021	09:15:54	43.33	12.61	9	2.4

Chapter 3

Seismic hazard scenario of the Venetian Plain and the effect of shear-wave velocity gradients

3.1 Introduction

The average shear-wave velocity (v_s) of the first 30 meters of subsoil and the depth of the engineering bedrock are considered the key parameters for simplified seismic site response modelling. [1] However, a reliable estimate of the site amplification should consider the entire shear-wave velocity profile from the Earth's surface down to the engineering bedrock. In deep alluvial basins, a typical geological context where the soil-bedrock interface may lie below the penetration depth of most common prospect-

[1] This chapter has been published as "Velocity gradients choice affecting seismic site response in deep alluvial basins: Application to the Venetian Plain (Northern Italy)" on The Journal of Geophysics and Engineering, 19(1), 1-13.
CONTRIBUTION: Data Collection, Data Processing and Interpretation

ing methods, only the shallow velocity profile can be obtained in detail, while the deeper structures are commonly extrapolated with linear equations. The choice of a realistic interpolation between the shallow and deep soil still remains an open issue. We compute the 1D seismic site response of two sectors of the Venetian Plain (Northern Italy) characterized by gravelly and sandy deep formations, respectively. We model the 1D soil columns using theoretical non-linear gradients proposed in literature for deep alluvial basins. In this chapter we perform several 1D seismic site analyses in the Venetian Plain area (Northern Italy), a large and deep sedimentary basin. In particular we consider two different sectors where a detailed set of seismic surveys were performed to obtain shallow v_s profiles, while the deeper structures remain un-investigated. To fill the gap between the shallow and deeper v_s structures, we adopt general gradients, proposed for the modelling of several alluvial basins as the Lower Rhine Basin (Germany; Budny [1985]), the Grenoble Basin (France; Guenguen et al., [2007]) and the Lucerne Basin (Switzerland; Poggi et al. [2012]). These sites (red stars in Figure 3.1) are in fact characterized by deep sedimentary covers, similarly to the Venetian Plain. In order to compare modelling and experimental data we analyzed real seismograms coming from a borehole in the Po Plain, where deep and surface seismic recording stations were available. 1D seismic site response modelling were compared to the recording amplifications, testing different gradients. We aim to assess how the choice of gradient can modify the seismic site response in deep sedimentary basins, where no information about the deeper structures are available. A realistic modelling of the ground motion is the key parameter for ground shaking scenario, used by civil engineers for the design of earthquake-resistant constructions. Due to the limited knowledge of the deeper velocity structures, it could be more appropriate to model the soil column with

the gradient which allows for the most conservative results in terms of ground motion effects. This study demonstrates the importance of the v_s gradient on ground motion scenarios and the results are relevant for the seismic hazard evaluation in the deep sedimentary basins, which host the large urban environments around the world.

3.2 Geological Setting: The Venetian Plain

Our study area is the Venetian Plain region (Northern Italy), a large syntectonic alluvial basin actively affected by earthquakes occurrence (Figure 3.1).

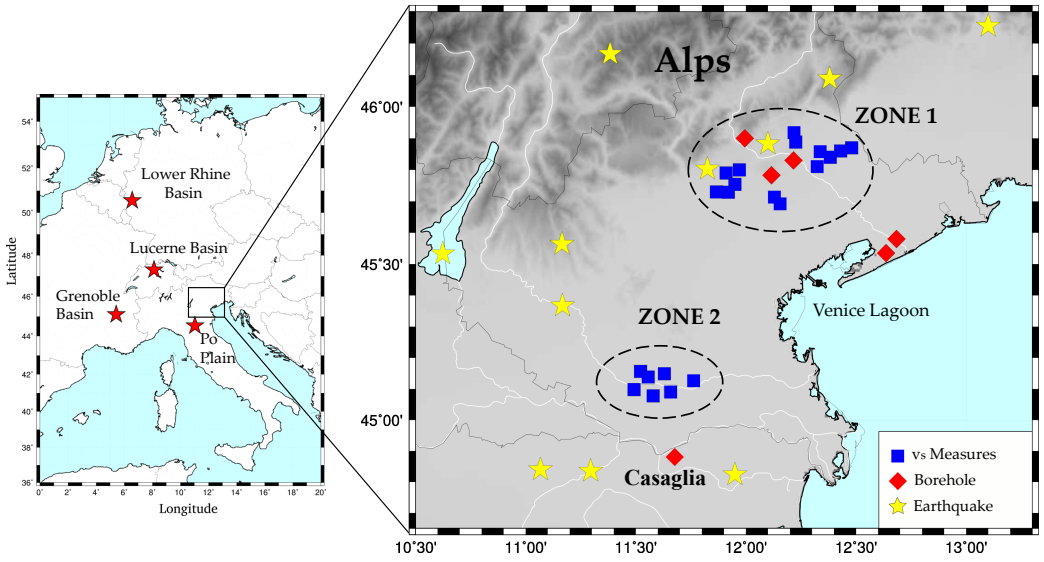

Figure 3.1: Left Panel: Europe chart and deep alluvial basins' locations (red stars): Lower Rhine Basin (Germany); Lucerne Basin (Switzerland); Grenoble Basin (France); Po Plain (Italy). Right Panel: zoom of Venetian Plain (Italy). Blue squares represent in-situ measurement locations. Red diamonds represent ENI/AGIP deep boreholes. Yellow stars indicate the epicentre of the main seismic events from 1117 to 2012 (5.5 $<M_w$ <6.8).

Together with the Po Plain, the Venetian Plain represents the foreland of the S-

verging central-southern Alps and of the N-NE-verging northern Apennine belt (Doglioni [1993]). The effect of the north-propagating Apennine foredeep, started in the late Miocene, affect the southern sectors of the Venetian Plain and lead to a regional southward tilting recorded up to Venice Lagoon. The thickness of Quaternary formations varies from 2 km in the southern part of the Venice Lagoon, and gradually pinch out eastward (Carminati et al. [2003]). The buried active fronts of Northern Apennines and Southern Alps are considered seismic sources capable of destructive earthquakes (Poli et al. [2008]). The epicentres distribution of historical and instrumental earthquakes is shown in Figure 3.2. Although the seismicity is concentrated along the foothills area of the Southern Alps and the Northern Apennines, it is widely recognized that the Venetian Plain is influenced by strong seismic site effects (Vuan et al. [2011]). The 3D structural models of the Venetian Plain are principally based on old geophysical information from oil explorations (Doglioni [1993]). They are also based on the TRANSALP, a deep seismic reflection measurement collected in the Eastern Alps (Cassinis [2006]). In this study we consider two different sectors of the Venetian Plain with different Quaternary sedimentary fillings: the "high" (Northern) and "low" (Southern) plain, where several shallow v_s measurements were performed (Figure 3.1). The high plain or pre-Alpine zone, here called ZONE 1, has a fluvial and glacial origin and is principally composed of gravel. The low plain, hereafter ZONE 2, extends from the gravel deposits transition to the Adriatic coast; the subsoil is composed mainly of silt and clay layers with intercalations of sandy layers (Carraro et al. [2015]).

3.3 Method

3.3.1 Shear-waves velocity profiles

The effects of local geology on seismic ground motion have been widely studied in geotechnical earthquake engineering in order to estimate response spectra for building restoration and construction(Martin et al. [1994]). The shear-wave velocity (v_s) is one of the key parameters adopted for site classification in several seismic regulations (Boore et al. [1993]). v_s profiles estimate the rigidity of the soil column when excited by seismic shear stress, which is the most important action controlling the seismic site response (Martin et al. [1994]). Seismic site amplification can be in fact described as the motion modification due to the soft soil during the wave propagation through the stratigraphic column, from the basement bedrock upward to the ground surface (Rathje et al. [2010]). Several seismic regulations propose different approaches in order to evaluate the seismic amplification due to the soil properties. The soils are often classified into different categories, based on the average v_s of the top 30 m of a soil profile (also called v_s30) as in the Italian Building Code ("Norme tecniche per le costruzioni-NTC"; Ministero delle Infrastrutture e dei Trasporti 2008); or the Eurocode 8-EC8; and the National Earthquake Hazard Reduction Program-NEHRP provisions (Building Seismic Safety Council-BSSC 2003). The v_s30 parameter adopted by the seismic site classification refers to the depth of investigation for common geophysical and geotechnical analysis, that are logistically and economically often limited to the first subsoil (generally around tens of meters depth). Seismic surveys to retrieve v_s values can be made either in boreholes (downhole seismic testing, Cardarelli et al. [2018]) or with surface methods as the multichannel analysis of surface waves (MASW,Strobbia et al. [2011]) and SH

refraction analysis. Regardless the method adopted in common engineering projects, the investigation depth rarely exceeds the first subsoil, being limited by the logistically achievable efforts such as: seismic source power, extension of the survey length due to urban conditions, borehole penetration etc. Thus, most of the seismic site response studies are based on the properties of the subsurface soils down to 30 meters (Boore et al. [1993], Martin et al. [1994]). The Italian and European seismic codes define the engineering bedrock as the depth at which $v_s \geq 800$ m/s (soil category A = stiff soil or rock, see EC8). Softer soils, with $v_s \geq 800$ m/s, are expected to amplify the seismic action, therefore the correct estimation of the site amplification should consider the entire soil profile from the ground surface down to the engineering bedrock. Nevertheless, in deep alluvial basins, a clear soft soil-bedrock interface may not be evident but buried under hundred meters of soft sediments (Guéguen et al. [2007],Poggi et al. [2012], Mascandola et al. [2019]). In these geological contexts, thick and soft sediments are expected to amplify the seismic ground motion. The site classifications that consider only the v_s30 might lack in correct seismic action estimation, leading to inaccurate evaluations of the ground amplification level (e.g., Borcherdt [1994], Pitilakis et al. [2006]). Several available techniques, such as passive surveys and travel-time seismic tomography allow a deeper soil characterization, down to hundreds of meters depth. The passive methods, based on the recording of ambient vibrations, use 2D arrays of receivers (e.g. SPAC; frequency-wavenumber method), linear arrays (Re-Mi, Louie [2001], Strobbia et al. [2015]) or single stations measurements (HVSR, Nakamura [1989]). Passive methods are powerful and cost effective, but they could suffer from a non-uniform distribution of noise sources and/or be biased by 2D site effects. Travel-time tomography use signals from earthquakes or low-frequency seismic ambient noise

to retrieve deep geological structures. Berbellini et al. [2017] propose that the reference bedrock depth of deep alluvial basins could be extrapolated using regional models inferred from travel-time seismic tomography. However, since tomographic approaches are oriented to large scale modelling, retrieved models are sufficiently accurate at depth (i.e., at the kilometric scale), but they often do not present enough resolution for local-scale seismic waveform studies, as needed for local hazard assessment and evaluation of earthquake scenarios. As matter of fact, the v_s profile characterizing the soil column may be accurate for the first tens of meters, thanks to local geophysical/geotechnical surveys, and at few kilometres in depth, if regional tomographic models are available. However, the velocity structure between the uppermost velocities (e.g., v_s30) and the engineering bedrock ($v_s \geq 800$ m/s) may be not accurately defined, especially in deep alluvial basins. The most adopted ground motion modelling approaches, such as one-dimensional 1D seismic site response, need the complete characterization of the soil column, at least until the reference engineering bedrock depth. For these reasons, several seismic codes propose simplified approaches to describe the soil column. The Italian seismic code (ICMS 2018), for example, proposes an extrapolation of v_s in depth through linear gradients with different slopes (depending on the geological site conditions) until the depth of the engineering bedrock depth (Figure 3.2).

It is known that the seismic motion can be decomposed in different sets of waves such as body waves (P, SH, SV) or surface waves (Rayleigh, Love) and seismic motion amplification may be different. However, it is a common practice in earthquakes engineering design norms focusing of the effect of near-surface geology for vertically propagating shear body waves (see Eurocode 8).

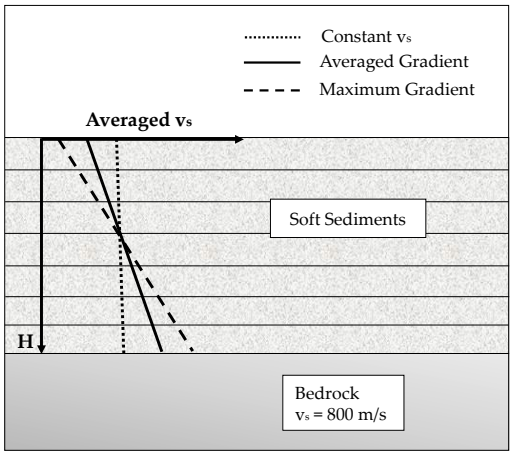

Figure 3.2: Extrapolation of v_s profiles with linear gradients suggested by the Italian Seismic Code (ICMS 2018, modified).

3.3.2 One dimensional seismic site response

In this work we simulate the 1D seismic site response of two sectors of the Venetian Plain: the ZONE 1, representing the pre-Alpine sector of the alluvial plain characterized by coarse deposits; the ZONE 2, representing the alluvial plain sector with sandy-clay formations (Figure 3.1). We analyze different sedimentary deposits with a wide granulometry range, which cover an important breadth of different soil types. In seismic engineering practice, the deep alluvial basin environments are usually represented with one-dimensional geometry of horizontal layering, allowing 1D seismic analysis. With STRATA software (Kottke and Rathje [2009]) it is possible to perform stochastic seismic site response analysis with the equivalent-linear approach, assuming horizontal soil layer boundaries with an infinite lateral extension and a vertically-propagating-horizontally-polarized shear waves (SH waves). In particular, STRATA code needs: (1) the input motions (acceleration time-histories); (2) the soil properties down to

the engineering bedrock: the v_s profiles, shear-modulus (G) and Damping ratio (D) non-linear curves (Boaga et al. [2012]), and total unit weight.

Input Motions

The seismic site response analysis requires the definition of seismic input terms of acceleration time series. The waveforms can be previously recorded accelerograms belonging to a seismic database, such as the European Strong Motion Database. We select a target response spectrum considering the local probabilistic seismic hazard analysis of the Veneto Region (Northern Italy). We adopt an average expected acceleration of 0.13g with 10 PERCENT of probability of non-exceedance in 50 years for a return period of 475 years (Italian Seismic Hazard Map, INGV 2004) (Figure 3.3a).

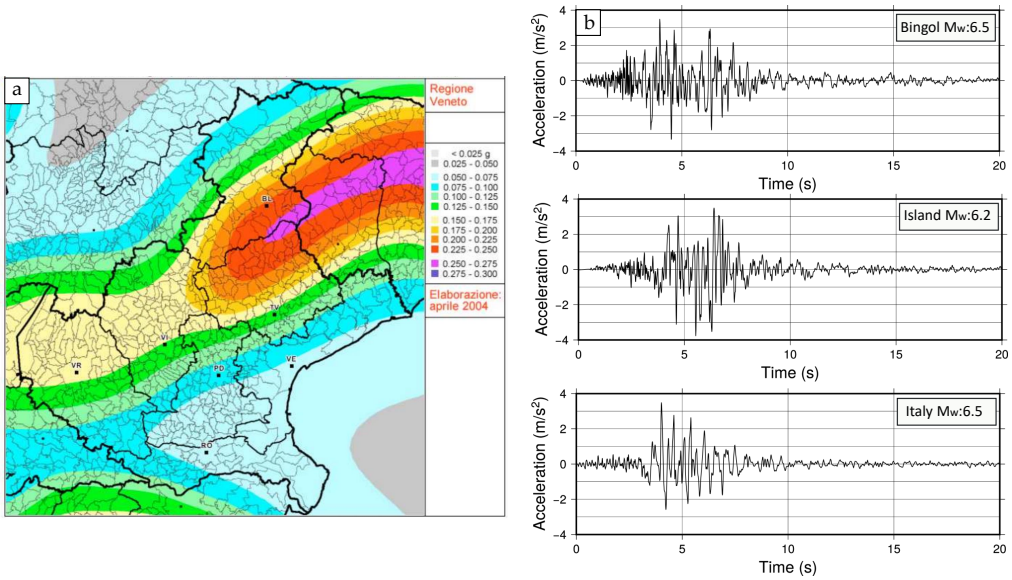

Figure 3.3: (a) Seismic hazard map of Veneto region, Italy (Italian Seismic Hazard Map, INGV 2004, modified); (b) The three-real selected accelerograms used as input motion in our stochastic 1D response simulations.

We use the Rexel program (Iervolino et al. [2010]) in order to select a set of one-

component real accelerograms. The research criteria consist of an upper and lower tolerance, with respect to the target spectrum, of 30% and 10% respectively, in a period range between 0.15s and 2s. Three accelerograms are finally selected for our simulation (Figure 3.3b).

Definition of v_s profiles

In order to characterize the two sites of the Venetian Plain (ZONE 1 and ZONE 2), some geophysical testing campaigns were carried out, including 31 MASW and 36 Re.Mi. surveys. Figure 3.1 shows the different tests locations, marked by blue squares. The resulting 67 v_s profiles, down to 30 m, are plotted in Figure 3.4. From the plot, it is possible to clearly distinguish between higher v_s formations in ZONE 1, characterizing by coarse sediments and lower v_s in ZONE 2, where sand formations are prevalent. The different granulometric distribution of the two study sectors are also confirmed by deep exploration boreholes log, close to the geophysical measurement locations (red diamonds in Figure 3.1), available on ViDEPI website (videpi.com). The average v_s profiles for the ZONE 1 and the ZONE 2, marked by red lines in Figure 3.4, match with the velocity structure proposed in the Eurocode 8 for gravelly and sandy soils, respectively. The averaged v_s profiles allow to construct the first 30 m of the 1D soil columns representatives of the two sectors of the Venetian Plain.

We model the deeper layers (below the 30 meters until the engineering bedrock) of the 1D soil columns with v_s gradients found in literature. The velocity gradients used in this study are meant to be used for generic deep alluvial basins, characterized by an average sedimentary cover that, in terms of seismic velocity, is similar to the shallow geological formations of the Venetian plain. Seven different gradients are selected, that

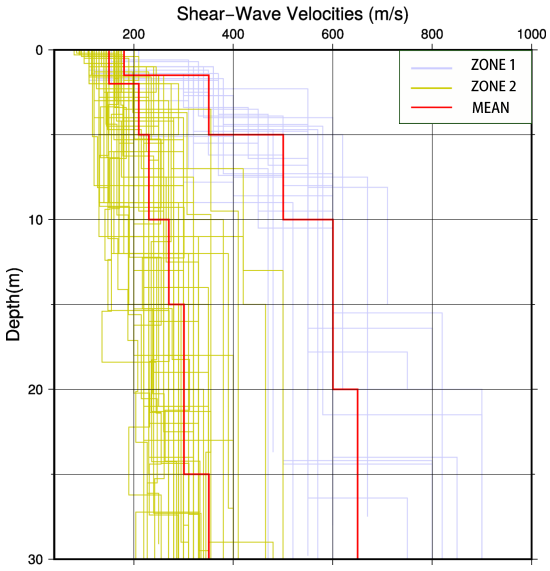

Figure 3.4: The 67 v_s profiles inferred from geophysical measurements in ZONE 1 (yellow) and ZONE 2 (blue). The red lines represent the mean v_s profiles for the two zones, representative of the shallow part (0-30 m) of the soil columns

we will refer to as: EXP (Exponential); PAR (Parabolic); SQR (square root trend); LIN (linear); GEN1 and GEN2, (Generics); HYP, (Hyperbolic). The adopted gradients can be subdivided in two categories. Gradients that don't include the bedrock depth parameter to model the v_s profile (EXP, PAR, SQR) fall into the first category. These gradients make it possible to define the engineering bedrock at different depths, depending on the selected gradient shape. Gradients that include the a priori information of the bedrock depth (LIN, GEN1, GEN2, HYP) belong to the second category. Considering the geological context of the Venetian Plain, there is no evidence in literature of bedrock depth in ZONE 1, while the ZONE 2 was recently investigated by Mascandola et al. [2019], who mapped the engineering bedrock of the Po Plain, that represents the southern propagation of the Venetian Plain (Figure 3.1). On the basis of the available information, we can model the soil columns of the ZONE 1 with gradients

belonging to the first category, while the ZONE 2 is modelled with gradients belonging to the second category, fixing the engineering bedrock at 400m depth (Mascandola et al. [2019]). The theoretical gradients used in this study are described below. In formula, the v_0 parameter represents the v_s at the ground surface (z = 0).

EXP: Exponential gradient defined as:

$$v_s(z) = v_0(1+z)^x \tag{3.1}$$

where x is an exponential coefficient controlling the dependence of velocity with the depth z (0 <x <1). This equation holds for granular media only. Saturation level, fluid pressure and cementation can affect the exponent x (Albarello et al. [2011]). This is the most common form of the v_s gradients, used to model tectonic basins such as Lower Rhine Basin (Germany) (Budny [1985]). In particular, to better define the parameter x for ZONE 1, we use the value found by Budny [1985]) for coarse sedimentary cover, equal to 0.285 (yellow curve in Figure 3.5a).

PAR: Parabolic gradient defined as:

$$v_s(z) = v_0 S_v 0^p \tag{3.2}$$

where S_v0 represents the total vertical overburden stress (considering a constant value of the soil unit weight) and p is a model parameter, generally varying between 0.1 and 0.3 (Andreotti et al. [2018]). Equation 3.2 allows the modelling of a parabolic profile of v_s and is proposed for sedimentary basins by Santamarina et al. [2001]. In order to link this curve to the shallow profile we set S_v0= 20 kN/m^3 which is the total

unit weight adopted for the 1D soil columns analyzed in this study. The p parameter is set to 0.15 (reference value as suggested by Andreotti et al. [2018]; red curve in Figure 3.5a).

SQR: v_s as a function of the square root of the depth, in formula:

$$v_s(z) = v_0 + a\sqrt{z} \tag{3.3}$$

where a is a constant (Gueguen et al. [2007]). This gradient is considered as a polynomial variation with depth. This equation represents a benchmark basin velocity model inferred from borehole data in Grenoble Basin (France), an Alpine basin with a maximum depth of more than 1 km. It is characterized by a Quaternary infill of coarse glacial deposits, which in terms of velocity, is similar to the sedimentary cover of the high Venetian Plain. In our model, we set a equal to 19, which is a reference value taken from Gueguen et al. [2007] (purple curve in Figure 3.5a).

LIN: Linear Gradient, defined as:

$$v_s(z) = mz + q \tag{3.4}$$

It is the easiest interpolation between the shallow subsoil (v_s min) and bedrock (v_s max = 800 m/s). This simplified approach is currently suggested by the Italian Seismic Code (2018) (Figure 3.2). We obtain the linear coefficients with a simple interpolation between the average shear-wave velocity at 30 meters depth (v_s min = 350 m/s) and the bedrock velocity at 400 meters depth. This results in a slope of m = 1.21 and an intercept of q = 313.51 m/s (Dashed red line in Figure 3.5b).

GEN1: The velocity gradient proposed by Regnier et al. [2016]).

$$v_s(z) = v_{smin} + (v_{smax} - v_{smin})(\frac{z - z_0}{z_2 - z_0})^a \tag{3.5}$$

This gradient is used to model simple soil conditions, where v_s increase regularly with depth. v_smin min and v_smax are the expected minimum and maximum shear wave velocities, z0 is the depth of the shallower low velocity layer and z_2 is the bedrock depth. The parameter a is an exponent set equal to 0.25, a reference value taken from Regnier et al. [2016]. In our model z0 is equal to 30 m, z_2 is equal to 400 m; v_smin and v_smax are equal to 350 m/s and 800 m/s respectively (Dashed yellow curve in Figure 3.5b)

GEN2: Generic v_s gradient This relationship was proposed by Poggi et al. [2012] for a seismic characterization of the alpine environment in Lucerne Basin (Switzerland). The gradient formula is:

$$v_s(z) = (v_{smax} - v_{smin})(1 - a^{\frac{z_0 - z}{b}}) + v_{smin} \tag{3.6}$$

This equation, similar to GEN 1, adopts curvature coefficients, a and b, which in our model are set to 2.3 and 81.7, so that the basement is reached at 400 m depth (Dashed purple curve in Figure 3.5b).

HYP: Hyperbolic profile This gradient represents the Gibson 2nd kind model (Gibson [1967]). The proposed gradient formula is:

$$v_s(z) = v_0 + \sqrt{\frac{z_2}{z_2 - z}} \tag{3.7}$$

z_2 is the bedrock depth (in our case S_v0 = 350 m/s and z_2 = 400 m). (Dashed

green curve in Figure 3.5b)

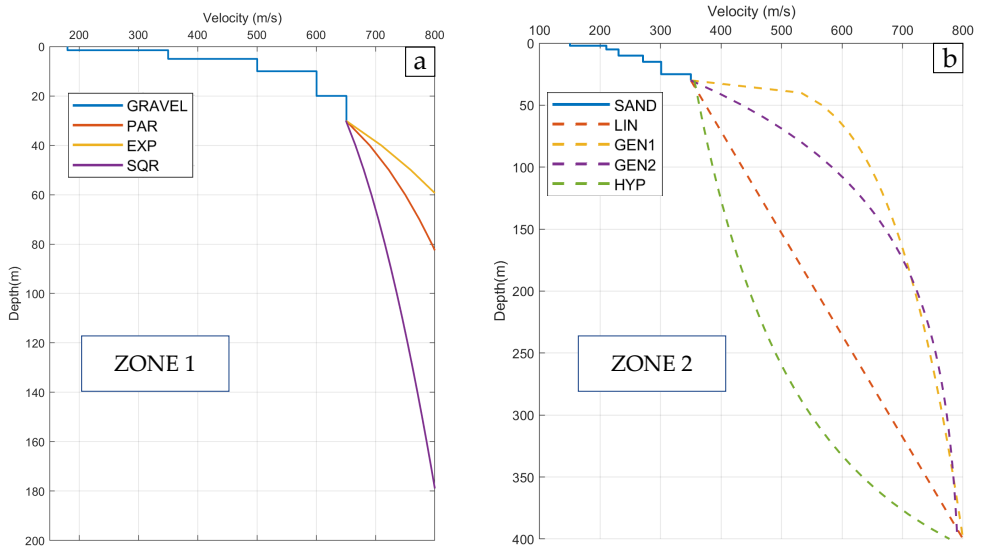

Figure 3.5: Velocity models adopted for 1D seismic site response for (a) ZONE 1 (case with unknown bedrock depth) and (b) ZONE 2 (case with bedrock depth $z_2 = 400$ m).

Stochastic 1D Seismic Analysis

The entire 1D soil columns with discretized layers are defined in order to compute the seismic site analysis. We analyze the different velocity profiles shown in Figure 3.5a, 3.5b. The shallow layers correspond to the average v_s profiles as indicated in Figure 3.4, while the deeper layers are obtained by discretizing the v_s gradient curves with 10 m thick intervals. The non-linear soil properties are generally represented with shear-modulus reduction (G/Gmax vs shear strain) and damping ratio (D vs shear strain) curves. In our case, the subsoil is modelled using the modulus reduction and damping curves as proposed by Idriss [1990] for gravel with a total unit weight of 20 kN/m^3 for the soil column of ZONE 1 (solid curves in Figure 3.6a and 3.6b). The soil profile

characterizing the ZONE 2 is modelled with the non-linear curves as proposed by Seed et al. [1986] for sandy silt with a total unit weight of 19 kN/m^3 (dashed curves in Figure 3.6a and 3.6b).

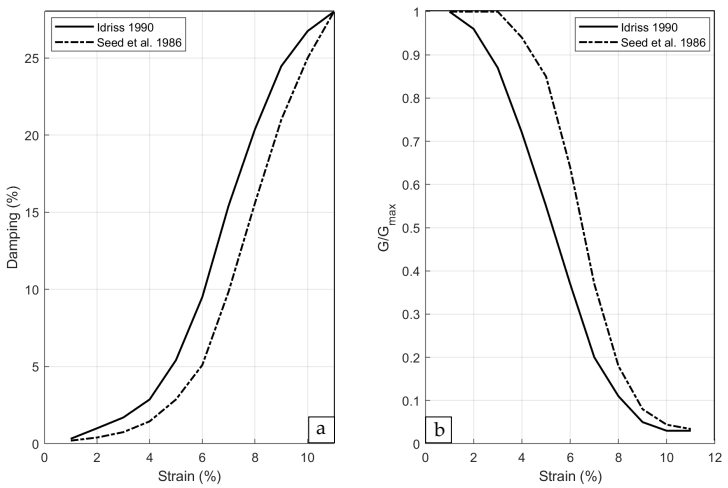

Figure 3.6: (a) Shear modulus and (b) damping curves adopted for 1D seismic analysis of ZONE 1 (Idriss 1990) and ZONE 2 (Seed et al. [1986].

Once the stratigraphic models are defined, a stochastic analysis via Monte Carlo simulations is performed in order to consider the local variability. The method consists in an iterative calculation of a deterministic model defined with a set of random realizations. The input parameters are randomly generated on the basis of previously defined probability distributions. In this way it is possible to simulate the sampling process of a real population in order to consider the uncertainty of the measurements. In our study, we randomize only the shallow v_s profile in the first 30 m, considering the standard deviation inferred from the statistical distribution of the 67 v_s profiles obtained by in-situ measurements (Figure 3.4). The variability of the shallow soil profiles adopted for the stochastic analysis is displayed in Figure 3.7a and 3.7b, which illustrate 100 v_s

profiles randomly generated. During the simulations the set of accelerograms described previously (shown in Figure 3.3b) are used as input at the bottom of each soil column. Thus, we perform 300 Monte Carlo simulations for each soil column (100 realizations for each of the three acceleration-time-histories), for a total of 2100 simulations.

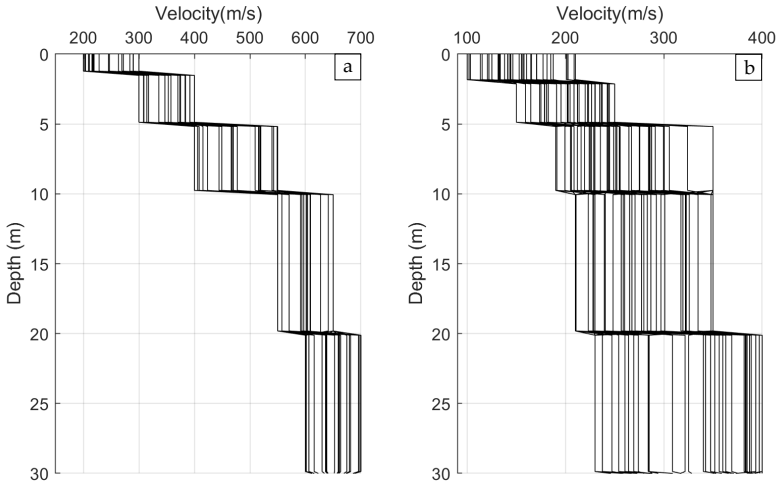

Figure 3.7: Example of 100 realizations of v_s profiles for (a) ZONE 1 and (b) ZONE 2.

3.4 Results

The results, derived from the stochastic 1D seismic site response analysis through Monte Carlo simulations, are presented in terms of surface acceleration response spectra (with a damping ratio, ξ, of 5%), peak ground accelerations (PGA), and Housner Spectrum Intensity (Housner [1952]). This last parameter is defined as:

$$S_I(\xi) = \int_{0.1}^{2.5} S_v(\xi, T) dT \tag{3.8}$$

The time integral considers the area under the pseudo-velocity response spectra

Sv over the period range T between 0.1s and 2.5s, with a damping ratio (ξ) of 5%. This is an important parameter (expressed in cm), commonly adopted to evaluate the seismic input energy and buildings damage capacity (Housner [1952]). STRATA software generates different outputs such as the acceleration time histories and the response spectra. The PGA and Housner Intensity are calculated a posteriori. The resulting spectral acceleration curves for ZONE 1 and ZONE 2 are shown in Figure 3.8a and 3.8b, respectively.

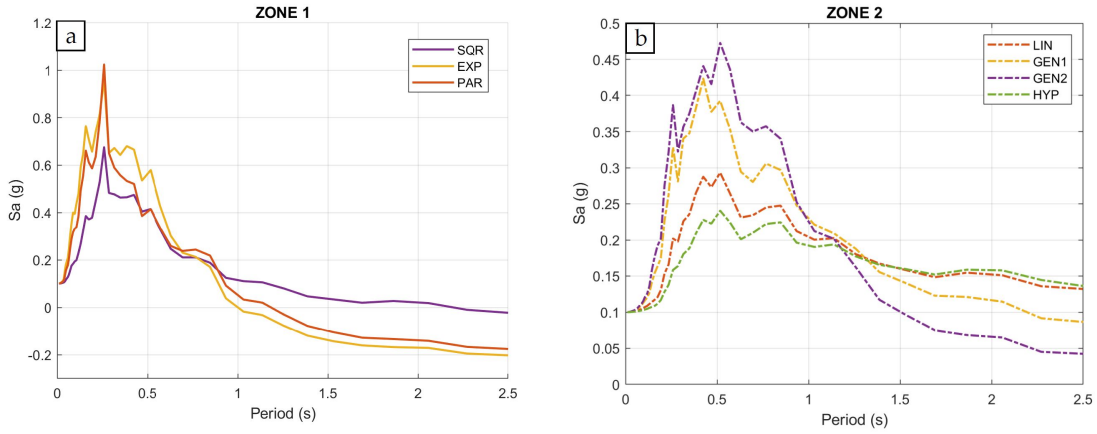

Figure 3.8: Mean response spectra at the ground surface for the different velocity gradients used to define the v_s profiles in (a) ZONE 1 and (b) ZONE 2.

They are computed as the mean of all Monte Carlo simulations. Each curve is normalized to the common initial value of spectral acceleration, which is equal to 0.1 g. The response spectra obtained from the simulation of the velocity gradients of ZONE 1 and ZONE 2 show significant amplifications in the period range of engineering interest, with high amplifications at low periods. The peak value of spectral acceleration increases gradually from 0.64 g to 1.3 g for ZONE 1 and from 0.25 g to 0.48 g for ZONE 2. It is possible to observe the same relative differences in PGA values (Figure 3.9). In particular, the values of PGA span from 0.51 g to 0.68 g for ZONE 1 (Figure 3.9a), and

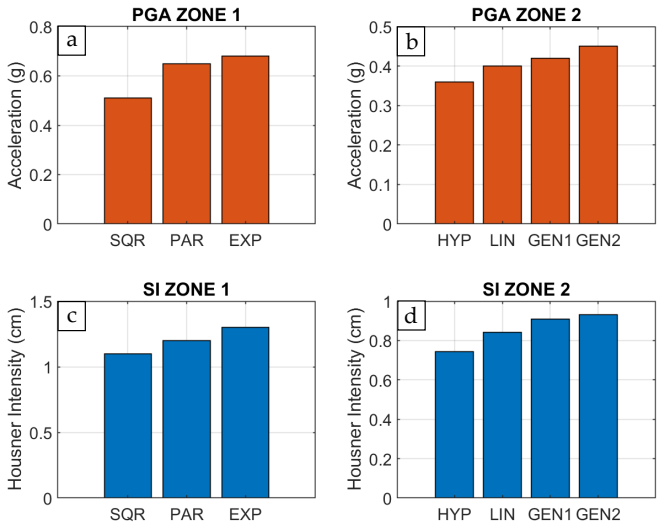

Figure 3.9: PGA (a-b) and Housner Spectrum Intensity SI (c-d) values, inferred from the simulations.

between 0.36 g and 0.45 g for ZONE 2 (Figure 3.9b). Figure 3.9 shows the Housner Spectrum Intensity values inferred from the spectra for each velocity gradient adopted in this study. The Housner Spectrum Intensities range between 1.1 cm and 1.3 cm for ZONE 1 (Figure 3.9c), and between 0.74 cm and 0.93 cm for ZONE 2 (Figure 3.9d).

3.4.1 Comparison with real accelerogram

In this paragraph we compare the results of 1D seismic site response and real data collected in Casaglia site where a borehole was available (see location in Figure 3.1).

In this site the borehole is located in Po alluvial plain (the geological context called "ZONE 2" in this study). The borehole reaches the quaternary basement at 132 m depth. The sedimentary coverage is represented by holocenic alluvial deposits, varying from clay to coarse loose sand poorly compacted. The site can be classified as soft-soil, according to cross-hole and down-hole measurements of Pesaresi et al. [2014]. On the basis of this specific stratigraphic information until 132 m depth, we model the 1D shear-wave velocity structure. The first 30 m are modelled with the mean v_s profile which characterise the ZONE 2 (Figure 3.4). The engineering bedrock depth is assumed to be at 132 m, as suggested by the stratigraphic log, so the deeper velocity structures are extrapolated with LIN and GEN2 gradients (Equation 3.4 and 3.6). The v_s profiles adopted for seismic site response are shown in Figure 3.10a. The borehole was equipped with two broad-band seismometers, one at the surface (OG010, a Lennartz velocimeter) and other at a depth of 135 m, within the quaternary basement (FERB, a Guralp CMG-3TB seismometer). The available recorded waveforms refer to a seismic event occurred on 12 February 2013, with $M_L = 3.8$ and an epicentral distance of 170 km (Pesaresi et al. [2014]). The East-component waveforms (expressed in m/s) are converted in

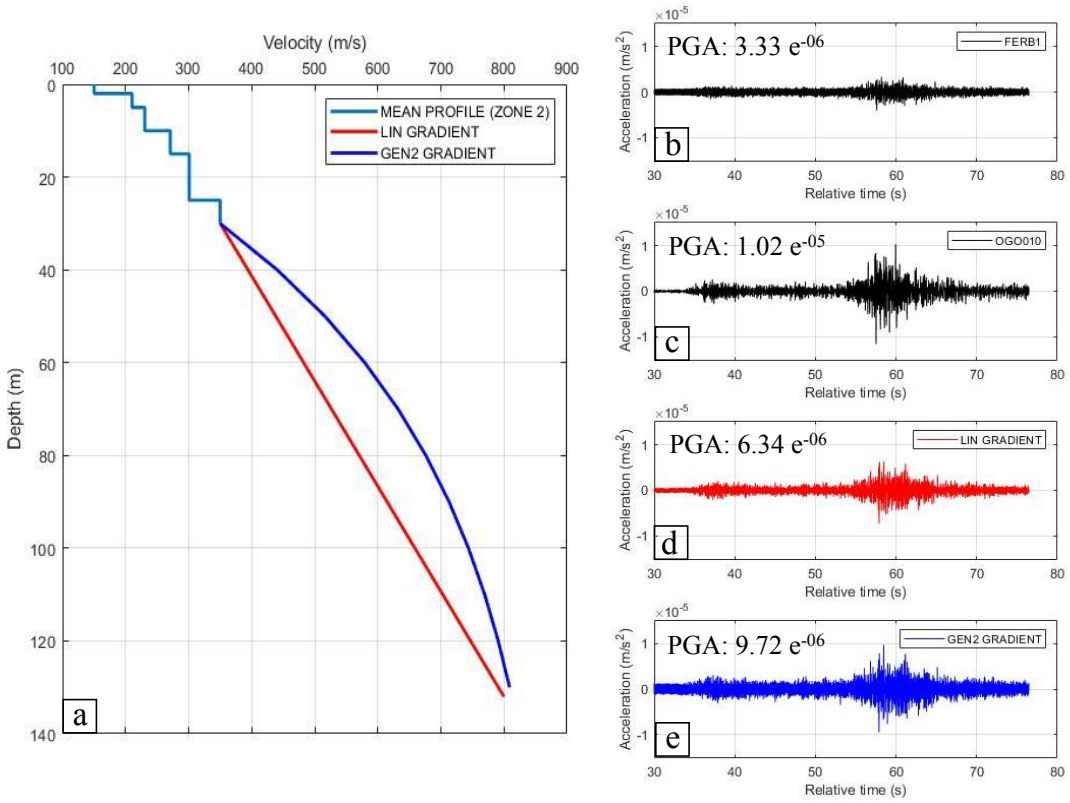

Figure 3.10: (a) Shear-wave velocity structures used as model for the alluvial sedimentary cover in Casaglia site (see Figure 3.1); b) Accelerogram of the seismic event occurred on 12 February 2013 recorded by the borehole seismic stations (FERB); c) the same seismic event recorded by the surface station located at the top of the borehole (OG010); d) simulated accelerogram inferred from a linear gradient LIN; e) simulated accelerogram inferred from an exponential gradient GEN2.

accelerograms and are shown in Figure 3.10b and 3.1c for the borehole sensor and surface sensor respectively, with their corresponding PGAs. It is worth noticing that the PGA recorded by the borehole station is smaller than the one recorded by the surface station, due to the soft layer amplification of motion. In order to compare the gradient method, the waveform recorded by the borehole station was used as input motion for the 1D seismic site response computed with STRATA Software. Figure 3.10c and 10d show the simulated accelerograms for the LIN and GEN2 gradients. The computed PGA are also displayed. As expected, the linear gradient LIN (as suggested by the norms) underestimates the amplification effects, with a variation of the amplification effects of 43%. On the contrary, the synthetic accelerogram computed with the non-linear gradient GEN2 is characterized by a PGA value similar to the real ones recorded at the surface.

3.4.2 Discussions and Conclusions

We compute the 1D seismic site response of two sectors of the Venetian Plain (ZONE 1 and ZONE 2), where deep v_s profiles are unknown, adopting several shear-wave velocity gradients found in literature. In ZONE 1, where the bedrock depth is unknown, the choice of the velocity gradient determines the engineering bedrock depth, ranging between 60 and 180 m (Figure 3.5a). In this case, the different results depend mainly on the variable thickness of the soft sedimentary layer, which is excited by the seismic input during the simulation. In ZONE 2, where the bedrock depth is known, the soft soil column has a constant thickness of 400 m, but the shape of the velocity profiles between the 30 m and the engineering bedrock is significantly different (Figure 3.5b). The stochastic simulation performed in STRATA and based on the use of different

literature velocity gradients shows differences up to 20%. The smaller site response is associated to the LIN (Linear) and HYP (Hyperbolic) gradients, characterized by lower values of v_s, e.g., softer soils. The softer sites are able to accumulate larger strains and experience more damping. In particular, considering the case of a thick soil column, the damping is much more pronounced; thus, in this condition, the attenuation phenomena become dominant. Keeping a conservative approach for seismic design, it appears more appropriate to model the soil column with generic gradients, which allow to obtain the highest values of PGA, Spectral Acceleration and Housner Spectrum Intensity. We evaluate the effect of the v_s gradient choice also considering real seismic data recorded at 135 m depth and at the surface in a borehole located in the Po Plain. In this way we investigate the site amplification of the sedimentary columns between the downhole and surface station, modelled with different types of gradients. The linear gradient method (as suggested by several seismic design norms) here again underestimates the seismic site amplification, while the non-linear gradient (GEN2) reliably estimates the site amplification effect.

Chapter 4

Ambient Noise Analysis

4.1 Introduction

In this chapter we explore the third aim of this Thesis, related to the ambient seismic noise analysis and noise interferometry. This application relies on the basic property of the surface waves, i.e., the frequency dependent phase and group velocities in heterogeneous media. The analysis of noise cross correlations across multiple frequency bands can in fact provides constraint on vertical velocity structure. Measuring dispersion curves (the frequency dependence of the velocity) is the key issue in modeling or imaging a medium using surface waves. (e.g. Scherbaum et al. [2003], Rozenberg and Ritter [2005], Boaga et al. [2007]). [1]

Therefore, we can apply the noise interferometric technique to infer shear-wave velocity models in the Venetian Plain. It has been demonstrated in the previous chapters

[1]DECLARATION: The part of this chapter related to anthropic noise has been published as "The 2020 Coronavirus lockdown and seismic monitoring of anthropic activity in Northern Italy" in *Scientific Report, vol. 10, pp. 1-8, 2020*
CONTRIBUTION: Maps realization, Data Interpretation

the importance of reliable information about the subsoil for site effects analysis, wave propagation scenarios and, in general, seismic hazard assessment. Nowadays, ambient noise studies are one of the fastest growing fields in the Earth sciences, bearing low costs and having relatively low environmental impacts. Passive methods are based on seismic noise and are independent from earthquake activity or active seismic sources. This is a significant advantage in areas where the natural seismicity is low and/or where active seismic sources (explosions, large vibrators) can't be used (Boaga et al. [2007]). Theoretical and experimental studies have shown that the cross correlation of the diffuse ambient noise wavefield provides an estimate of the impulse response, or empirical Green's Function, of the subsurface between the two stations being correlated (e.g. Boschi and K. [2015]; Campillo and Paul [2003]; Roux et al. [2005]; Shapiro and Campillo [2004]; Weemstra et al. [2016]). In this cross-correlation technique, often referred to as seismic interferometry, the first station becomes a virtual source of the seismic wave recorded at the second (Shapiro et al. [2005]). Noise interferometry has been widely adopted for seismological and geophysical applications, but for the first time, we will try to perform this technique using the long continuous time series recorded by the ASX1000 MEMS sensors prototype, the new instrument proposed in this Thesis. In particular, we intend to apply this technique using the four MEMS sensors located in northern Italy, in Veneto Region in order to characterize the Venetian Plain in terms of shear-wave velocity profiles. Firstly, we discuss the concept of seismic noise in seismology, focusing on the typical noise sources. In this context, the unexpected situation of Coronavirus lockdown during 2020 gave us the unique opportunity to discriminate ambient noise of natural origin from man-made noise in North Italy (see the paper "The 2020 Coronavirus lockdown and seismic monitoring of anthropic

activity in Northern Italy", APPENDIX A). Then we describe the noise interferometric technique performed with ASX1000 MEMS sensors prototype. Finally, we perform ambient noise analysis using the long continuous seismic data recorded by broad-band, high-quality seismic stations belonging to the INGV (Istituto Nazionale di Geofisica e Vulcanologia) seismic network. This last part of the work was carried out abroad, at the TU Delft University (Delft University of Technology, Netherlands) during the ending phase of the PhD period, thus only our preliminary results are shown.

4.2 Method

4.2.1 Seismic Ambient Noise

Recorded seismic signals always contains noise which can have two origins: (1) the noise generated in the instrumentation. All electronic components as well as the sensors itself generate noise. (2) the seismic-ambient noise from Earth vibrations: a superposition of seismic signals excited by numerous natural and man-made physical processes. In this chapter we will focus on this second category of noise.

The natural noise represents the vibrations of the ground caused by tides, water-waves striking the coast, standing water waves in the open seas due to storm systems, air pressure changes, turbulent wind or wind-induced vibrations of trees or tall buildings. The natural noise can have characteristic frequencies depending on the source of disturbance. Most studies have focused on surface waves within the microseismic frequency band (0.05 - 0.2 Hz) which contain strong signals produced by ocean waves (Longuet-Higgins [1950]). Man-made noise (often referred to as "cultural" noise) is generated by human activities (trains, traffic machinery, industrial activities etc.). This

type of noise is characterized by a large difference between days, night or holidays time (Halliday et al. [2017]; Zhang et al. [2009]). Anthropic noise is thought to include frequencies from 1 to 10 Hz approximately, attenuating quickly with distance (a few km) and disappearing quickly with increasing depth. The natural, low-frequency noise, that provides unique observations of surface-wave propagation allowing to map the structure of the Earth's lithosphere (Shapiro and Campillo [2004]). Cultural noise, instead, is of interest to geoscientists and engineers, as it can be used at relatively small scales, for instance in characterizing shallow subsoils (Louie [2001],Boaga et al. [2007]).

4.2.2 Noise Interferometric Technique

"The term interferometry generally refers to the study of interference phenomena between pairs of signals in order to obtain information from the differences between them." Curtis et al., 2006

Basic Theory

The term "seismic interferometry" refers to the principle of generating new seismic responses by cross-correlating seismic observations at different receiver locations (Wapenaar and Fokkema [2006], Boschi and Weemstra [2015]). The cross-correlation C_xy(t, ω), function of time t and frequency ω, of ambient surface wave signal u recorded at two seismic instruments, located at positions x and y, is defined as:

$$C_xy(t,\omega) = \frac{1}{2\pi}\int_{-T}^{T} u(x,\tau,\omega)u(y,t+\tau,\omega)d\tau \tag{4.1}$$

with the parameter T defining the size of the window over which the cross-correlation is computed. In particular, many authors showed theoretically (e.g. Boschi and Weem-

stra [2015], Campillo and Paul [2003]; Wapenaar and Fokkema [2006]) and experimentally (e.g. Weaver and Lobkis [2001]) that the Green's function of a medium between two stations can be derived by the cross-correlation of recordings of a coherent random wave field at those points (Figure 4.1).

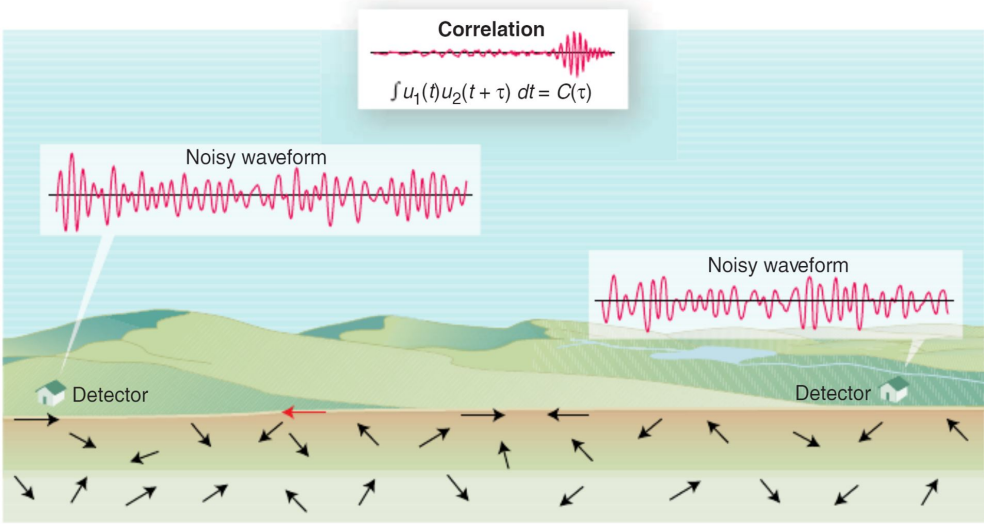

Figure 4.1: When a diffuse wave field is generated by distant sources and/or by multiple scattering, detectors report random signals. Occasionally a ray (for example, the one shown in red) passes through both detectors. As a result, the signals are correlated.

The elastodynamic Green's function (e.g., Aki and Richards [2002]) is essentially the impulse response of a medium. The Green's functions between pairs of seismographs can be estimated from the time-derivative of the long-time cross-correlation of ambient seismic noise and are related to velocity dispersion. In particular, the most energetic part of the estimated Green's functions is associated with surface wave propagation. From the vertical component ambient noise cross-correlation it is possible to extract the vertical component of the Rayleigh-wave Green's function (e.g., Boschi et al. [2019]). Theoretically, the resulting cross-correlations should show the same ve-

locity and dispersion features on both positive and negative lags, since waves travelling in opposite directions between station-pairs sample the same structures. Noise interferometry evolved quickly to become an important and widely used tool in seismology. For example, this method provides high-resolution tomography studies from the local (e.g. Bussat and Kugler [2009]; Boaga et al. [2007]) to the continental (e.g. Shapiro et al. [2005]) scale. This application of seismic interferometry is commonly called ambient noise tomography.

Ambient Noise Interferometry

A Python-based script was developed in order to perform the ambient noise processing in this work. The applied processing routine is basically the same as the one described by Bensen et al. [2007]. The first phase of data processing consists of preparing waveform data from each single station. A long (e.g. one day) continuous noise signal is subdivided into shorter time windows (e.g. one hour). Each time window is demeaned, detrended and band-pass filtered. An example of this step is shown in Figure 4.2, where we compare raw seismic data with the processed ones.

For this example, we take in account seismic data recorded by two stations in Northern Italy (CTI, Trentino A.A. Region and CAVE, Emilia Romagna Region), belonging to the INGV network. The seismic data are filtered in the frequency band 0.05- 0.2 Hz. After this first step the time windows are normalized in the time-domain so that the effects of possible ballistic signal (i.e. large earthquakes, passing vehicles etc.) or instrumental irregularities present in the data are minimized. In this study the temporal normalization is done by converting each record into one-bit signals. This method, called "one-bit" normalization retains only the sign of the raw signals,

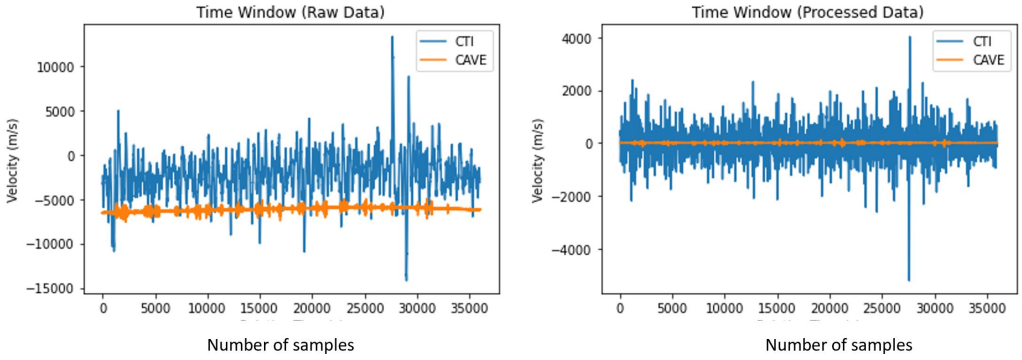

Figure 4.2: Example of a 1-hour long time window (expressed with number of samples) inferred from long continuous sequences of seismic noise recorded by CTI and CAVE stations. In the left panel we show the raw data; in the right panel we show the demeaned and filtered data.

replacing all positive amplitudes with a "1" and all negative amplitudes with a "-1". It has been demonstrated that this approach increases the signal-to-noise ratio (SNR) when employed in acoustic experiment in the laboratory and in seismological application (Campillo and Paul [2003]). An example of one-bit application is shown in Figure 4.3.

4.4c). Spectral whitening is then applied to each time window. The whitening broadens the band of the ambient noise recording and also remove the effects caused by persistent monochromatic source. The purpose of this phase is to accentuate broad-band ambient noise by attempting to remove earthquake signals and other irregularities that tend to obscure ambient noise. In this Thesis, the spectral whitening is applied considering the ratio between the spectrum obtained through Fast Fourier Transform (FFT) and the smoother spectrum (inferred from a convolution function). In Figure 4.4a we show an example of spectrum (black curve) and the smoothed spectrum (red curve). The resulting ratio (Spectrum/Smoothed Spectrum) is shown in Figure 4.4b. In this way, the frequency spectrum is flattened through spectral whitening. In order

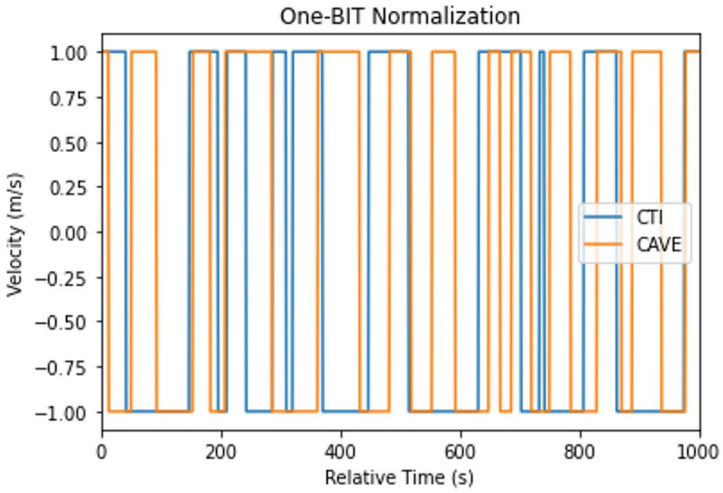

Figure 4.3: One-bit normalization applied to the time series shown in 4.2

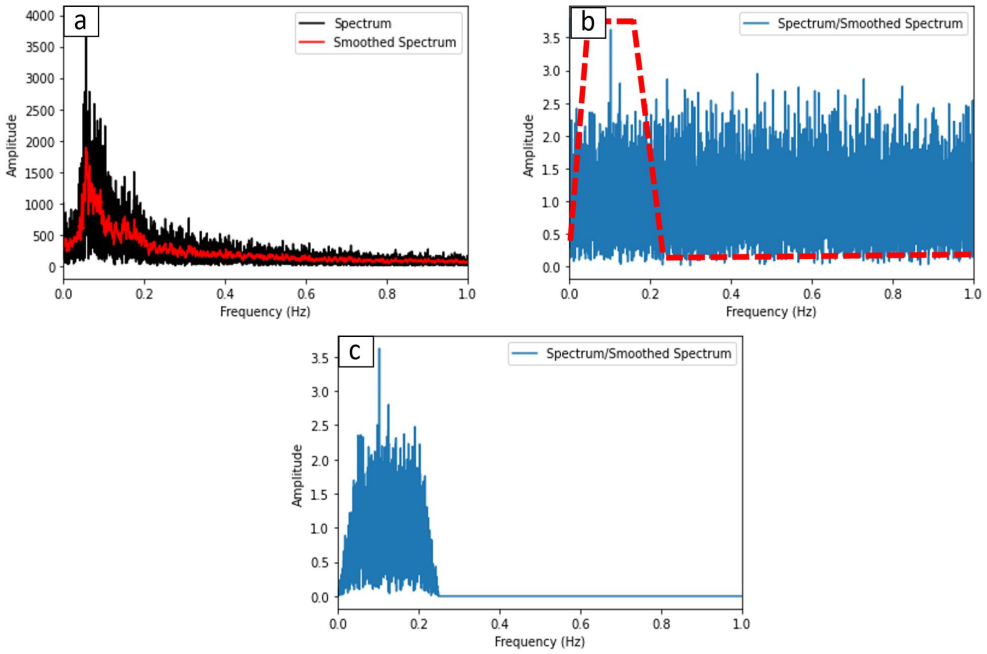

Figure 4.4: (a) Amplitude spectrum inferred from the signal recorded by CTI station, shown in 4.3 (black curve) and the smoothed amplitude spectrum (red curve). (b) The Ratio between the spectrum and the smoothed one. (c) Spectrum filtered in the frequency range 0.05- 0.2 Hz.

to retrieve the frequency range of interest, a trapezoidal function, built around the initial frequency band filter (0.005 -0.2 Hz) is applied (Figure 4.4c). The final step of the data processing scheme, as proposed by Bensen et al. [2007], is represented by the cross-correlation (in frequency domain, which is computationally faster with respect to cross-correlation in time domain) of each time window and the final stacking. In the stacked phase, the cross-correlations resulted for each time window are added to one another. The use of long time-series optimizes the signal-to-noise ratio of the final cross-correlation function and allows to observe the coherent surface waves signal.

4.3 Results

4.3.1 Cultural noise during the 2020 Coronavirus lockdown

In 2020, Italy thus became the first country in the world, with the exception of The Hubei Region (China), to enact lockdown measures as a consequence of the COVID-19 outbreak and the need to contain it. In March 2020 the Italian government drastically reduced vehicle traffic and interrupted all nonessential industrial activities over the entire national territory. We analysed continuous data from an array of different seismic stations belonging to INGV network, located in the vicinity of known industrial districts in northern Italy in Lombardy, Emilia-Romagna, and Tuscany (Figure 4.5a). In particular, we quantified the effects of the March/Avril 2020 Coronavirus lockdown on the seismic ambient noise field. We found that, confirming earlier estimates, anthropic noise becomes dominant at frequencies above ˜2 Hz, where most stations show a ˜50% reduction in the energy associated with ambient signal. It then grows with increasing frequency, up to about 20 Hz for most stations (Figure 4.5b). For detailed results,

see the paper "The 2020 Coronavirus lockdown and seismic monitoring of anthropic activities in Northern Italy" in the APPENIDX A of this Thesis.

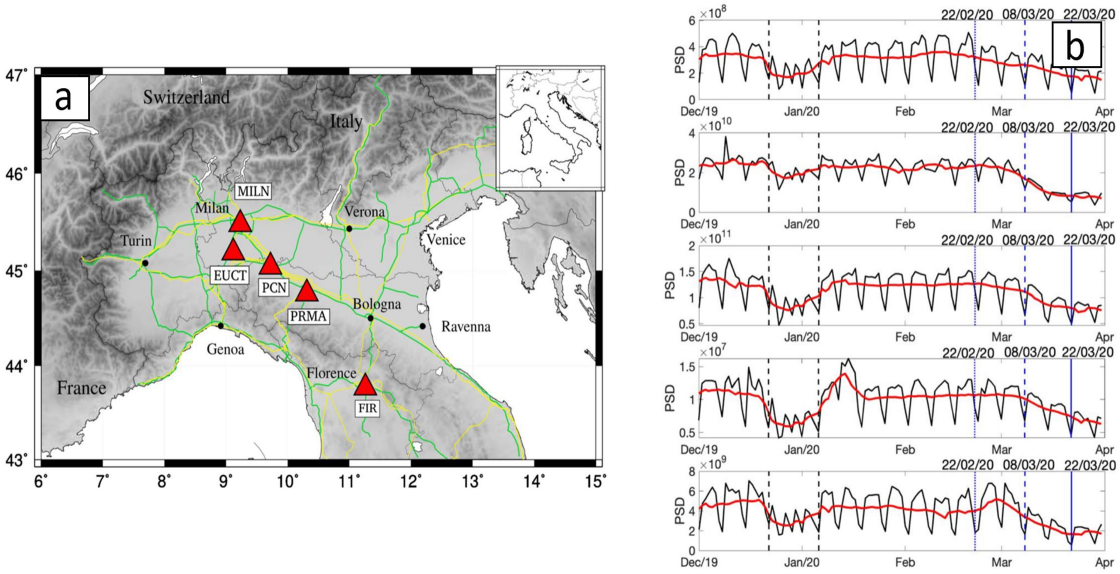

Figure 4.5: (a): Map of the seismic stations marked here by red triangles and acronyms. Green and yellow lines denote major highways and railways, respectively. (b) PSD curves of the analysed seismic ambient noise, obtained by averaging over the entire frequency range of interest (1 to 40 Hz), without (black line) and with (red) smoothing. The dates of mentioned governmental decrees are highlighted in blue with continuous and dash-dotted lines.

4.3.2 Noise Cross-Correlation with ASX1000 prothotype

In this paragraph we present the results related to the cross-correlation of the signal recorded by the ASX1000 MEMS sensors prototype. In fact, the installed MEMS sensors, which is the experimental network proposed in this Thesis, are characterized by a continuous recording. Long continuous datasets of seismic ambient noise are stored and can be downloaded from the ADEL website platform, (See Chapter 2, Paragraph 2.2.1). For the ambient noise analysis, we take in account the MEMS sensors

installed in the Veneto Region (CASTELFRANCO, BASSANO D.G., ISTRANA and MONTEBELLUNA) (Figure4.6), in order to infer shear waves velocity models of a sector of the Venetian Plain.

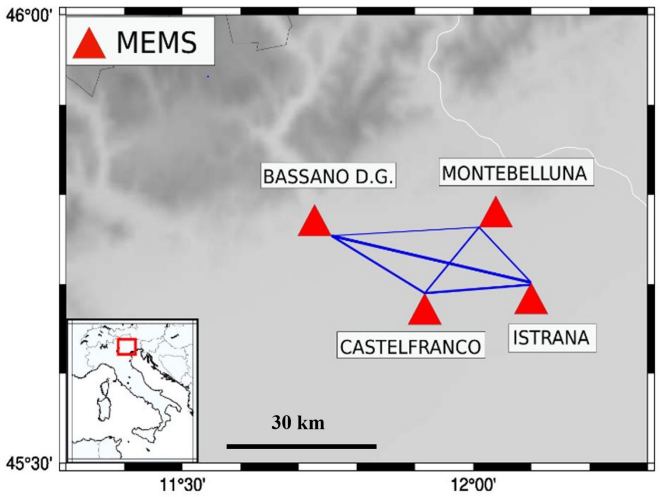

Figure 4.6: Map of the MEMS sensors installed in Veneto Region, selected for the ambient-noise cross-correlation analysis. We perform the cross-correlation of ambient noise recorded by our MEMS sensors prototype, considering all the possible permutations (blue lines).

We download 1 week-long continuous signal for each seismic sensor. The longer time window which can be downloaded from the platform is 1-hour long. Thus, the daily signals are built concatenating the sorted downloaded files. The vertical-Z component noise records are processed using the method proposed by Bensen et al. [2007] and explained in paragraph 4.2.2.2. In this study, daily waveforms at each station are filtered in two different frequency range (0.1 - 0.5 Hz and 0.1 -1 Hz) Cross-correlation is performed daily in the frequency domain. After being transformed back to the time domain (with an Inverse Fast Fourier Transform, IFFT), daily cross-correlations are stacked and plotted as a function of the Lag Time (expressed in seconds 's'). The

results are shown in Figure 4.7a and 4.7b.

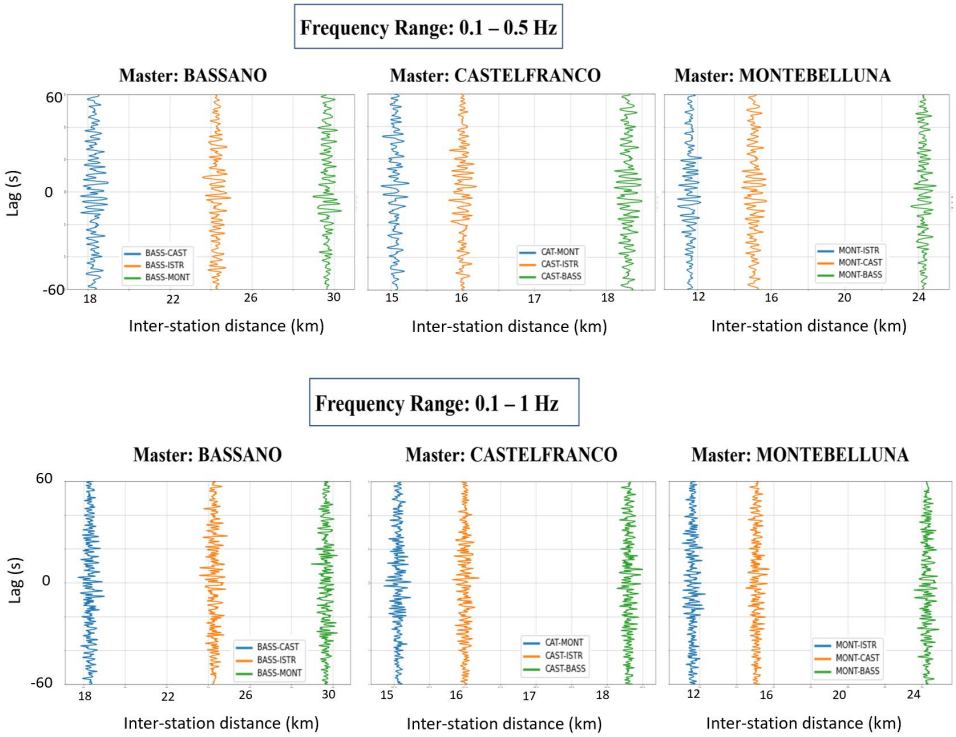

Figure 4.7: Cross-correlation inferred from different master signals, plotted as function of the interstation distances. The ambient noise data are filtered in the frequency bands 0.1-0.5 Hz and 0.1-1 Hz.

4.3.3 Noise Cross-Correlation with high-quality and broad-band seismic stations (Preliminary Results)

In this paragraph we present the preliminary results related to the cross-correlation of seismic stations belonging to the IV network operated by INGV. This part of the Thesis was developed with the collaboration of the Delft University of Technology (TU Delft, Netherlands). The high-quality and broad-band recordings from the IV network are available. In fact, data are distributed through the Orfeus European Integrated

Data Archive (EIDA) federation and International Federation of Digital Seismograph Networks (FDSN) under an open license. The Venetian Plain presents a good coverage of these seismic stations and could allow to perform ambient seismic noise technique to obtain high-resolution Rayleigh waves dispersion curves. The map of the selected seismic stations for ambient noise analysis is shown in Figure 4.8.

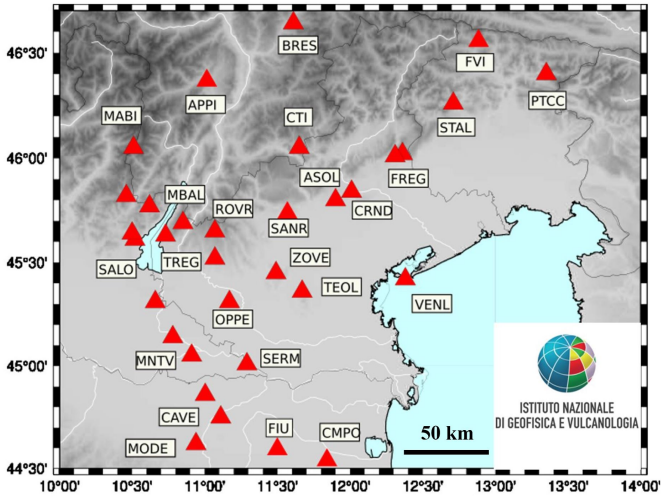

Figure 4.8: Map of the selected high-quality, broad-band seismic stations belonging to the IV network, managed by the INGV.

We collect the continuous broad-band vertical component seismic data recorded by 33 stations from the IV network from December 2019 to January 2021. The selected stations consist of about 25 high broad-band and high-gain seismometers and 8 short-period seismometers. The stations have a sampling rate of 100 Hz, with the exception of seismic stations MBAL which has a sampling rate of 200 Hz. The long continuous data are downloaded through obspyDMT, an open-source software toolbox for the query, retrieval, processing and management of seismological data, including long continuous dataset. The Data recorded by the 33 selected seismic stations are stored in a 2 TB

Hard-Disk. For this analysis, we consider the vertical-Z component. The collected seismic data are down-sampled for an ease storage and handling, in our case to 10 Hz from originally 100 Hz. The data are subdivided in 1-hour length time windows; they are processed through trend and mean removal; are band-pass filtered between 0.05 and 0.2 Hz, normalized in time domain and whitened. The 1-hour segment are finally cross-correlated between all station-pairs and then stacked into a single-time series. In Figure 4.9 we show an example of the cross-correlations with the fixed master which is the CTI seismic stations. In order to obtain a clearer figure, we plot only 17 cross-correlation functions representative of different azimuthal coverage.

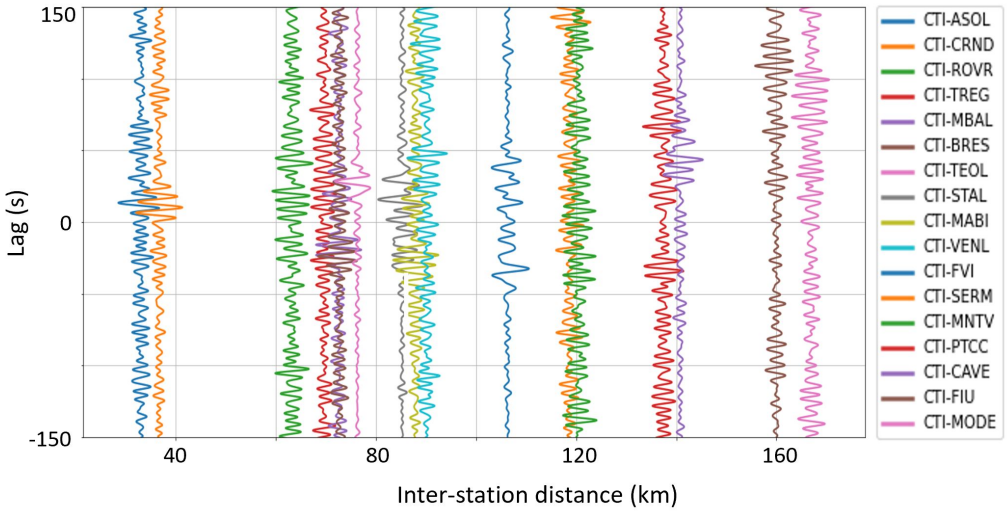

Figure 4.9: Cross-correlation functions with the common master (CTI seismic station).

4.3.4 Discussions and Conclusions

This Chapter explores the ambient noise analysis.

First, we perform a detailed analysis of the cultural noise. The unexpected situation of the Coronavirus outbreak gave us the unique occasion to discriminate cultural noise

from the ambient noise of natural origins. This result could be useful in the future for local subsoil mapping and monitoring studies (see APPENDIX A, section A.2).
We evaluate also the possibility to perform noise interferometric technique with the ASX1000 MEMS sensor prototypes installed in Northern Italy, in order to infer shear-wave velocity model of this sector. As expected, it is not possible to observe coherent signal in the obtained time-domain cross-correlation functions (Figure 4.7a and 4.7b). The instrumental noise level which characterizes the ASX1000 MEMS sensor prototype is significantly high. We are just measuring the recording system noise and not the seismic ambient noise. Moreover, nowadays the cross-correlation analysis with the ASX1000 prototypes involve time series with a duration of only one week, while noise analysis generally requires 1-year or more long time series. Currently, the ADEL platform allows to download recorded time windows with a maximum length of 60 minutes, one station at time. So, the availability of time series longer that one week are logistically complicated. Finally, we perform ambient noise analysis using the long continuous seismic data recorded by broad-band, high-quality seismic stations belonging to the INGV seismic network, installed in Veneto Region. In several cases it is possible to observe clear signals, presumably related to the Rayleigh wave propagation (CTI-ASOL, CTI-CRND, CTI-TEOL, CTI-CAVE) (Figure 4.9). Due to not perfectly isotropic noise field distribution, asymmetric cross-correlation are often observed. In particular, the station-pair CTI-TEOL exhibits coherent signals in both positive and negative lags, suggesting a more diffuse source noise. The remaining station pairs seem to provide incoherent results. We expect to improve these results by selecting the night-time hours, or day-time hours of the recorded ambient noise.

Chapter 5

Conclusion

This chapter summarizes the contribution of the thesis and discusses avenues for future research. We include the conclusion of each aim discussed in this work. We present a new MEMS sensor prototype named ASX1000 adopted to to build two experimental networks in Northern Italy and Central Italy, installing 16 of these new sensors. The accelerometers prototypes proposed in this study are smalls, inexpensive, low power demanding and allow for a rapid and fast installation with screw and plugs. Their dynamic range and frequency band make these sensors suitable to monitor not only large earthquakes, but even small, discrete and moderate seismic events. The performance of the ASX1000 prototypes is examined on the basis of the results of the laboratory experiments (shake table and noise-floor evaluation) and field recording (earthquake detection). To summarize, the ASX1000 prototype is capable of recording:

1. small seismic events ($1.5 < M_L < 2.5$) at short epicentral distances, with a maximum of 15 km (Cascone et al. [2021]).

2. discrete seismic event ($2.5 < M_L < 4$) at distances in the order of 80 km.

3. moderate seismic event (M_L >5) at distances in the order of more than 300 km.

A detailed discussion related to the micro-seismicity monitoring with the ASX1000 prototype is reported in APPENDIX A, section A.1. We remark that generally a seismic network is deployed considering an installation of the sensors, which is as insensitive to ambient noise sources (human and environmental) as possible, so that the sensitivity for earthquake generated signal is high. The ASX1000 prototypes are installed in urban contexts, within noisy telecommunication infrastructures and they are still able to record extremely low energetic events, with local magnitude lower than 2.0. Then, the comparison to the highest-quality accelerometers (such as those belonging to the RAN network) in terms of PGA and Sa confirms that the signals are in good agreement. All these considerations suggest that the ASX1000 prototype is a promising tool to integrate the existing seismic networks or seismic arrays (which are generally small seismic networks installed to have a detailed investigation of small-scale phenomena such as small earthquake swarms or induced seismicity). This thesis represents an experimental phase, where the sensitivity of the ASX1000 prototypes are tested and evaluated. However, at the moment, the earthquake's information can be retrieved only after few minutes from the origin time of seismic event. In order to have a quick parameterization of an earthquake through automatic production of shake maps, several seismological implementations (such as a ring-server, a central trigger and selected time-window) are necessary. In the future we expect to build multi-sensors accelerometers which allow to improve significantly the SNR of the acquired signals.

The second aim of this work is related to a detailed study of seismic site response in the Venetian Plain, one of the study areas (Cascone et al. [2022]). In particular, we compute the 1D seismic site response of two sectors of the Venetian Plain, where deep

v_s profiles are unknown, adopting several shear-wave velocity gradients found in literature. Our study demonstrates how the choice of the velocity gradient curves has a significant impact on the seismic site response in terms of PGAs, Spectral Accelerations and Housner Intensities. These three parameters are fundamental for strong ground motion prediction and they are the most adopted in engineering a-seismic design. The stochastic simulation based on the use of different literature velocity gradients shows differences up to 20%. Keeping a conservative approach for seismic design, it appears more appropriate to model the soil column with generic gradients, which allow to obtain the highest values of ground motion parameters. We evaluate the effect of the gradient choice also considering real seismic data recorded at 135 m depth and at the surface in a borehole located in the Po Plain. In this way we investigate the site amplification of the sedimentary columns between the downhole and surface station, modelled with different types of gradients. The linear gradient method underestimates the seismic site amplification, while the non-linear gradient GEN2 reliably estimates the site amplification effect. This experimental study case confirms the importance of choosing an appropriate gradient in alluvial plains for an estimation of seismic effects. However, the only available accelerograms for the 1D seismic site response analysis of Casaglia site are characterized by small acceleration values, thus it could be difficult to establish the real implication on structural a-seismic design. In order to avoid estimation errors induced by an arbitrary choice of the velocity gradient, the regional deep basin structure should be determined through deep geophysical investigations (e.g. seismic reflection surveys, passive surface wave techniques, etc.). When these seismic surveys are not logistically possible, it seems more appropriate to model the soil column with the v_s gradient which allows obtaining the most conservative approach, i.e. the stronger

seismic ground motion.

The third aim of this thesis is related to the ambient noise analysis.The first important result related to this topic regards a detailed analysis of the cultural noise during the 2020 coronavirus lockdown. (APPENDIX A, section A.2). Our results suggest that the lockdown, imposed by the Italian Government, only reduces noise of anthropic origin. By comparing the Fourier Spectra of seismic ambient noise before and after the lockdown, one can attempt to characterize anthropic noise. The seismic data recorded during the lockdown will be useful to characterize specific source of anthropic noise, which in the future could become useful in local subsoil mapping and monitoring studies.

Finally, in this thesis we evaluate the possibility to perform noise interferometric technique with the ASX1000 MEMS sensor prototype. The current results suggest that these MEMS prototypes are not suitable for passive surveys. The high level of instrumental noise and their limited bandwidth obscure the ambient noise sources. As suggested in Chapter 2, in the next future we expect to develop new multi-sensor MEMS prototypes characterized by a significantly lower level of instrumental noise. Moreover, from the ADEL website will be updated for the download of longer recorded time windows. We strongly believe that the future technological improvements of the MEMS sensor field will enable the use of MEMS device also for passive prospective aims. This will open interesting perspective, since it is planned to install hundreds of MEMS in this territory in the next few years. This will allow theoretically a dense interferometric study, in order to retrieve detailed subsoil models at local scale.

In this thesis we present also the preliminary results of the noise interferometric technique applied to the seismic data recorded by the high-quality and broad-band seismic

stations. In this case, the instrument noise is well below the seismic noise. For this aim, we consider 33 seismic stations belonging to the INGV network, located in proximity of the Venetian Plain. Several station pairs give reasonable results in the frequency range 0.05 -0.2 Hz.

In the next future we expect to:

1. improve the cross-correlation results, performing the correlation of only night-time hours, or day-time hours. This approach could improve the cross-correlation functions.

2. consider higher frequency ranges in order to investigate the shallow subsoil.

3. extract the phase velocities and invert the obtained dispersion curves with the inversion algorithm developed by the TU Delft University. The extracted phase velocities between 0.05 Hz and 0.2 Hz (and presumably, higher frequencies) will be used in the tomographic inversion for imaging the velocity structures of the Venetian Plain.

4. test passive interferometry on new multi-MEMS sensor prototypes (under construction), which is able to reduce drastically the sensors noise.

Appendix A

APPENDIX A: Refereed Papers

A.1 Small local earthquake detection using low-cost MEMS accelerometers: Example in Northern and Central Italy

The Seismic Record
A journal of the Seismological Society of America

Small Local Earthquake Detection Using Low-Cost MEMS Accelerometers: Examples in Northern and Central Italy

Valeria Cascone*[1], Jacopo Boaga[1], and Giorgio Cassiani[1]

Abstract

This study evaluates the seismicity detection efficiency of a new low-cost triaxial accelerometer prototype based on microelectromechanical systems (MEMS) technology. Networks of MEMS sensors were installed in telecommunication infrastructures to build two small arrays in northern and central Italy. The sensor prototypes recorded major earthquakes as well as nine small seismic events with $2.0 < M_L < 3.0$. Where possible, MEMS were compared to the closest high-quality seismic stations belonging to the national accelerometric network. The comparison, in terms of peak ground accelerations and spectral responses, confirms that the signals are in good agreement. The tested inexpensive MEMS sensors were able to detect small local events with epicentral distances as large as 50 km and provided an efficient characterization of the main motion parameters. This confirms that the proposed accelerometer prototypes are promising tools to integrate into traditional networks for local seismicity monitoring.

Cite this article as Cascone, V., Boaga, J., and Cassiani, G. (2021). Small Local Earthquake Detection Using Low-Cost MEMS Accelerometers: Examples in Northern and Central Italy. *The Seismic Record*. **1**, 20–26, doi: 10.1785/0320210007.

Supplemental Material

Introduction

Microelectromechanical systems (MEMS) sensors are miniaturized integrated circuit batch processing devices, with size ranging from a few micrometers to millimetres (Homeijer *et al.*, 2011). They are widely adopted in many industrial applications such as telecommunication, automotive, game controllers, and so on (Shi *et al.*, 2009). As a consequence of such widespread use, MEMS sensors are the most economic motion detector (Fleming *et al.*, 2009; Cochran *et al.*, 2012; D'Alessandro and D'Anna, 2013; Evans *et al.*, 2014; Lawrence *et al.*, 2014; Nof *et al.*, 2019). Moreover, the performance of MEMS sensors is rapidly growing, being already comparable to high-quality accelerometers (Kong *et al.*, 2016). Recent advances in micromachined sensors provide adequate sensitivity for measurement in geophysical applications. For example, several MEMS devices are suitable for volcanic activity studies (Andò *et al*, 2011), gravimetric and geodetic observations (Cenni *et al.*, 2019; Mustafazade *et al.*, 2020), and seismological and earthquake engineering projects (Holland, 2003; Cochran *et al.*, 2012). These sensors can reach an efficient performance for moderate ($5.0 > M_w > 5.9$) to large ($M_w > 6.0$) earthquake detection at distances on the order of tens of kilometres (Boaga *et al.*, 2019; Liu *et al.*, 2011). Because of the low cost of the MEMS motion sensors (~ two orders of magnitude less than a classical high-quality seismological stations), they could be adopted for the installation of dense accelerometric networks. Ground-motion wavefield recording is limited to relatively coarse spatial sampling due to a limited number of installed sensors and large instrument spacing (on the order of tens of kilometres). This can lead to spatial aliasing of the wavefield and consequently an underestimation of the effective peak ground acceleration (PGA) as well as uncertainties in the estimation of local effects on the resulting shake maps (Wald *et al.*, 2008). These are the reasons why several

1. Department of Geosciences, University of Padova, Padova, Italy, https://orcid.org/0000-0001-7402-0985 (VC); https://orcid.org/0000-0001-8588-3962 (JB)

*Corresponding author: valeria.cascone@phd.unipd.it

dense low-cost MEMS networks have been recently tested for the monitoring of strong earthquakes ground shaking (Cochran *et al.*, 2009; Lawrence *et al.*, 2014). The question remains whether such technology is suitable for low-magnitude seismicity detecting. In particular, an interesting use of these sensors could be the monitoring of possible induced seismicity, an issue of growing public concern in face of some of the practices in the energy industry (oil and gas production, gas and CO_2 storage, geothermic operations, Valoroso *et al.*, 2009; Clarke *et al.*, 2014). Induced seismicity usually generates moderate seismic events of magnitude rarely larger than 3.0 (Ellsworth, 2013; Westaway and Younger, 2014; Walsh and Zoback, 2015; Weingarten *et al.*, 2015). For most of the national regulations, reaching magnitude values of the order of $M_w = 3.0$ puts operations at risk. Most of the induced earthquakes recorded in the world are of $M_w < 3$ and often much lower, but this may nevertheless trigger the public concern that larger events may follow (e.g., Majer *et al.*, 2007). As a consequence, subsoil activities must provide a suitable seismic monitoring plan that involves the installation of an expensive network of sensors. The use of advanced MEMS low-cost sensors could greatly improve these applications, freeing resources on one hand and providing better monitoring on the other.

In this study, we tested the performance of a MEMS sensor prototype designed by the Italian company ADEL srl to monitor small local events. A selection of these sensors that are digital, multirange, triaxial MEMS accelerometers (named ASX1000) were installed in seismic zones of northern and central Italy, to evaluate their performance in recording low-energy events.

We performed an analysis of the detected seismicity ($M_L < 3.0$), comparing the data as recorded by the MEMS sensors with the nearest available high-quality accelerometers managed by the Italian National Protection Service (Rete Accelerometrica Nazionale [RAN]). The results are promising and open new perspectives for the extensive use of such low-cost MEMS sensors for the monitoring of local seismicity.

Methodology

The MEMS sensor prototype adopted in this work (Adel ASX1000) is a triaxial MEMS accelerometer, with an internal circuit of transduction and digital output. The sensor has three sensing elements oriented along mutually orthogonal axes. It operates in high sensitivity mode for an acceleration range of $\pm 2g$ ($g = 9.80665$ m/s^2). The prototype frequency bandwidth is set to 0–62.5 Hz at 250 Hz sampling. ASX1000 has a micro-SD memory card that stores the recorded data and three

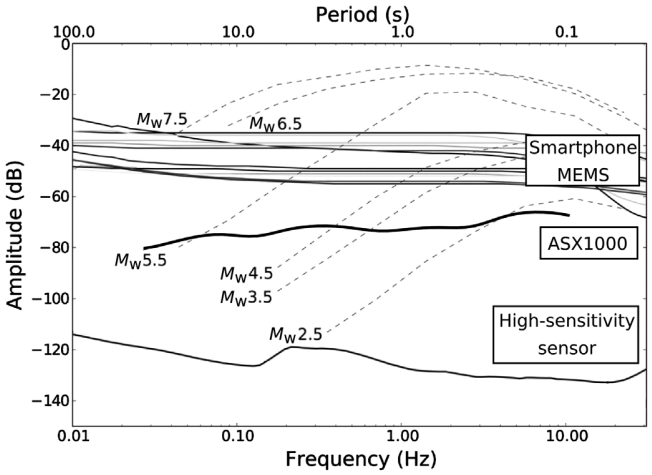

Figure 1. Noise floor of the ASX1000 microelectromechanical systems (MEMS) prototype compared to the most common smartphone MEMS sensors and high-quality force balance instruments. Dashed black lines are typical ground-motion amplitudes of earthquakes measured at 10 km from the epicenter for various magnitudes (from Kong *et al.*, 2016, modified).

communication channels for the remote control and data transmission (a serial channel RS-422 or RS485, a LAN Ethernet 10/100 Mbit/s, and an USB 2.0). The MEMS sensor prototype was calibrated in the laboratory on a shake table with a sweeping signal characterized by a frequency range between 0 and 100 Hz, a duration of 60 s, and a maximum amplitude of ± 0.2 m/s^2. The prototype proved to be in very good agreement with the laser motion reference for the frequency response up to 80 Hz. Noise analysis of the single components detects a power spectral density (PSD) with a general downward trend between −80 and −65 dB in the 0.2–10 Hz frequency range, interesting for earthquake engineering (Fig. 1). Figure 1 compares the detectable magnitude of seismic events measured at distances of 10 km, as in Kong *et al.* (2016), with the obtained PSD from the horizontal component of the ASX1000 MEMS prototype, common industrial phone MEMS sensors, and seismological high-quality stations. Lab tests suggested that ASX1000 has the potential sensitivity to record local events with magnitude $M_w > 2.5$ in the 2–10 Hz frequency range, which is the most critical frequency range of seismological interest.

To test the performance in detecting small seismic events, 15 ASX1000 prototypes were installed at two seismic active areas of Italy: the inner part of the Umbria Valley (central Italy, Chiaraluce *et al.*, 2017) and the southern-east Alpine Front (northern Italy, Galadini *et al.*, 2005). Figure 2 shows

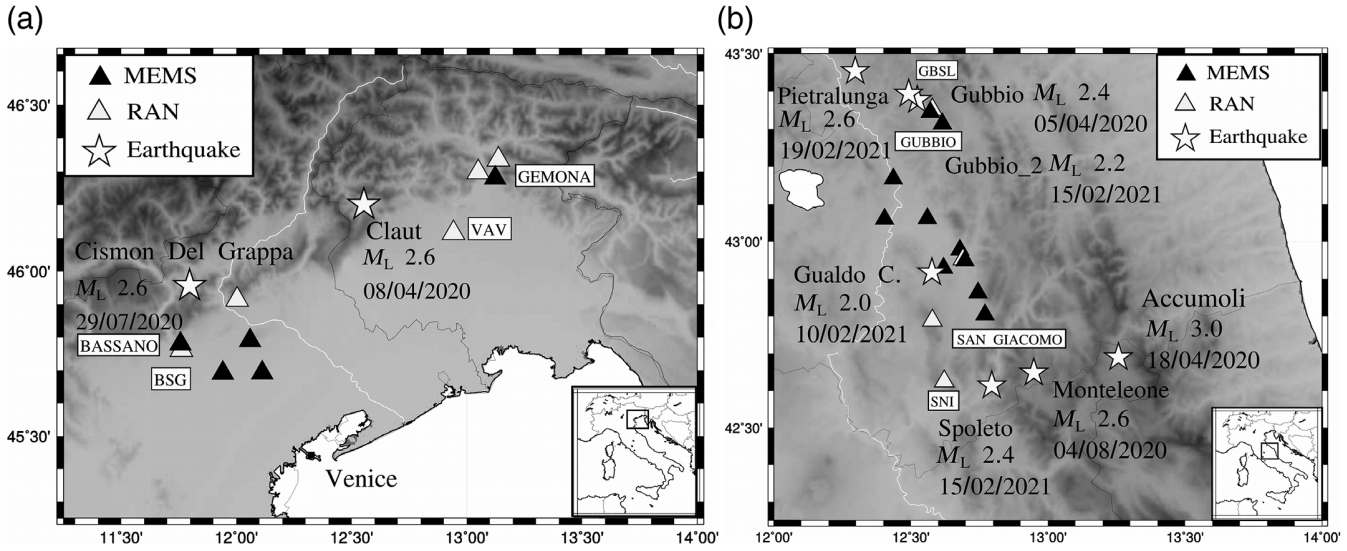

Figure 2. MEMS sensors arrays in (a) northern and (b) central Italy. Black triangles are the MEMS accelerometers, the white triangles are the high-quality available stations. The stars represent the epicenters with $M_L < 3$ discussed in this study. The insets display the Italian Peninsula with black squares, representing the selected study areas.

the locations of the MEMS arrays, the locations of the closest national strong-motion high-quality sensors (RAN that use Kinemetrics Episensor ES-T sensors), and the epicenters of the recorded seismic events analyzed in this study. The MEMS sensors were installed inside telecommunication infrastructures at the base of the local server room, and the sensors were firmly coupled with the ground with screws and plugs. Raw data were transmitted to a central service in real time through a LAN connection.

Results

The MEMS sensors were able to detect nine small local earthquakes with $2.0 < M_L < 3.0$ between April 2020 and February 2021. The corresponding epicenters are shown in Figure 2. The location and the local magnitude of the recorded events were retrieved from the National Seismic Institute earthquakes database (Istituto Nazionale di Geofisica e Vulcanologia [INGV]). Figure 3 shows the time series signal as recorded by the ASX1000 MEMS prototypes (horizontal-transverse component), the earthquake's ID name, and the distance between the sensors and the epicenters.

Even small events are clearly visible, especially for the nearest epicenters (e.g., Gubbio, Gualdo C., and Gubbio_2 earthquakes in Fig. 3a,f,h, respectively). From the recorded waveforms, we determined the PGA values and the acceleration response spectra (5% damped spectral acceleration [SA]), to be compared with the recordings of the high-quality stations belonging to the RAN. The RAN accelerograms can be downloaded from the Italian Civil Protection website (see Data Availability Statement). Figure 4 shows a comparison between the horizontal-transverse components recorded by our MEMS stations and by the high-quality accelerometers for the events having similar epicentral distances and soil conditions; this comparison avoids, as much as possible, unreliable comparison due especially to local effects (e.g., stations installed on hard rock vs. soft sediments). The considered events were named Gubbio, Cismon, Claut, and Pietralunga, as recorded respectively by the MEMS Gubbio, Bassano, Gemona, and the high-quality stations GBSL, BSG, and VAV (see Fig. 2).

As apparent from Figure 4, MEMS recordings are in very good agreement with the high-quality stations, both in terms of PGA and spectral response, especially for the closest events (consider the Gubbio–GBSL stations comparison in Fig. 4a).

In Table 1, we report the PGA values as recorded by the ASX1000 MEMS prototypes and by the closest high-quality RAN seismic stations for the earthquakes considered in Figure 4 along with the station–event distances, the MEMS–RAN distances (interstation distances), and the discrepancy of the PGAs ($\Delta PGAs = PGA_{MEMS} - PGA_{RAN}$).

The PGA values are very similar, especially for the horizontal components, presenting an average discrepancy between MEMS sensors and high-quality accelerometers of <15%.

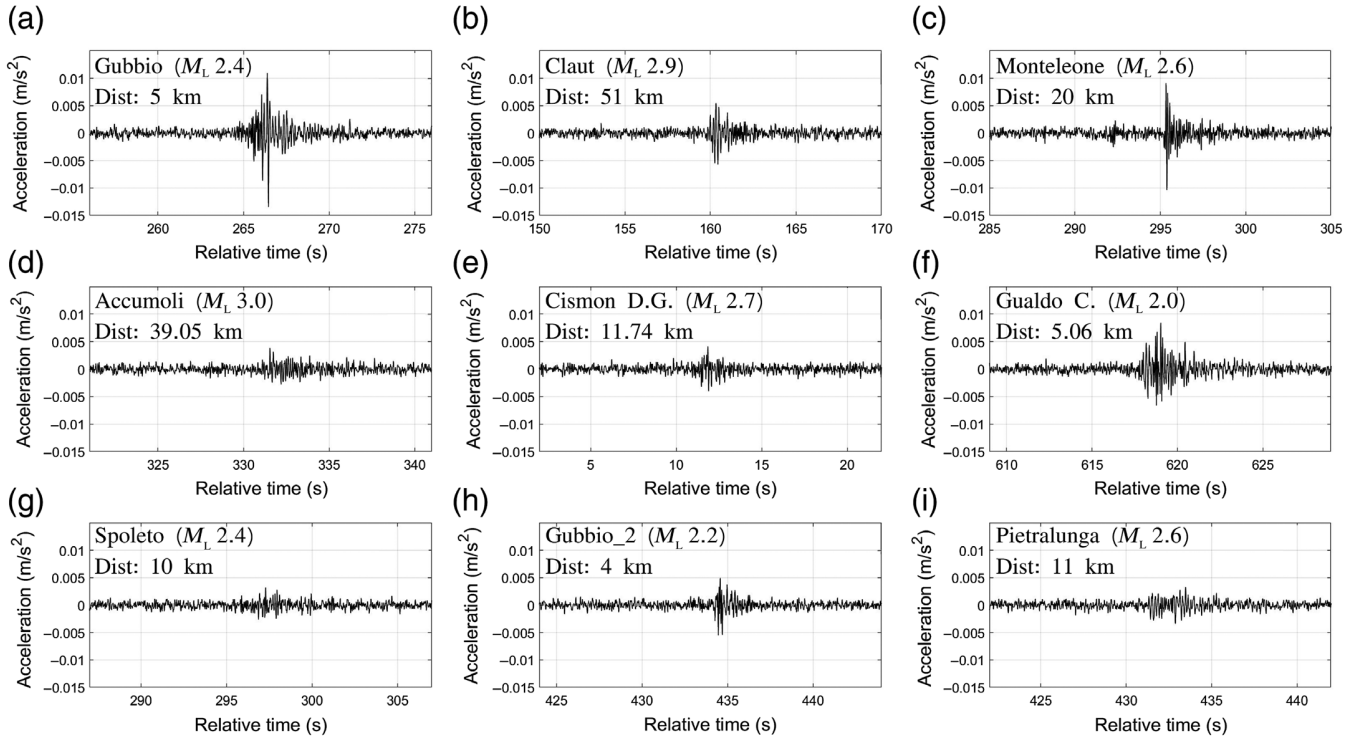

Figure 3. Time series of the seismic events as recorded by the horizontal component of the ASX1000 MEMS prototype. Each panel shows the event name, the estimated local magnitude M_L, and the sensor–event distance. (a) Gubbio earthquake; (b) Claut earthquake; (c) Monteleone earthquake; (d) Accumoli earthquake; (e) Cismon earthquake; (f) Gualdo C. earthquake; (g) Spoleto earthquake; (h) Gubbio_2 earthquake; and (i) Pietralunga earthquake (see Fig. 2 for locations; and for details, see Data Availability Statement).

The best match between the two sensors is given by the Gubbio earthquake recordings in which the high-quality station RAN and the MEMS sensor have nearly the same location. In this case discrepancy is ~6%. Higher discrepancy is observed for the vertical component (Z) of the Gubbio–GBSL stations, possibly related to installation issues. The ASX1000 MEMS responds in agreement with high-quality stations even for remote and small earthquakes, such as the case of the Claut event (with the epicenter 51 km away from the recording stations).

Discussion and Conclusions

MEMS sensors are often used to detect strong-motion events. Our tests show the reliability of MEMS also for low magnitude ($2.0 < M_L < 3.0$) seismicity monitoring. This study investigates the performance of the low-cost ASX1000 MEMS prototype accelerometer under small earthquake ($M_L < 3.0$) excitation. Sensors have been initially tested using a calibrated shake table. Under the controlled sweep excitation, the MEMS sensor shows a good performance in the frequencies up to 80 Hz, critical for the earthquake engineering aims, and the self-noise test shows that the PSD is around −80 dB in the 0.2–10 Hz range. Our field results show that the low-cost ASX1000 MEMS prototypes are suitable to record seismic events with a minimum local magnitude of $M_L = 2.0$ and epicentral distance <20 km or $M_L \sim 3$ at 50 km distance. The comparison of the PGA and spectral responses inferred from our MEMS sensors and the nearest high-quality accelerometers (belonging to the RAN) yields a good match, especially at smaller epicenter distances and when the interstation distances (MEMS–RAN) are lower than 2 km.

We note that these sensors are installed in urban telecommunication infrastructures. Although they are located in a noisy environment, not intended for seismic monitoring, they are still capable of recording small local earthquakes.

The use of low-cost sensors for small or local earthquakes monitoring will allow the development of dense accelerometric networks, thus mitigating the spatial sampling issues and providing highly detailed ground shaking maps, even for small

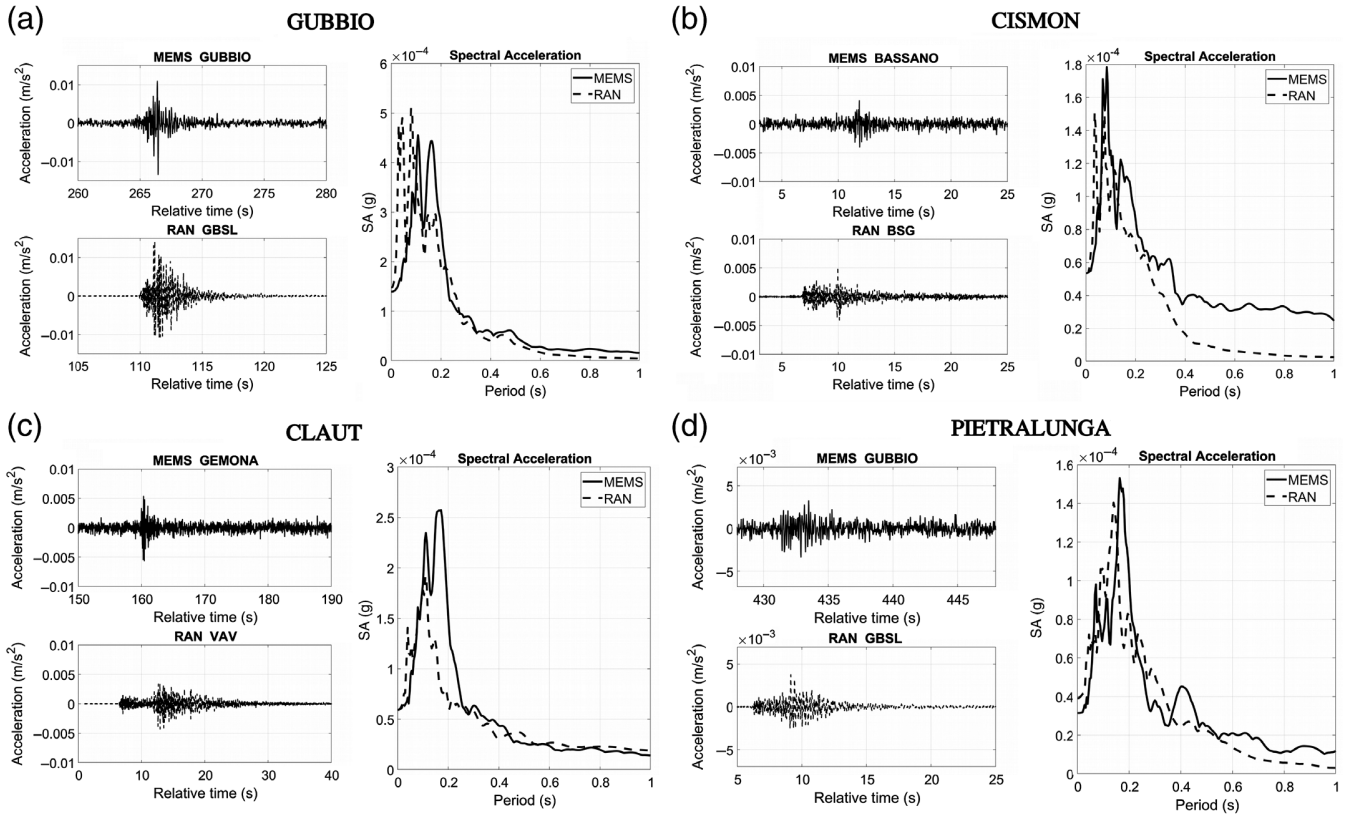

Figure 4. Acceleration time histories and corresponding normalized response spectra for both the MEMS stations and the RAN high-quality stations. For each event, the MEMS signal is shown above (solid line) and RAN signal below (dashed line). In the spectra plots, solid lines are the MEMS response and dashed lines are RAN response spectra. Events: (a) Gubbio, (b) Cismon, (c) Claut, and (d) Pietralunga.

events that are of course also very frequent. A well-defined shaking pattern inferred from small earthquakes can help identify local site effects that are often overlooked.

On the basis of these results, the ASX1000 MEMS prototype could be efficiently integrated into existing national seismic networks (as suggested by D'Alessandro *et al.*, 2019).

Moreover, the MEMS sensor prototype evaluated in this study could potentially be adopted for induced seismicity detection. A dense network with MEMS sensors distributed in the immediate proximity of industrial activity sites (such as oil and gas production, geothermic operation, etc.) could improve low-magnitude seismicity monitoring.

While a promising geophysical tool, the low-cost ASX1000 prototype still suffers from a high level of internal noise, which is usually considered to limit their use for several seismological purposes, such as accurate earthquake locations or origin time estimations. Nevertheless, the fast improvement of sensors quality combined with decreasing costs suggests that in the near future MEMS-based motion networks will play a relevant role in the monitoring of lower-level seismicity, which still conveys important seismologic information such as local seismic response to large, destructive events.

Data and Resources

Data availability statement: The public data used in this article are available at http://ran.protezionecivile.it and http://terremoti.ingv.it/. Other data are available upon request for scientific purposes.

The microelectromechanical systems (MEMS) data supporting the conclusions of this article, being property of a private company, is made available by the authors only upon request for scientific purposes. The Rete Accelerometrica Nazionale (RAN) accelerometric data are public and can be downloaded from the Italian Civil Protection website (http://ran.protezionecivile.it, available only for earthquakes with $M_L \geq 2.5$, and only upon request for smaller M_L). The event locations and timing are public data and can be downloaded from the National Institute of Geophysics and Volcanology

Table 1
Selected Earthquakes for the Comparison between the Microelectromechanical Systems (MEMS) Sensors and Rete Accelerometrica Nazionale (RAN) High-Quality Stations

Earthquakes ID, Date, Time (yyyy/mm/dd hh:mm:ss, UTC)	M_L	PGA MEMS (m/s^2)	PGA RAN (m/s^2)	Event–MEMS Distance (km)	Event–RAN Distance (km)	Interstation Distance (km)	ΔPGAs (m/s^2)
GUBBIO, 2020/04/05 14:33:48 (X comp)	2.4	0.0134	0.0143	5.5	5	0.5	−0.0009
GUBBIO, 2020/04/05 14:33:48 (Y comp)	2.4	0.0086	0.0119	5.5	5	0.5	−0.0033
GUBBIO, 2020/04/05 14:33:48 (Z comp)	2.4	0.0073	0.0110	5.5	5	0.5	−0.0037
CLAUT, 2020/04/08 15:10:46 (X comp)	2.9	0.0057	0.0042	51	38.1	34.9	0.0015
CLAUT, 2020/04/08 15:10:46 (Y comp)	2.9	0.0056	0.0047	51	38.1	34.9	0.0009
CLAUT, 2020/04/08 15:10:46 (Z comp)	2.9	–	–	51	38.1	34.9	–
CISMON, 2020/07/29 22:26:34 (X comp)	2.7	0.0041	0.0052	20	19.1	2	−0.0011
CISMON, 2020/07/29 22:26:34 (Y comp)	2.7	0.0032	0.0034	20	19.1	2	−0.0002
CISMON, 2020/07/29 22:26:34 (Z comp)	2.7	0.0044	0.0042	20	19.1	2	0.0002
PIETRALUNGA, 2021/02/19 23:42:45 (X comp)	2.6	0.0034	0.0037	11	5	0.5	−0.0003
PIETRALUNGA, 2021/02/19 23:42:45 (Y comp)	2.6	0.0033	0.0030	11	5	0.5	0.0003
PIETRALUNGA, 2021/02/19 23:42:45 (Z comp)	2.6	0.0039	0.0024	11	5	0.5	0.0015

Columns 2–8 show the local magnitude (M_L); peak ground acceleration (PGA) recorded by MEMS and RAN sensors; distances between the MEMS sensors and epicenters; distances between RAN stations and epicenters; interstation (RAN MEMS) distances; ΔPGA that is the difference between the PGAs recorded by MEMS and RAN sensors ($PGA_{MEMS} - PGA_{RAN}$).

(INGV) website (http://terremoti.ingv.it/). All websites were last accessed in February 2021. Supplemental material for this article includes the complete technical information of the MEMS sensor prototype and the calibration experiment on the shake table.

Declaration of Competing Interest

The authors declare no conflict of interest.

Acknowledgments

The authors wish to thank ADEL srl for the use of their proprietary data and TIM SpA for the permission granted to microelectromechanical systems (MEMS) installation in their infrastructures. The authors would also like to thank David Zuliani of the Seismological Research Center of Istituto Nazionale di Oceanografia e Geofisica Sperimentale (OGS) for the calibration experiment on the shake table apparatus.

References

Andò, B., S. Baglio, G. L'Episcopo, V. Marletta, N. Savalli, and C. Trigona (2011). A BE-SOI MEMS for inertial measurement in geophysical applications, *IEEE Trans. Instrum. Meas.* **60,** no. 5, 1901–1908.

Boaga, J., F. Casarin, G. De Marchi, M. R. Valluzzi, and G. Cassiani (2019). 2016 central Italy earthquakes recorded by low-cost MEMS-distributed arrays, *Seismol. Res. Lett.* **90,** no. 2A, 672–682.

Cenni, N., J. Boaga, F. Casarin, G. D. Marchi, M. R. Valluzzi, and G. Cassiani (2019). 2016 Central Italy Earthquakes: Comparison between GPS signals and low-cost distributed MEMS arrays, *Adv. Geosci.* **51,** 1–14.

Chiaraluce, L., R. Di Stefano, E. Tinti, L. Scognamiglio, M. Michele, E. Casarotti, M. Cattaneo, P. De Gori, C. Chiarabba, G. Monachesi, *et al.* (2017). The 2016 central Italy seismic sequence: A first look at the mainshocks, aftershocks, and source models, *Seismol. Res. Lett.* **88,** no. 3, 757–771.

Clarke, H., L. Eisner, P. Styles, and P. Turner (2014). Felt seismicity associated with shale gas hydraulic fracturing: The first documented example in Europe, *Geophys. Res. Lett.* **41,** no. 23, 8308–8314.

Cochran, E. S., J. F. Lawrence, C. Christensen, and R. S. Jakka (2009). The quake-catcher network: Citizen science expanding seismic horizons, *Seismol. Res. Lett.* **80,** no. 3, 26–30.

Cochran, E. S., J. F. Lawrence, A. Kaiser, B. Fry, A. Chung, and C. Christensen (2012). Comparison between low-cost and traditional

MEMS accelerometers: A case study from the M7. 1 Darfield, New Zealand, aftershock deployment, *Ann. Geophys.* **54,** no. 6, doi: 10.4401/ag-5268.

D'Alessandro, A., and G. D'Anna (2013). Suitability of low-cost three-axis MEMS accelerometers in strong-motion seismology: Tests on the LIS331DLH (iPhone) accelerometer, *Bull. Seismol. Soc. Am.* **103,** no. 5, 2906–2913.

D'Alessandro, A., A. Costanzo, C. Ladina, F. Buongiorno, M. Cattaneo, S. Falcone, C. La Piana, S. Marzorati, S. Scudero, G. Vitale, *et al.* (2019). Urban seismic networks, structural health and cultural heritage monitoring: The national earthquakes observatory (INGV, Italy) experience, *Front. Built Environ.* **5,** 127.

Ellsworth, W. L. (2013). Injection-induced earthquakes, *Science* **341,** no. 6142, doi: 10.1126/science.1225942.

Evans, J. R., R. M. Allen, A. I. Chung, E. S. Cochran, R. Guy, M. Hellweg, and J. F. Lawrence (2014). Performance of several low-cost accelerometers, *Seismol. Res. Lett.* **85,** 147–158, doi: 10.1785/0220130091.

Fleming, K., M. Picozzi, C. Milkereit, F. Kuhnlenz, B. Lichtblau, J. Fischer, C. Zulfikar, and O. Ozel (2009). The self-organizing seismic early warning information network (SOSEWIN), *Seismol. Res. Lett* **80,** no. 5, 755–771.

Galadini, F., M. E. Poli, and A. Zanferrari (2005). Seismogenic sources potentially responsible for earthquakes with M ≥ 6 in the eastern Southern Alps (Thiene-Udine sector, NE Italy), *Geophys. J. Int.* **161,** no. 3, 739–762.

Holland, A. (2003). Earthquake data recorded by the MEMS accelerometer: Field testing in Idaho, *Seismol. Res. Lett.* **74,** no. 3, 20–26.

Homeijer, B., D. Lazaroff, D. Milligan, R. Alley, J. Wu, M. Szepesi, B. Bicknell, Z. Zhang, R. G. Walmsley, and P. G. Hartwell (2011). Hewlett packard's seismic grade MEMS accelerometer, *2011 IEEE 24th International Conf. on Micro Electro Mechanical Systems*, IEEE, 585–588.

Kong, Q., R. M. Allen, L. Schreier, and Y. W. Kwon (2016). MyShake: A smartphone seismic network for earthquake early warning and beyond, *Sci. Adv.* **2,** no. 2, e1501055, doi: 10.1126/sciadv.1501055.

Lawrence, J. F., E. S. Cochran, A. Chung, A. Kaiser, C. M. Christensen, R. Allen, J. W. Baker, B. Fry, T. Heaton, D. Kilb, *et al.* (2014). Rapid earthquake characterization using MEMS accelerometers and volunteer hosts following the M 7.2 Darfield, New Zealand, earthquake, *Bull. Seismol. Soc. Am.* **104,** no. 3, 184–192.

Liu, C. M., B. C. Chou, R. C. F. Tsai, N. Y. Shen, B. S. Chen, E. C. Cheng, H. C. Tuan, A. Kalnitsky, S. Cheng, C. H. Lin, *et al.* (2011). MEMS technology development and manufacturing in a CMOS foundry, *2011 16th International Solid-State Sensors, Actuators and Microsystems Conf.*, IEEE, 807–810.

Majer, E. L., R. Baria, M. Stark, S. Oates, J. Bommer, B. Smith, and H. Asanuma (2007). Induced seismicity associated with enhanced geothermal systems, *Geothermics* **36,** no. 3, 185–222.

Mustafazade, A., M. Pandit, C. Zhao, G. Sobreviela, Z. Du, P. Steinmann, X. Zou, R. T. Howe, and A. A. Seshia (2020). A vibrating beam MEMS accelerometer for gravity and seismic measurements, *Sci. Rep.* **10,** no. 3, 1–8.

Nof, R. N., A. I. Chung, H. Rademacher, L. Dengler, and R. M. Allen (2019). MEMS Accelerometer Mini-Array (MAMA): A low-cost implementation for earthquake early warning enhancement, *Earthq. Spectra* **35,** no. 3, 21–38.

Shi, G., C. S. Chan, W. J. Li, K. S. Leung, Y. Zou, and Y. Jin (2009). Mobile human airbag system for fall protection using MEMS sensors and embedded SVM classifier, *IEEE Sensor J.* **9,** no. 5, 495–503.

Valoroso, L., L. Improta, L. Chiaraluce, R. Di Stefano, L. Ferranti, A. Govoni, and C. Chiarabba (2009). Active faults and induced seismicity in the Val d'Agri area (southern Apennines, Italy), *Geophys. J. Int.* **178,** no. 3, 488–502.

Wald, D., K. W. Lin, K. Porter, and L. Turner (2008). ShakeCast: Automating and improving the use of ShakeMap for post-earthquake decision-making and response, *Earthq. Spectra* **24,** no. 2, 533–553.

Walsh, F. R., and M. D. Zoback (2015). Oklahoma's recent earthquakes and saltwater disposal, *Sci. Adv.* **12,** no. 5, e1500195, doi: 10.1126/sciadv.1500195.

Weingarten, M., S. Ge, J. W. Godt, B. A. Bekins, and J. L. Rubinstein (2015). High-rate injection is associated with the increase in US mid-continent seismicity, *Science* **348,** no. 6241, 1336–1340.

Westaway, R., and P. L. Younger (2014). Quantification of potential macroseismic effects of the induced seismicity that might result from hydraulic fracturing for shale gas exploitation in the UK, *Q. J. Eng. Geol. Hydrogeol* **47,** no. 4, 333–350.

Manuscript received 20 March 2021
Published online 13 May 2021

A.2 The 2020 coronavirus lockdown and seismic monitoring of anthropic activities in Northern Italy

SCIENTIFIC REPORTS
nature research

OPEN

The 2020 coronavirus lockdown and seismic monitoring of anthropic activities in Northern Italy

Piero Poli[1] ✉, Jacopo Boaga[2], Irene Molinari[3], Valeria Cascone[2] & Lapo Boschi[2,3,4]

In March/April 2020 the Italian government drastically reduced vehicle traffic and interrupted all non-essential industrial activities over the entire national territory. Italy thus became the first country in the world, with the exception of Hubei, to enact lockdown measures as a consequence of the COVID-19 outbreak and the need to contain it. Italy is also a seismically active area, and as such is monitored by a dense permanent network of seismic stations. We analyse continuous seismic data from many stations in northern and central Italy, and quantify the impact of the lockdown on seismic ambient noise, as a function of time and location. We find that the lockdown reduces ambient noise significantly in the 1–10 Hz frequency range; because natural sources of seismic noise are not affected by the lockdown, the seismic signature of anthropic noise can be characterised with unprecedented clarity, by simply comparing the signal recorded before and after the lockdown. Our results correlate well with independent evaluations of the impact of the lockdown (e.g., cell phone displacements), and we submit that ambient-noise seismology is a useful tool to monitor containment measures such as the coronavirus lockdowns.

On March 9, 2020, the Italian government issued a decree prohibiting movement in public places except for justifiable work reasons, basic necessities and health emergencies, canceling sporting events and public gatherings, closing schools, universities, and recreational facilities on the entire national territory. This followed smaller-scale lockdowns of eleven municipalities in the North (February 21), soon expanded to the entire region of Lombardy and fourteen neighbouring provinces (March 8), decided in an attempt to contain a major outbreak of the COVID-19 pandemic.

On March 22, through another decree, all non-essential industries were closed down throughout the country; inter-city movement was further restricted, requiring travellers to provide justification and documentation to authorities on any movement between cities. At the time of completing this manuscript, all these lockdown measures are still ongoing.

It has been pointed out that containment measures in Belgium (for example) have resulted in a conspicuous drop in the continuous signal recorded by broadband seismic stations[1]. This means that all the anthropic activities interrupted by the lockdown contribute importantly to "the hum of vibrations in the planet's crust;" it also means, then, that the lockdown is an opportunity for students of "seismic ambient noise"[2,3] to clearly separate its anthropic vs. natural components, normally intermingled and not easily distinguishable.

Ambient noise, or seismic signal recorded in the absence of earthquakes, is known to largely consist of "microseisms" resulting from the coupling between oceans and the solid earth at frequencies mostly below 1 Hz[4]. At relatively high frequencies, however, it also includes the so-called "anthropic" or "cultural" noise[5–7] associated with human activities at or near the surface of the Earth, namely machinery in power plants and factories, and train and road traffic. Anthropic noise is thought to include frequencies from 1 to 10 Hz approximately, attenuating quickly with distance (a few km) and disappearing quickly with increasing depth; its total energy changes daily (day vs. night), weekly (working days vs. weekends), and with the occurrence of holidays (the Christmas break is particularly prominent in many countries). Just like the "natural", low-frequency noise, that provides unique observations of surface-wave propagation allowing to map the structure of the Earth's lithosphere[8], anthropic

[1]ISTERRE, Université de Grenoble, Grenoble, France. [2]Dipartimento di Geoscienze, Università degli Studi di Padova, Padova, Italy. [3]Istituto Nazionale di Geofisica e Vulcanologia, via Donato Creti 12, Bologna, Italy. [4]Sorbonne Université, CNRS, INSU, Institut des Sciences de la Terre de Paris, ISTeP UMR 7193, F-75005, Paris, France. ✉e-mail: piero.poli@univ-grenoble-alpes.fr

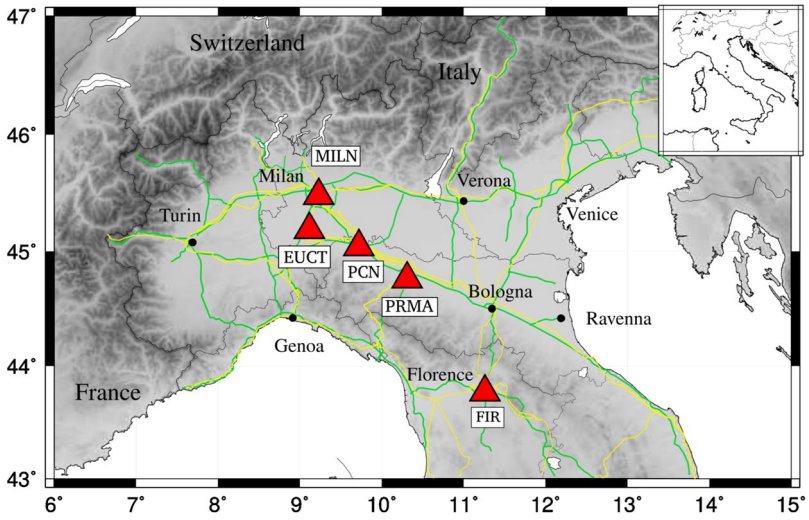

Figure 1. All data analysed in our study were recorded at the broadband seismic stations marked here by red triangles and acronyms; all stations are part of the Italian National Seismic Network operated by the Istituto Nazionale di Geofisica e Vulcanologia. Green and yellow lines denote major highways and railways, respectively.

noise is of interest to geoscientists, as it can be used at relatively small scales, for instance in mapping and monitoring efforts[9,10].

While earlier studies have attempted to characterise high-frequency seismic noise[7,11–14], the current lockdown of industrial activities and reduction in road and train traffic in Italy is an unprecedented opportunity to discriminate it from ambient noise of natural origin. Italy is a highly industrialized and urbanized country, densely covered with non-stationary noise sources[15], such as traffic and industry-induced vibration[16]. This is particularly true in its northern regions, which account for 70% of the country's entire industrial output, and where lockdown measures have been enacted earlier than everywhere else in Europe. We analyse continuous data from an array of broadband seismic stations, located in the vicinity of known industrial districts in Lombardy, Emilia-Romagna and Tuscany (Fig. 1); we identify the spectral signature of the March 2020 lockdown, and take advantage of the lockdown to quantify and evaluate the spectral signature of anthropic activities. Importantly, measuring the overall reduction in seismic energy associated with the lockdown is also a way to quantify its effects; this is relevant to governmental entities, wishing to monitor the effectiveness of the measures being taken.

Data

We downloaded publicly available, continuous, three-component seismic recordings from a set of permanent broadband stations, part of the Italian National Seismic Network operated by the Istituto Nazionale di Geofisica e Vulcanologia[17]. All instruments have a flat response at frequencies between ~0.01 and ~10 Hz, or broader; we remove ("deconvolve") instrument response from the data prior to our analysis. The locations of stations employed in most of our study are shown in Fig. 1. Stations were selected based on their proximity to industrial districts; in particular, MILN is located near the city of Milano, with a particularly high concentration of vehicle traffic and industrial activities.

Seismic Ambient Noise Before and After the Lockdown

The seismic signature of the containment measures in Italy is apparent from a relatively simple analysis of continuous recordings at station MILN, located within the city limits of Milano, in a busy area near the University of Milano campus and the Lambrate train station. We compute spectrograms (Fig. 2) by Fourier-transforming 1-hour-long segments of continuous signal, with a 30-minute overlap between subsequent segments; for each calendar day, all segments are then averaged, and the squared modulus of the resulting average Fourier transform is computed: this way, a single "power-spectral density" (PSD) function is obtained, for each station, component (East-West, North-South, vertical) and calendar day.

Figure 2 shows clearly that the lockdown has a relevant impact on recorded seismic noise over a broad frequency range; its effect disappears at frequencies below 1 Hz, where anthropic noise is weaker. The energy drop associated with the lockdown is comparable with that occurring every weekend and during the winter break, both in 2018/19 and 2019/20. Interestingly, loss of energy is gradual over time, starting with the first lockdown measures on February 21, and increasing with time until a plateau is reached around March 22 (interruption of non-essential industrial activities). A trend similar to that seen in Fig. 2 has also been found through the analysis of cell phone displacements[18]. This suggests that vehicle traffic, which was significantly reduced (particularly in and around Milano) already with the February measures, contributes significantly to the entire spectrum of anthropic noise; there is also episodical evidence from the press that a number of factories were closed based on the unilateral decision of their owners, before the government-imposed lockdown.

The analysis applied to station MILN is repeated for all seismic stations of Fig. 1, and the results are illustrated in Figs. 3 and 4.

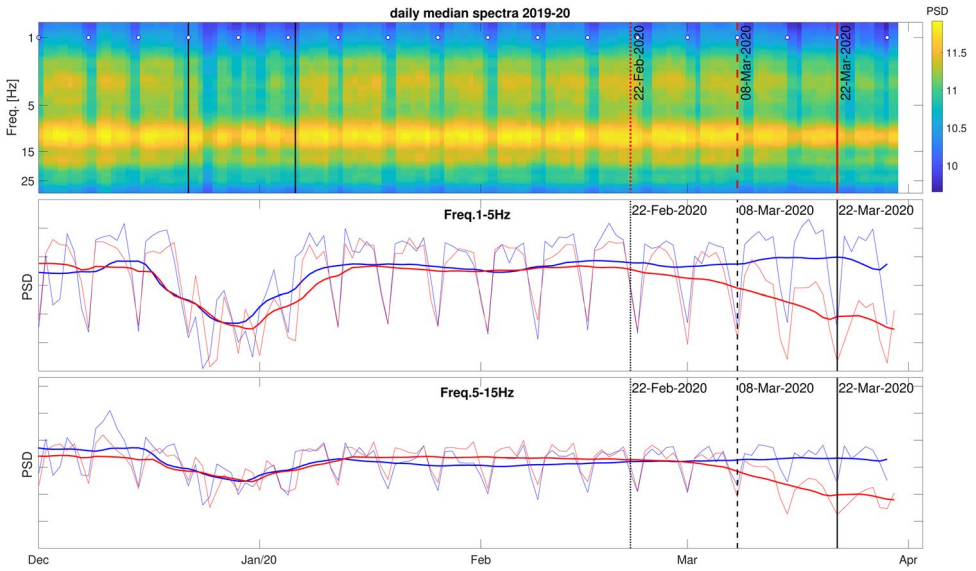

Figure 2. Spectrogram of ambient signal recorded on the vertical component of station MILN, December 1st 2019-present (top); the same spectrogram, averaged (red lines) at frequencies from 1 to 5 Hz (middle) and from 10 to 15 Hz (bottom), compared with results obtained in the same way, from recordings made December 2018-April 2019 at the same station (blue). (The East-West and North-South components show very similar trends, albeit slightly less pronounced.) The 2018/2019 curve is slightly offset, in order for weekends to be "in phase" with those of 2019/20. To emphasize relatively-long term (weekly rather than daily) effects, curves are also smoothed over time (thicker lines). The dates when specific containment measures were first implemented are marked by a dotted line (lockdowns of eleven municipalities in the North), a dashed line (restriction of movement and closure of schools in the entire country) and a solid line (interruption of all non-essential industrial activities).

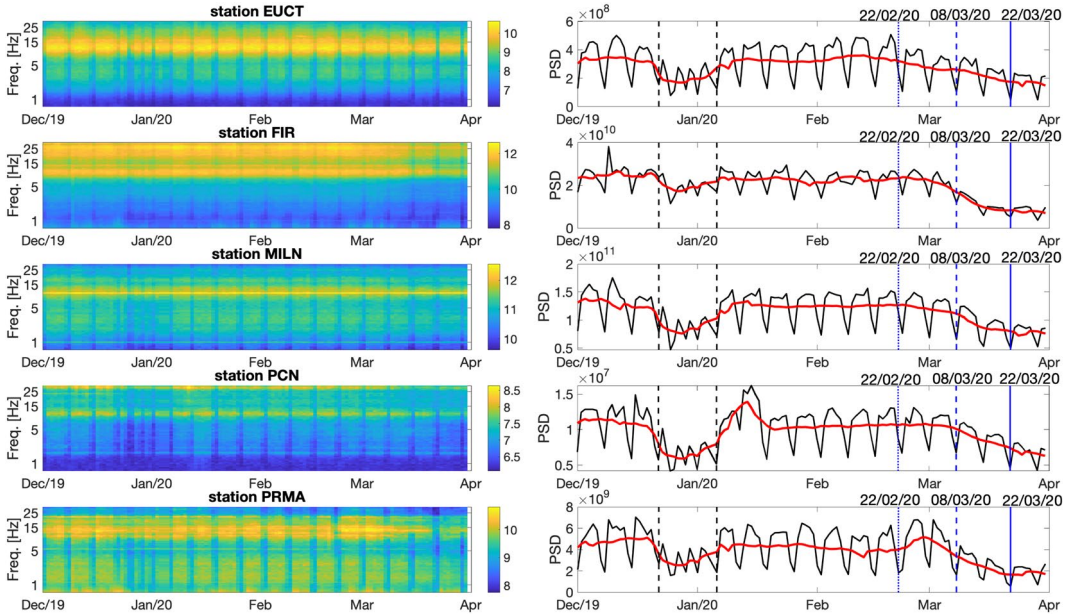

Figure 3. Spectrograms (left) of signal recorded on the vertical components of stations (top to bottom) EUCT, FIR, MILN, PCN, PRMA. To the right, curves obtained from the same spectra, by averaging over the entire frequency range of interest (1 to 40 Hz), without (black line) and with (red) smoothing, similar to Fig. 2. The dates of mentioned governmental decrees are highlighted as in Fig. 2, and so are the typical initial and final days of winter break.

Lockdown measures apparently impact all stations under consideration, but the character of their effects changes in various ways with station location. In the case of FIR, located in the city of Florence, the signature of the winter break is almost negligible, while the February/March lockdown still has a prominent effect; it might be

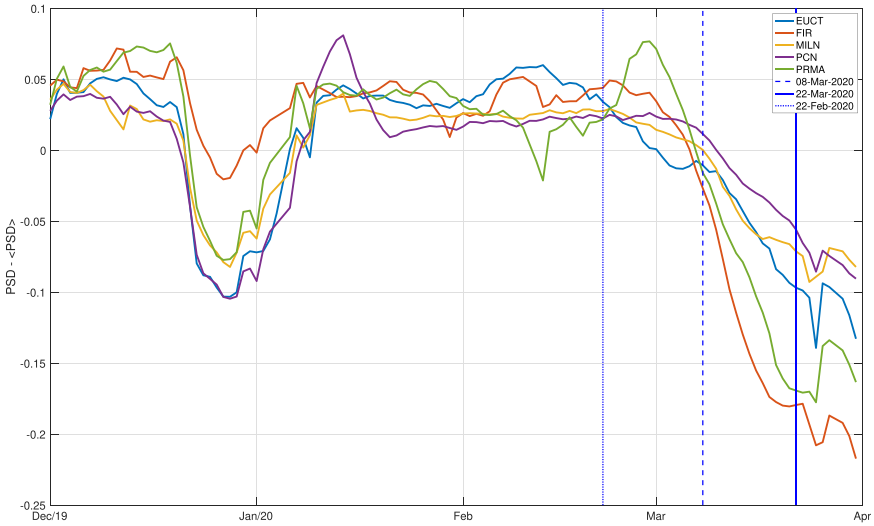

Figure 4. The smoothed red curves shown in Fig. 3 are plotted here on a single graph, for comparison; for each station, the average value of the PSD observed in the time interval of interest is subtracted from the corresponding curve, prior to plotting, as this can change significantly from station to station, but is not relevant to our analysis. Each colour corresponds to one station, as specified. Again, the dates of mentioned governmental decrees are highlighted as in Fig. 2.

possible to interpret this observation through the analysis of anthropic activities usually taking place in the area (e.g., tourism, which is presumably not reduced by the holiday). The drop is gradual at all stations, with no specific governmental decree standing out with respect to the others. At station PRMA, a slight increase in ambient noise occurs after February 21 and before March 9.

The Spectral Signature of "Cultural" Seismic Noise

We next characterise anthropic noise by evaluating variations in the spectra of seismic ambient noise before and after the implementation of lockdown measures. We compute the ratios of the PSD measured (as described in sec. 3) on Tuesday March 31 2020, to that measured at the same station on Tuesday December 3 2019. We carry out this calculation separately for each component, and for all stations analysed thus far; the results of this exercise are shown in Fig. 5. The energy associated with ambient signal is clearly reduced for all stations, at all frequencies in the range of interest. At each station, PSD ratios change with frequency almost exactly in the same way for all components. Near 1 Hz, all stations show a more or less rapid decline in the PSD ratio, with ambient noise being more effectively reduced as frequency grows. This trend continues all the way to 20 Hz at stations EUCT and PRMA, while other stations show a more complex behaviour. Above 10 Hz station MILN stands out, its PSD ratio growing quickly with frequency.

Anthropic noise is known to be relevant at frequencies above 1 Hz, and to consist of a range of different excitation mechanisms[7,15,19,20]. Natural sources such as rain, wind[21] and sea/ocean waves are typically characterized by frequencies below 1 Hz, and are obviously not affected by the lockdown. We infer that, by taking the ratio of noise spectra before and after the lockdown, an estimate of the spectral character of anthropic noise is obtained, and the spectra in Fig. 5 can help us estimate the nature of anthropic noise in the region of interest, independent of the lockdown; the frequencies where the PSD of ambient signal is most reduced by the lockdown are those where, in normal times, the contribution of anthropic activities to seismic ambient noise is most important. The fact that most energy loss associated with the lockdown is at frequencies between 1–10 Hz is coherent with what is known of the typical signature of industrial activity and vehicle traffic[22]. Seismic data recorded during the lockdown might be particularly useful in identifying sources of anthropic noise, which could be employed by geophysicists, after the lockdown, e.g. to characterise the upper subsoil by cross correlation of ambient signal[23,24].

We further analysed the relationship between ambient noise recorded on different components, finding the "H/V" ratio between the PSDs of horizontal-component and vertical-component signals: first, the PSD of each component of signal recorded on a given day is averaged in the frequency range 1–10 Hz; then the arithmetical average of the resulting East-West-component and North-South-component values is taken; finally, the ratio of the resulting horizontal PSD to the vertical one is computed. The procedure is iterated for each station and for each day between December 1 and March 31, and the results are shown in Fig. 6.

In general, the value of H/V is related to how seismic energy in the ambient-noise field is distributed in the form of compressional, shear and surface waves[7,25,26]; changes in H/V after vs. before the lockdown would reveal whether the reduction in anthropic noise affects one of these seismic phases/components more or less importantly than the others; in other words, whether traffic and industry-induced vibration can be associated to one particular constituent of the seismic field. Figure 6 shows that the lockdown measures have no effect on H/V, and we infer that, while anthropic noise is reduced significantly by the lockdown (Fig. 5), the relative contributions of compressional, shear and surface waves remain approximately constant: the noise wave field is stable in the

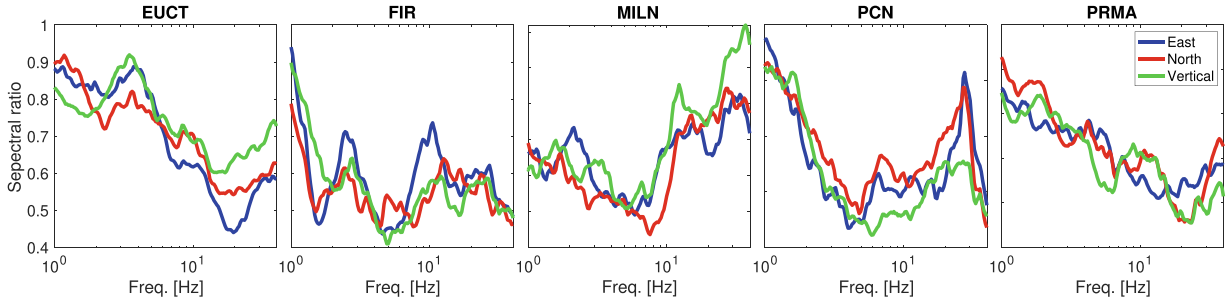

Figure 5. Ratio of PSD after vs. before the lockdown, at stations (left to right) EUCT, FIR, MILN, PCN and PRMA, in the frequency range 1–40 Hz. Different-colour curves indicate different instrument components, i.e. blue, red and green for the East-West, North-South and vertical components, respectively.

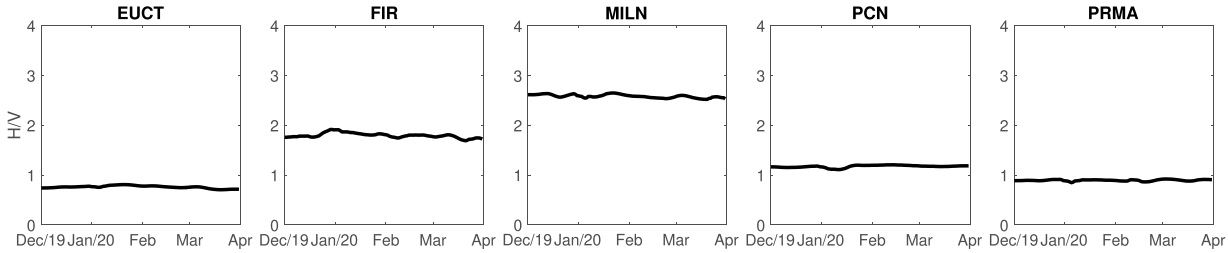

Figure 6. Ratio of horizontal to vertical PSD, averaged over frequency, shown as a function of time from the beginning of December 2019 to the end of March 2020. From left to right, ratios obtained at stations EUCT, FIR, MILN, PCN, PRMA are shown, respectively.

1–10 Hz frequency band, and can thus represent a reliable source of information about geological features of the subsoil[7] or to monitor the evolution of subsurface velocity[10,26].

Geographic Distribution of Anthropic Noise

The Italian territory is densely covered by seismic instruments, and by repeating our analysis on the entire network of available stations we are able to quantify the spatial dependence of anthropic noise reduction. For each station, for each day, the PSD of signal recorded 6 AM to 8 PM is computed, and averaged over different frequency bands. In practice, we employ the direct Fourier method[27], as implemented in the Obspy package[28,29]: this is standard procedure to identify artefacts related to station operation, episodic cultural noise, overall station quality and level of Earth noise at each site. To emphasize the change in ambient noise with the lockdown, we plot the difference between the values so obtained on three dates in 2020, and reference values obtained conducting the same calculation on data recorded for five months until the lockdown, and averaging. We include as Supplementary Material S1 an animated version of Fig. 7, showing the PSD at the same stations, October 7, 2019 through April 1, 2020; through this time-dependent visualization, the drastic effects of the lockdown are further emphasized.

Our main result, that noise be strongly reduced after the lockdown in the "cultural" frequency range, is confirmed by Fig. 7, and extended to most of Northern Italy. Between 1–3 Hz, the lockdown effects are more pronounced in the Lombardy and Veneto regions than in Central Italy and along the Apennine range. The most important reductions in ambient noise are recorded by stations along the Alpine arc, near Torino, Milano and Verona, and in the city of Florence.

Summary

We have analysed continuous data from northern Italy, and quantified the effects of the March 2020 coronavirus lockdown on the seismic ambient noise field. We confirm that this effect is significant, and easily observed in our data: see in particular Figs. 3 and 4. The Italian government first imposed a reduction of people (and therefore vehicle) movement, on March 9; we find that this date marks the beginning of a gradual loss in ambient-noise energy at all frequencies, which we attribute to the reduction of road and railroad traffic in the region of interest. Depending on the station, the energy curve flattens out, or starts to decline more slowly towards the beginning of April, despite the more stringent measures imposed at that time (interruption of all non-essential industrial activities). A similar trend has been found from cell-phone displacement data[18]. One implication of our observations is that seismic data could be useful for governmental institutions to monitor the effectiveness of measures involving a reduction or interruption of human activity in a given area.

It is understood that the lockdown only reduces noise of anthropic origin; it follows that by comparing the Fourier spectrum of seismic ambient noise before and after the lockdown (Fig. 5), one can attempt to characterise anthropic noise. We find that, confirming earlier estimates[30,31], anthropic noise becomes dominant at frequencies

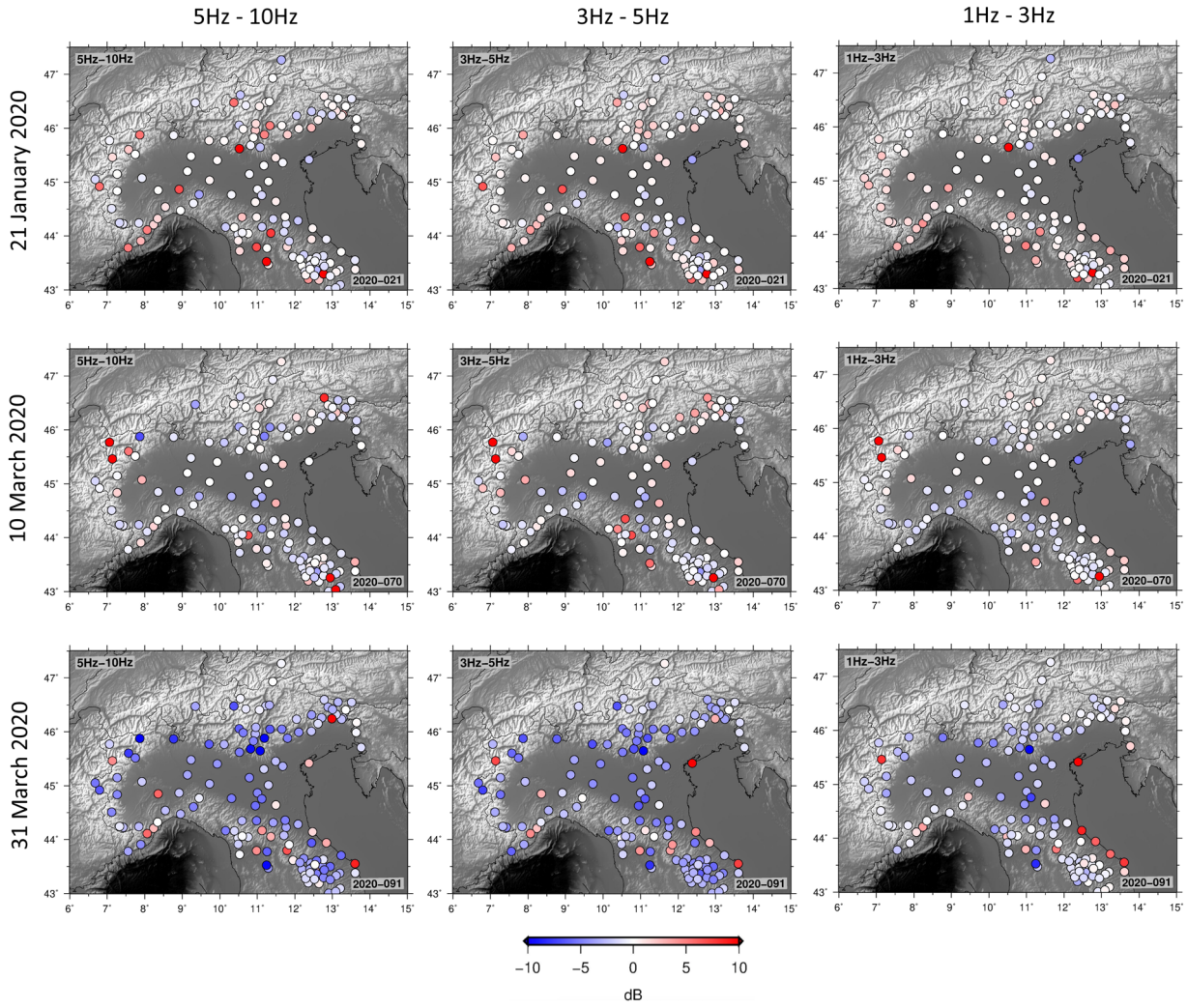

Figure 7. Difference between PSD (6 AM–8 PM) on a given day (top to bottom: January 21, March 10 and March 31: all are Tuesdays), and average PSD calculated for all week days (6 AM–8 PM) from 1–10–2019 to 1-4-2020. The calculation is conducted within three frequency bands (left to right: 5–10 Hz, 3–5 Hz and 3–1 Hz). Values for each station are plotted, through the shown colour code, at the station location.

above ~2 Hz, where most stations show a ~50% reduction in the energy associated with ambient signal. It then grows with increasing frequency, up to about 20 Hz for most stations. Other than that, the spectrum associated with each station has a unique nature, and knowledge of anthropic activity occurring in its vicinity is probably needed for its interpretation. Our results suggest that seismic data recorded during the lockdown will be useful to identify and characterise specific sources of anthropic noise, which in the future could become useful in local subsoil mapping and monitoring studies[32–37].

Received: 6 April 2020; Accepted: 18 May 2020;
Published online: 10 June 2020

References

1. Gibney, E. Coronavirus lockdowns have changed the way Earth moves. *Nature*, pages, https://doi.org/10.1038/d41586-020-00965-x (2020).
2. Campillo, M. & Roux, P. Seismic imaging and monitoring with ambient noise correlations. In Romanowicz, B. & Dziewonski, A. M.editors, *Treatise of Geophysics. Vol. 1*. Elsevier (2014).
3. Boschi, L. & Weemstra, C. Stationary-phase integrals in the cross-correlation of ambient noise. *Rev. Geophys.*, **53**, https://doi.org/10.1002/2014RG000455 (2015).
4. Longuet-Higgins, M. S. A theory of the origin of microseisms. *Phil. Trans. R. Soc. Lond.* **243**, 1–35 (1950).
5. Bungum, H., Mykkeltveit, S. & Kvaerna, T. Seismic noise in Fennoscandia, with emphasis on high frequencies. *Bull. Seism. Soc. Am.* **75**, 1489–1513 (1985).
6. Given, H. K. Variations in broadband seismic noise at IRIS/IDA stations in the USSR with implications for event detection. *Bull. Seism. Soc. Am.* **80**, 2072–2088 (1990).
7. Bonnefoy-Claudet, S., Cotton, F. & Bard, P.-Y. The nature of noise wavefield and its applications for site effects studies: A literature review. *Earth-Science Reviews* **79**, 205–207 (2006).

8. Shapiro, N. M. & Campillo, M. Emergence of broadband Rayleigh waves from correlations of the ambient seismic noise. *Geophys. Res. Lett.*, 31(7) (2004).
9. Louie, J. N. Faster, better: shear-wave velocity to 100 meters depth from refraction microtremor arrays. *Bull. Seism. Soc. Am.* **91**, 347–364 (2001).
10. Bontemps, N., Lacroix, P., Larose, E., Jara, J. & Taipe, E. Rain and small earthquakes maintain a slow-moving landslide in a persistent critical state. *Nature Communications* **11**, 2041–1723, https://doi.org/10.1038/s41467-020-14445-3 (2020).
11. Junge, A. Characterization of and correction for cultural noise. *Surveys in Geophysics* **17**, 361–391 (1996).
12. Bonnefoy-Claudet, S. *et al*. H/V ratio: a tool for site effects evaluation. Results from 1-D noise simulations. *Geophys. J. Int.* **167**, 827–837, https://doi.org/10.1111/j.1365-246x.2006.03154.x (2006).
13. Cara, F. *et al*. On the stability and reproducibility of the horizontal to vertical spectral ratio on ambient noise: Case study of Cavola, northern Italy. *Bull. Seism. Soc. Am.* **100**, https://doi.org/10.1785/0120090086 (2010).
14. Scafetta, N. & Mazzarella, A. Cultural noise and the night-day asymmetry of the seismic activity recorded at the Bunker-East (BKE) Vesuvian Station. *Journal of Volcanology and Geothermal Research* **349**, 117–127 (2018).
15. Latorre, D., Amato, A., Cattaneo, M., Carannante, S. & Michelini, A. Maninduced low frequency seismic events in Italy. *Geophys. Res. Lett.* **41**, 8261–8268, https://doi.org/10.1002/2014GL062044 (2014).
16. Cattaneo, M. *et al*. A catalogue of non-tectonic earthquakes in central-eastern Italy. *Ann. Geophys.* **57**, S0328, https://doi.org/10.4401/ag-6434 (2014).
17. ISIDe Working Group. *Italian Seismological Instrumental and Parametric Database (ISIDe)*. Istituto Nazionale di Geofisica e Vulcanologia (2007).
18. Pepe, E. *et al*. The reduction of social mixing in Italy following the lockdown. https://covid19mm.github.io/in-progress/2020/03/25/second-report.html (2020).
19. Peterson, J. R. *Observations and modeling of seismic background noise*. USGS, Albuquerque, New Mexico (1993).
20. Obermann, A. & Hillers, G. Recent advances in seismology. In Schmelzbach, C., editor, *Advances in Geophysics*. Elsevier (2019).
21. Burtin, A., Bollinger, L., Vergne, J., Cattin, R. & Nàbělek, J. Spectral analysis of seismic noise induced by rivers: A new tool to monitor spatiotemporal changes in stream hydrodynamics. *J. Geophys. Res.*, **113** (2008).
22. Inbal, A. *et al*. Sources of long range anthropogenic noise in Southern California and implications for tectonic tremor detection. *Bull. Seism. Soc. Am.* **108**, 3511–3527 (2018).
23. Boaga, J., Vaccari, F. & Panza, G. F. Shear wave structural models of Venice Plain, Italy, from time cross correlation of seismic noise. *Engineering Geology* **116**, 189–195 (2010).
24. Brenguier, F. *et al*. Train traffic as a powerful noise source for monitoring active faults with seismic interferometry. *Geophys. Res. Lett.* **46**, 9529–9536, https://doi.org/10.1029/2019GL083438 (2019).
25. Hennino, R. *et al*. Observation of equipartition of seismic waves. *Phys. Rev. Lett.* **86**, 3447 (2001).
26. Hillers, G. *et al*. Seismic velocity change patterns along the San Jacinto fault zone following the 2010 m 7.2 El Mayor-Cucapah and m 5.4 Collins Valley earthquakes. *J. Geophys. Res.* **124**, 7171–7192 (2019).
27. Cooley, J. W. & Tukey, J. W. An algorithm for the machine calculation of complex Fourier Series. *Math. Comp.* **19**, 297–301 (1965).
28. Krischer, L. *et al*. ObsPy: A bridge for seismology into the scientific Python ecosystem. *Comput. Sci. Dis.* **8**, 014003, https://doi.org/10.1088/1749-4699/8/1/014003 (2015).
29. McNamara, D. E. & Boaz, R. I. Seismic Noise Analysis System, Power Spectral Density Probability Density Function: Stand-Alone Software Package. United States Geological Survey Open File Report, No. 2005-1438 (2005).
30. Sheen, D., Shin, J. S. & Kang, T. Seismic noise level variation in South Korea. *Geosci. J.* **13**, 183–190, https://doi.org/10.1007/s12303-009-0018-0 (2009).
31. Hillers, G. *et al*. Global oceanic microseism sources as seen by seismic arrays and predicted by wave action models. *Geochem. Geophys. Geosyst.* **13**, Q01021, https://doi.org/10.1029/2011GC003875 (2012).
32. INGV Seismological Data Centre. Rete Sismica Nazionale (RSN). Istituto Nazionale di Geofisica e Vulcanologia (INGV), Italy, https://doi.org/10.13127/SD/X0FXnH7QfY (1997).
33. MedNet project partner institutions. Mediterranean Very Broadband Seismographic Network (MedNet). Istituto Nazionale di Geofisica e Vulcanologia (INGV), Italy, https://doi.org/10.13127/SD/fBBBtDtd6q (1988).
34. OGS (Istituto Nazionale di Oceanografia e di Geofisica Sperimentale) and University of Trieste). North-East Italy Broadband Network. International Federation of Digital Seismograph Networks, Other/Seismic Network, https://doi.org/10.7914/SN/NI (2002).
35. OGS (Istituto Nazionale di Oceanografia e di Geofisica Sperimentale). North-East Italy Seismic Network. International Federation of Digital Seismograph Networks, Other/Seismic Network, https://doi.org/10.7914/SN/OX (2016).
36. University of Genova. Regional Seismic Network of North Western Italy. International Federation of Digital Seismograph Networks, Other/Seismic Network, https://doi.org/10.7914/SN/GU (1967).
37. Wessel, P. *et al*. The Generic Mapping Tools version 6. *Geochem. Geophys. Geosyst.* **20**, 5556–5564, https://doi.org/10.1029/2019GC008515 (2019).

Acknowledgements

We downloaded and analysed continuous seismic data provided by the Istituto Nazionale di Geofisica e Vulcanologia, the Osservatorio Geofisico Sperimentale, the University of Genova. The Generic Mapping Tools were used to generate the map in Figure 1. Piero Poli was supported by the European Union Horizon 2020 Research and Innovation Programme (grant agreements, 802777-MONIFAULTS).

Author contributions

Conceptualization, P.P., L.B.; Methodology, P.P., L.B., J.B.; Validation. L.B., P.P.; Formal analysis. P.P., I.M.; Data curation P.P., I.M.; Writing—review and editing, L.B., P.P., I.M., J.B., V.C.

Competing interests

The authors declare no competing interests.

Additional information

Supplementary information is available for this paper at https://doi.org/10.1038/s41598-020-66368-0.

Correspondence and requests for materials should be addressed to P.P.

Reprints and permissions information is available at www.nature.com/reprints.

Publisher's note Springer Nature remains neutral with regard to jurisdictional claims in published maps and institutional affiliations.

A.3 Velocity gradients choice affecting seismic site response in deep alluvial basins: Application to the Venetian Plain (Northern Italy)

OXFORD

Journal of Geophysics and Engineering

Journal of Geophysics and Engineering (2022) **19**, 1–13 https://doi.org/10.1093/jge/gxab067

Velocity gradients choice affecting seismic site response in deep alluvial basins: Application to the Venetian Plain (Northern Italy)

Valeria Cascone*, Ilaria Barone and Jacopo Boaga

Geoscience Department, University of Padova, Via G. Gradenigo 6, Padova, 35131, Padova, Italy

*Corresponding author: Valeria Cascone. E-mail: valeria.cascone@phd.unipd.it

Received 15 December 2020, revised 10 September 2021
Accepted for publication 1 November 2021

Abstract

The average shear-wave velocity of the first 30 metres of subsoil and the depth of the engineering bedrock are considered the key parameters for simplified seismic site response modelling. However, a reliable estimate of the site amplification should consider the entire shear-wave velocity profile from the ground surface down to the engineering bedrock. In deep alluvial basins, a typical geological context where the soil–bedrock interface may lie below the penetration depth of most common prospecting methods, only the shallow velocity profile can be defined in detail, while the deeper structures are commonly extrapolated with linear equations. The choice of a realistic interpolation between the shallow and deep soil still remains an open issue. We compute the 1D seismic site response of two sectors of the Venetian Plain (Northern Italy) characterised by gravelly and sandy deep formations. We model the 1D soil columns using theoretical non-linear gradients proposed in literature for deep alluvial basins. The numerical modelling results, in terms of strong motion parameters, show variations in the seismic site response up to 20%. The effect of the velocity gradients is also evaluated comparing the numerical simulations with real accelerometers recorded by a deep borehole seismometer and a seismic station located at the top of the borehole. These results demonstrate that the selection of the velocity gradient is crucial for seismic site characterisation of deep alluvial basins. In particular, the study suggests which is the most conservative gradient among the ones tested in terms of ground motion hazard estimation.

Keywords: seismic site response, deep alluvial basins, shear-wave velocity, velocity gradients

1. Introduction

The effects of local geology on seismic ground motion have been widely studied in geotechnical earthquake engineering to estimate response spectra for building restoration and construction (Kramer 1996). The shear-wave velocity (V_s) is one of the key parameters adopted for site classification in several seismic regulations (Boore *et al.* 1993, Martin & Dobry 1994). V_s profiles estimate the rigidity of the soil column when excited by seismic shear stress, which is the most important action controlling the seismic site response (Martin & Dobry 1994). Seismic site amplification can be in fact described as the motion modification due to the soft soil during the wave propagation through the stratigraphic column, from the basement bedrock upwards to the ground surface (Langston 2003; Chong & Ni 2009; Rathje *et al.* 2010). Several seismic regulations propose different approaches to evaluate the seismic amplification due to the soil properties. The soils are often classified into different categories, based on the average V_s of the top 30 m of a

soil profile (also called V_{s30}) as in the Italian Building Code ('Norme tecniche per le costruzioni–NTC'; Ministero delle Infrastrutture e dei Trasporti 2008); or the Eurocode 8–EC8 (European Committee for Standardisation 2004); and the National Earthquake Hazard Reduction Program-NEHRP provisions (Building Seismic Safety Council–BSSC 2003).

The V_{S30} parameter adopted by the seismic site classification considers the first 30 metres of subsoil, which is the depth of investigation for common geophysical and geotechnical analysis, that are logistically and economically often limited to the first subsoil. Seismic surveys to retrieve V_S values can be made either in boreholes (down-hole seismic testing, Cardarelli *et al.* 2018) or with surface methods as the multichannel analysis of surface waves (MASW, Park *et al.* 2000; Strobbia *et al.* 2011) and SH refraction analysis, (Hunter *et al.* 2002). Regardless of the method adopted in common engineering projects, the investigation depth rarely exceeds the first subsoil, being limited by the logistically achievable efforts such as: seismic source power, extension of the survey length due to urban conditions, borehole penetration etc. Thus, most of the seismic site response studies are based on the properties of the subsurface soils down to 30 metres (Boore *et al.* 1993; Martin & Dobry 1994).

The Italian and European seismic codes define the engineering bedrock as the depth at which $V_S \geq 800$ m s^{-1} (soil category A = stiff soil or rock, see EC8). Softer soils, with $V_S \leq 800$ m s^{-1}, are expected to amplify the seismic action, therefore the correct estimation of the site amplification should consider the entire soil profile from the ground surface down to the engineering bedrock. Nevertheless, in deep alluvial basins, a clear soft soil–bedrock interface may not be evident but buried under hundreds of metres of soft sediments (Guèguen *et al.* 2007; Poggi *et al.* 2012; Faccioli *et al.* 2015; Mascandola *et al.* 2019). In these geological contexts, thick and soft sediments are expected to amplify the seismic ground motion (Kramer 1996). The site classifications that consider only the V_{S30} might lack a correct seismic action estimation, leading to inaccurate evaluations of the ground amplification level (e.g. Borcherdt 1994; Pitilakis *et al.* 2006). Several available techniques, such as passive surveys and travel-time seismic tomography allow a deeper soil characterisation, down to hundreds of metres deep. The passive methods, based on the recording of ambient vibrations, use 2D arrays of receivers (e.g. SPAC, Aki 1957; frequency–wavenumber method, Lacoss *et al.* 1969), linear arrays (Re-Mi, Louie 2001; Strobbia *et al.* 2015) or single station measurements (HVSR, Nakamura 1989). Passive methods are powerful and cost effective, but they could suffer from a non-uniform distribution of noise sources and can be biased by 2D site effects (Claprood & Asten 2010). Travel-time tomography use signals from earthquakes or low-frequency seismic ambient noise to retrieve deep geological structures. Barbellini *et al.* (2017) propose that the reference bedrock depth of deep alluvial basins could be extrapolated using regional models inferred from travel-time seismic tomography. However, since tomographic approaches are orientated to large scale modelling, retrieved models are sufficiently accurate at depth (i.e. at the kilometric scale), but they often do not present enough resolution for local-scale seismic waveform studies, as needed for local hazard assessment and evaluation of earthquake scenarios.

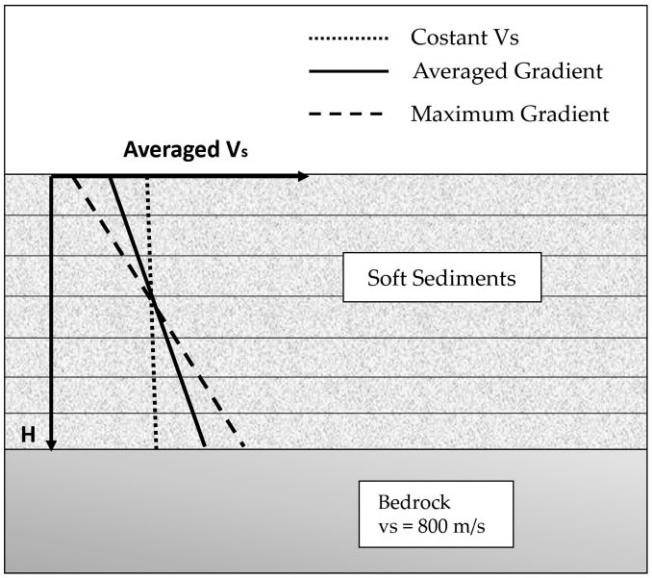

Figure 1. Extrapolation of V_S profiles with linear gradients suggested by the Italian Seismic Code (ICMS 2018, modified).

As matter of fact, the V_S profile characterising the soil column may be accurate for the first tens of metres, thanks to local geophysical/geotechnical surveys, and at few kilometres deep if regional tomographic models are available. However, the velocity structure between the uppermost velocities (e.g. Vs_{30}) and the engineering bedrock ($V_S \geq 800$ m s^{-1}) may be not accurately defined, especially in deep alluvial basins. The most adopted ground motion modelling approaches, such as the 1D seismic site response, need the complete characterisation of the soil column, at least until the reference engineering bedrock depth. For these reasons, several seismic codes propose simplified approaches to describe the soil column. The Italian Seismic Code (ICMS 2018), for example, proposes an extrapolation of V_S in depth through linear gradients with different slopes (depending on the geological site conditions) until the depth of the engineering bedrock depth (figure 1).

It is known that the seismic motion can be decomposed in different sets of waves such as body waves (P, SH, SV) or surface waves (Rayleigh, Love), and seismic motion amplification may be different. However, it is common practice in earthquake engineering design norms focusing of the effect of near-surface geology for vertically propagating shear body waves (see Eurocode 8, European Committee for Standardisation 2004).

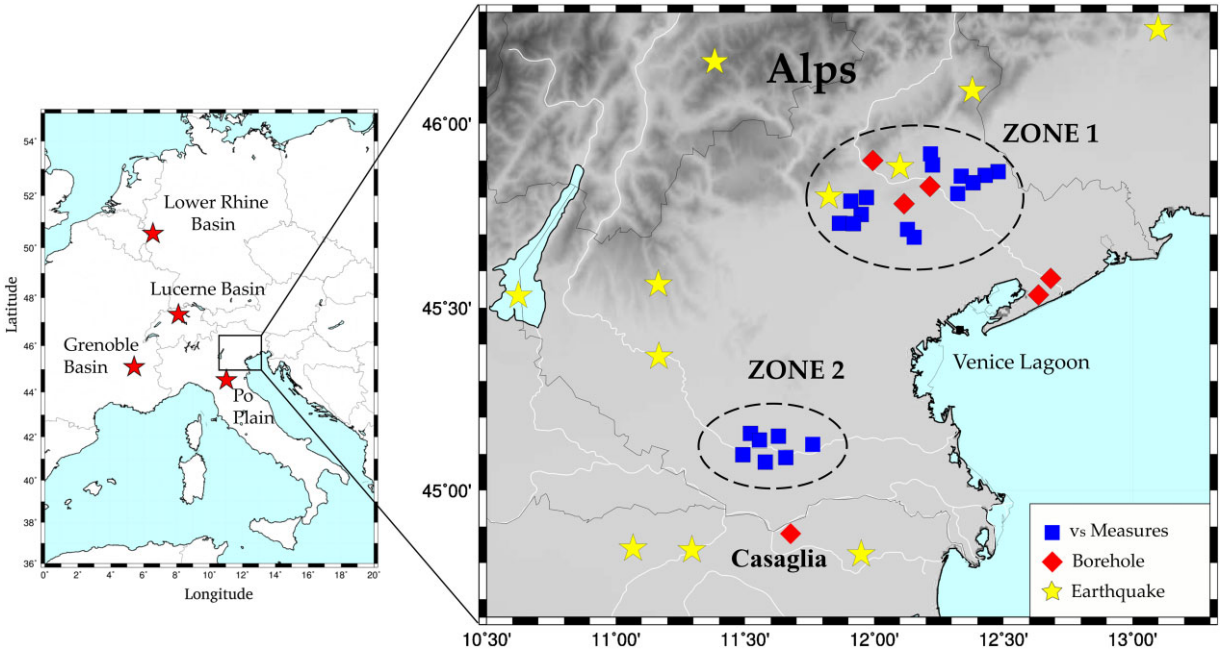

Figure 2. Left panel: Europe chart and deep alluvial basins' locations (red stars): Lower Rhine Basin (Germany); Lucerne Basin (Switzerland); Grenoble Basin (France) and the Po Plain (Italy). Right panel: zoom of Venetian Plain (Italy). Blue squares represent in situ measurement locations. Red diamonds represent ENI/AGIP deep boreholes. Yellow stars indicate the epicentre of the main seismic events from 1117 to 2012 ($5.5 > Mw > 6.8$).

In this study, we perform several 1D seismic site analysis in the Venetian Plain area (Northern Italy), a large and deep sedimentary basin (figure 2). In particular, we consider two different sectors where a detailed set of seismic surveys were performed to obtain shallow V_S profiles, while the deeper structures remain un-investigated. To fill the gap between the shallow and deeper V_S structures, we adopt general gradients, proposed for the modelling of several alluvial basins as the Lower Rhine Basin (Germany; Budny 1984), the Grenoble Basin (France; Guèguen *et al.* 2007) and the Lucerne Basin (Switzerland; Poggi *et al.* 2012). These sites (red stars in figure 2) are in fact characterised by deep sedimentary covers, similarly to the Venetian Plain.

To compare modelling and experimental data we analysed real seismograms coming from a borehole in the Po Plain, where deep and surface seismic recording stations were available. 1D seismic site response modelling was compared to the recording amplifications, testing different gradients.

We aim to assess how the choice of gradient can modify the seismic site response in deep sedimentary basins, where no information about the deeper structures is available. A realistic modelling of the ground motion is the key parameter for ground shaking scenario, used by civil engineers for the design of earthquake-resistant constructions. Due to the limited knowledge of the deeper velocity structures, it could be more appropriate to model the soil column with the gradient which enables the most conservative results in terms of ground motion effects. This study demonstrates the importance of the V_S gradient on ground motion scenarios and the results are relevant for seismic hazard evaluation in deep sedimentary basins, which host large urban environments around the world.

2. Study area: the Venetian Plain

Our study area is the Venetian Plain region (Northern Italy), a large syntectonic alluvial basin actively affected by earthquake occurrence (figure 2). Together with the Po Plain, the Venetian Plain represents the foreland of the S-verging central-southern Alps and the N-NE-verging northern Apennine belt (Doglioni 1993). The effect of the north-propagating Apennine foredeep started in the late Miocene affecting the southern sectors of the Venetian Plain and led to a regional southward tilting recorded up to Venice Lagoon. The thickness of Quaternary formations varies from 2 km in the southern part of the Venice Lagoon, and gradually pinches out eastward (Carminati *et al.* 2003). The buried active fronts of Northern Apennines and Southern Alps are considered seismic sources capable of destructive earthquakes (Poli *et al.* 2008). The epicentre distribution of historical and instrumental earthquakes is shown in figure 2. Although the seismicity is concentrated along the foothills area of the Southern Alps and the Northern Apennines, it is widely recognised that the Venetian Plain is influenced by strong seismic site effects (Vuan *et al.* 2011).

The 3D structural models of the Venetian Plain are principally based on old geophysical information from oil explorations (Doglioni 1993). They are also based on the

TRANSALP (TRANSALP Working Group 2002), a deep seismic reflection measurement collected in the Eastern Alps (Cassinis 2006).

In this study, we consider two different sectors of the Venetian Plain with different Quaternary sedimentary fillings: the 'high' (Northern) and 'low' (Southern) plain, where several shallow V_S measurements were performed (figure 2). The high plain or pre-Alpine zone, here called ZONE 1, has a fluvial and glacial origin and is principally composed of gravel (Carraro *et al.* 2015). The low plain, hereafter ZONE 2, extends from the gravel deposits transition to the Adriatic coast; the subsoil is composed mainly of silt and clay layers with intercalations of sandy layers (Carraro *et al.* 2015).

3. Method

In this work, we simulate the 1D seismic site response of two sectors of the Venetian Plain: the ZONE 1, representing the pre-Alpine sector of the alluvial plain characterised by coarse deposits; the ZONE 2, representing the alluvial plain sector with sandy-clay formations (figure 2). We analyse different sedimentary deposits with a wide granulometry range, which cover an important breadth of different soil types.

In seismic engineering practice, the deep alluvial basin environments are usually represented with 1D geometry of horizontal layering, allowing 1D seismic analysis. With STRATA software (Kottke & Rathje 2009), it is possible to perform stochastic seismic site response analysis with the equivalent-linear approach (Kramer 1996), assuming horizontal soil layer boundaries with an infinite lateral extension and vertically propagating horizontally polarised shear waves (SH waves).

In particular, STRATA code needs: (i) input motions (acceleration time histories); and (ii) soil properties down to the engineering bedrock: the V_S profiles, shear-modulus (G) and damping ratio (D) non-linear curves (Schnabel *et al.* 1972; Idriss & Sun 1992; Boaga *et al.* 2012, 2013), and total unit weight.

In section 4 we illustrate numerical simulations based on the effects of the different type of gradients on 1D seismic analysis. In section 5 we compare the results of a 1D seismic site response with different gradients and real data collected in the Casaglia site (figure 2). In this site, a borehole equipped with two broadband seismometers (a deep and a surface stations) was available (Pesaresi *et al.* 2014).

4. Numerical simulations

4.1. Input motions

The seismic site response analysis requires the definition of seismic input terms of acceleration time series. The waveforms can be previously recorded accelerograms belonging to a seismic database, such as the European Strong Motion Database. We select a target response spectrum considering the local probabilistic seismic hazard analysis of the Veneto Region (Northern Italy). We adopt an average expected acceleration of 0.13 g with 10% of probability of non-exceedance in 50 years for a return period of 475 years (Italian Seismic Hazard Map, Gruppo di Mappa di Pericolosità Sismica [GdL MPS] 2004) (figure 3a). We use the Rexel program (Iervolino *et al.* 2009) to select a set of one-component real accelerograms. The research criteria consist of an upper and lower tolerance, with respect to the target spectrum, of 30 and 10%, respectively, in a time range between 0.15 and 2 seconds. Three accelerograms are finally selected for our simulation (figure 3b).

4.2. Definition of V_S profiles

We model the soil columns combining a detailed shallow V_S profile (down to 30 m) obtained through geophysical surveys and V_S gradients proposed in literature to model deeper layers in alluvial basins. These gradients are adopted when no information is available and an extrapolation until the bedrock depth is required.

4.2.1. Shallow V_S profiles. To characterise the two sites of the Venetian Plain (ZONE 1 and ZONE 2), some geophysical testing campaigns were carried out, including 31 MASW and 36 Re.Mi. surveys. In figure 2 the blue squares represent the locations of the geophysical measurements. The resulting 67 V_S profiles, down to 30 m, are plotted in figure 4. From the plot, it is possible to clearly distinguish between the higher V_S formations in ZONE 1, characterised by coarse sediments, and the lower V_S in ZONE 2 where sand formations are prevalent. The different granulometric distribution of the two study sectors are also confirmed by a deep exploration boreholes log, close to the geophysical measurement locations (red diamonds in figure 2), available on the ViDEPI website (videpi.com). The average V_S profiles for the ZONE 1 and the ZONE 2, marked by red lines in figure 4, match with the velocity structure proposed in the Eurocode 8 (European Committee for Standardisation 2004) for gravelly and sandy soils, respectively. The averaged V_S profiles enable construction of the first 30 m of the 1D soil columns representatives of the two sectors of the Venetian Plain.

4.2.2. Deep Vs profiles. We model the deeper layers (below 30 m until the engineering bedrock) of the 1D soil columns with V_S gradients found in literature. The velocity gradients used in this study are meant to be used for generic deep alluvial basins, characterised by an average sedimentary cover that, in terms of seismic velocity, is similar to the shallow geological formations of the Venetian Plain. Seven different gradients are selected that we will refer to as: EXP (Exponential); PAR (Parabolic); SQR (square root trend); LIN

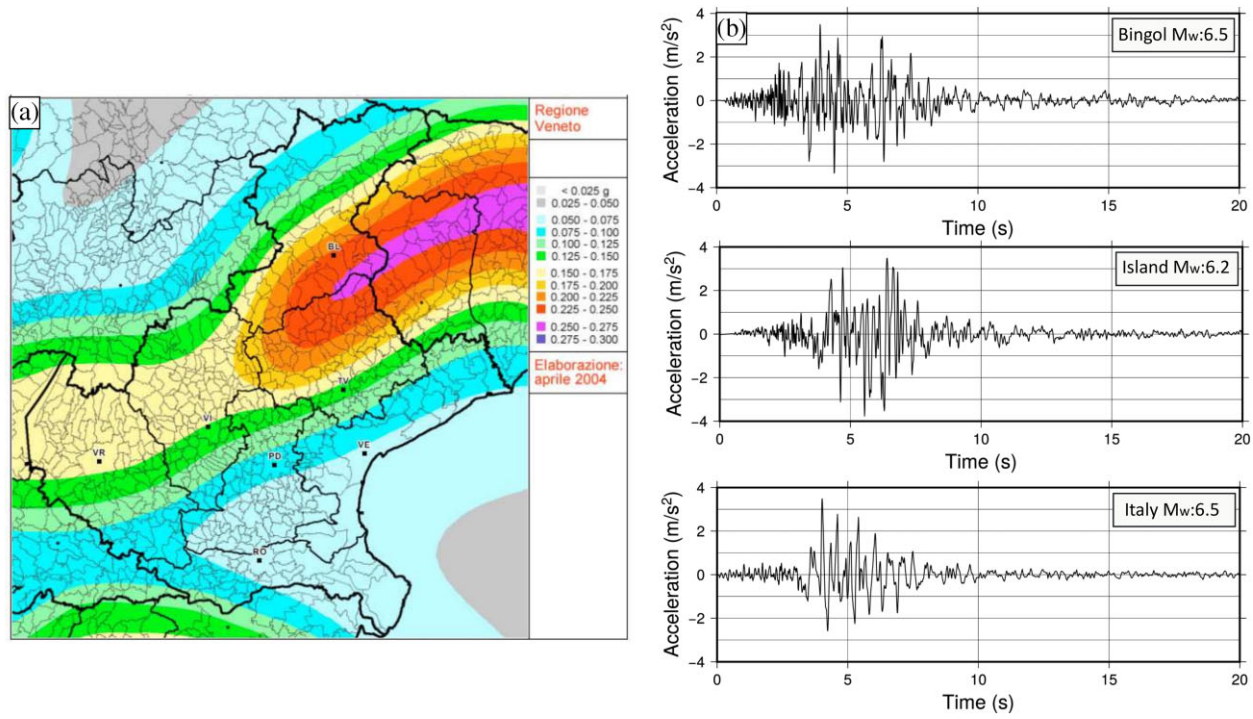

Figure 3. (a) Seismic hazard map of Veneto region, Italy (Italian Seismic Hazard Map, Gruppo di Mappa di Pericolosità Sismica (GdL MPS) 2004, modified). (b) The three-real selected accelerograms used as input motion in our stochastic 1D seismic site response simulations.

(linear); GEN1 and GEN2, (Generics) and HYP, (Hyperbolic). The adopted gradients can be subdivided in two categories. Gradients that do not include the bedrock depth parameter to model the V_S profile (EXP, PAR, SQR) fall into the first category. These gradients make it possible to define the engineering bedrock at different depths, depending on the selected gradient shape. Gradients that include the a priori information of the bedrock depth (LIN, GEN1, GEN2, HYP) belong to the second category.

Considering the geological context of the Venetian Plain, there is no evidence in the literature of the bedrock depth in ZONE 1, while the ZONE 2 was recently investigated by Mascandola *et al.* (2019), who mapped the engineering bedrock of the Po Plain that represents the southern propagation of the Venetian Plain (figure 2). On the basis of the available information, we can model the soil columns of the ZONE 1 with gradients belonging to the first category, while the ZONE 2 is modelled with gradients belonging to the second category, fixing the engineering bedrock at 400 m deep (Mascandola *et al.* 2019).

The theoretical gradients used in this study are described next. In equation (1), the v_0 parameter represents the V_S at the ground surface ($z = 0$).

EXP: Exponential gradient defined as:

$$V_s(z) = V_0(1+z)^x, \quad (1)$$

where x is an exponential coefficient controlling the dependence of velocity with the depth z ($0 < x < 1$). This equation holds for granular media only. Saturation level, fluid pressure and cementation can affect the exponent x (Albarello *et al.* 2011). This is the most common form of the V_S gradients, used to model tectonic basins such as Lower Rhine Basin (Germany) (Budny 1984). In particular, to better define the parameter x for ZONE 1, we use the value found by Budny (1984) for coarse sedimentary cover, equal to 0.285 (yellow curve in figure 5a)

PAR: Parabolic gradient defined as:

$$V_s(z) = V_0\,\sigma_{v0}^{p}, \quad (2)$$

where σ_{v0} represents the total vertical overburden stress (considering a constant value of the soil unit weight) and p is a model parameter, generally varying between 0.1 and 0.3 (Andreotti *et al.* 2018). Equation (2) allows the modelling of a parabolic profile of V_S and is proposed for sedimentary basins by Santamarina *et al.* (2001). To link this curve to the shallow profile we set $\sigma_{v0} = 20\ \mathrm{kN/m^3}$, which is the total unit weight adopted for the 1D soil columns analysed in this study. The p parameter is set to 0.15 (reference value as suggested by Andreotti *et al.* 2018; red curve in figure 5a).

SQR: V_S as a function of the square root of the depth, in the equation:

$$V_s(z) = V_0 + \alpha\sqrt{z}, \quad (3)$$

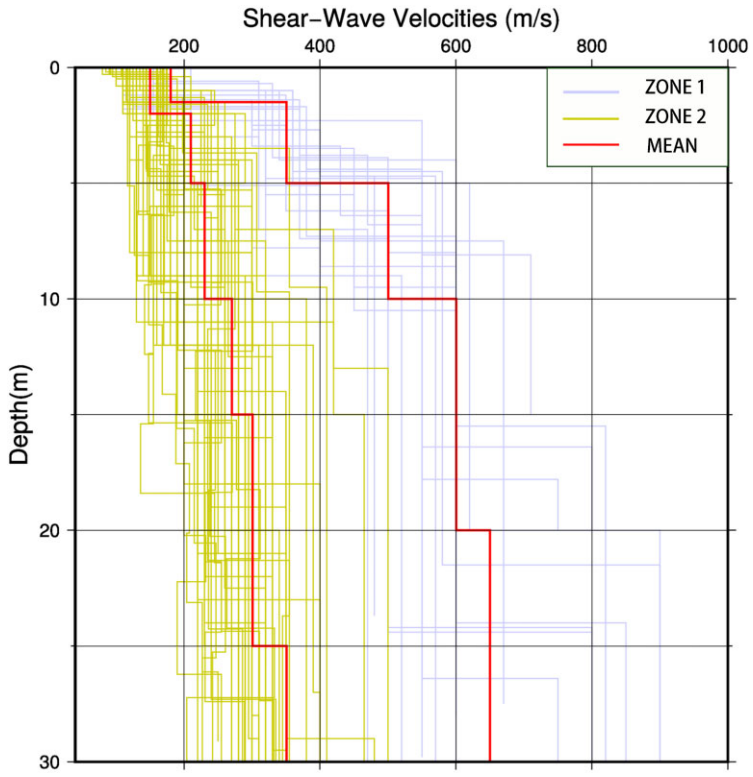

Figure 4. The 67 V_S profiles inferred from geophysical measurements in ZONE 1 (yellow) and ZONE 2 (blue). The red lines represent the mean V_S profiles for the two zones, representative of the shallow part (0–30 m) of the soil columns.

where α is a constant (Guèguen *et al.* 2007). This gradient is considered as a polynomial variation with depth. This equation represents a benchmark basin velocity model inferred from borehole data in Grenoble Basin (France), an Alpine basin with a maximum depth of more than 1 km. It is characterised by a Quaternary infill of coarse glacial deposits, which in terms of velocity is similar to the sedimentary cover of the high Venetian Plain. In our model, we set α equal to 19, which is a reference value taken from Guèguen *et al.* 2007 (purple curve in figure 5a).

LIN: Linear gradient, defined as

$$V_s(z) = mz + q. \tag{4}$$

This is the easiest interpolation between the shallow subsoil ($V_{S\,min}$) and bedrock ($V_{S\,max} = 800$ m s^{-1}). This simplified approach is currently suggested by the Italian Seismic Code (2018) (figure 1). We obtain the linear coefficients with a simple interpolation between the average shear-wave velocity at 30 m deep ($V_{S\,min} = 350$ m s^{-1}) and the bedrock velocity at 400 m deep. This results in a slope of $m = 1.21$ and an intercept of $q = 313.51$ m s^{-1} (dashed red line in figure 5b).

GEN1: The velocity gradient proposed by Régnier *et al.* (2016)

$$V_s(z) = V_{s\,min} + (V_{s\,max} - V_{s\,min}) \left(\frac{z - z_0}{z_2 - z_0} \right)^a. \tag{5}$$

This gradient is used to model simple soil conditions, where V_S increase regularly with depth. $V_{S\,min}$ and $V_{S\,max}$ are the expected minimum and maximum shear-wave velocities, z_0 is the depth of the shallower low velocity layer and z_2 is the bedrock depth. The parameter a is an exponent set equal to 0.25, a reference value taken from Régnier *et al.* (2016). In our model, z_0 is equal to 30 m, z_2 is equal to 400 m; $V_{S\,min}$ and $V_{S\,max}$ are equal to 350 and 800 m s^{-1}, respectively (dashed yellow curve in figure 5b).

GEN2: Generic V_S gradient

This relationship was proposed by Poggi *et al.* (2012) for aseismic characterisation of the Alpine environment in Lucerne Basin (Switzerland). The gradient equation is

$$V_s(z) = (V_{s\,max} - V_{s\,min}) \left[1 - a^{\frac{z_0 - z}{b}} \right] + V_{s\,min}. \tag{6}$$

This equation, similar to GEN 1, adopts curvature coefficients, a and b, which in our model are set to 2.3 and 81.7, so that the basement is reached at 400 m depth (dashed purple curve in figure 5b).

HYP: Hyperbolic profile

This gradient represents the second Gibson model (Gibson 1967). The proposed gradient equation is

$$V_s(z) = V_0 \sqrt{\frac{z_2}{z_2 - z}}, \tag{7}$$

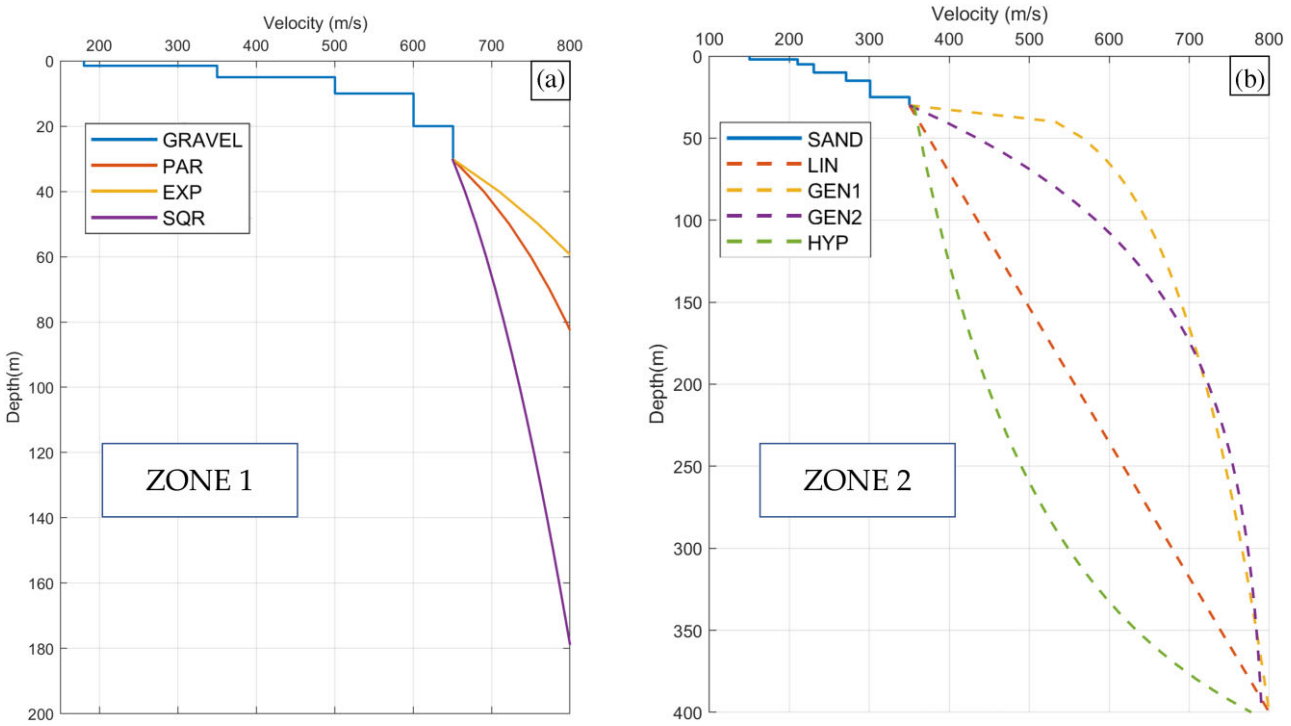

Figure 5. Velocity models adopted for 1D seismic site response for (a) ZONE 1 (case with unknown bedrock depth) and (b) ZONE 2 (case with bedrock depth $z_2 = 400$ m).

where z_2 is the bedrock depth (in our case $v_0 = 350$ m s^{-1} and $z_2 = 400$ m) (dashed green curve in figure 5b).

4.3. *Stochastic 1D seismic analysis*

The entire 1D soil columns with discretised layers are defined to compute the seismic site analysis. We analyse the different velocity profiles shown in figure 5a,b. The shallow layers correspond to the average V_S profiles as indicated in figure 4, while the deeper layers are obtained by discretising the V_S gradient curves with 10-m thick intervals.

The non-linear soil properties are generally represented with a shear-modulus reduction (G/G_{max} V_S shear strain) and damping ratio (D V_S shear strain) curves. In our case, the subsoil is modelled using the modulus reduction and damping curves as proposed by Idriss (1991) for gravel with a total unit weight of 20 kN/m^3 for the soil column of ZONE 1 (solid curves in figure 6a,b). The soil profile characterising the ZONE 2 is modelled with the non-linear curves as proposed by Seed *et al.* (1986) for sandy silt with a total unit weight of 19 kN/m^3 (dashed curves in figure 6a,b).

Once the stratigraphic models are defined, a stochastic analysis via Monte Carlo simulation is performed to consider the local variability. The method consists of an iterative calculation of a deterministic model defined with a set of random realisations. The input parameters are randomly generated on the basis of previously defined probability distributions. In this way, it is possible to simulate the sampling process of a real population to consider the uncertainty of the measurements. In our study, we randomize only the shallow V_S profile in the first 30 m, considering the standard deviation inferred from the statistical distribution of the 67 V_S profiles obtained by *in situ* measurements (figure 4).

The variability of the shallow soil profiles adopted for the stochastic analysis is displayed in figure 7 parts a,b, which illustrate 100 V_S profiles randomly generated. During the simulations, the set of accelerograms described previously (shown in figure 3b) are used as the inputs at the bottom of each soil column. Thus, we perform 300 Monte Carlo simulations for each soil column (100 realisations for each of the three acceleration time histories), for a total of 2100 simulations.

4.4. *Results*

The results, derived from the stochastic 1D seismic site response analysis through Monte Carlo simulations, are presented in terms of surface acceleration response spectra (with a damping ratio, ξ, of 5%), peak ground accelerations (PGA) and Housner Spectrum Intensity (Housner 1952). This last parameter is defined as

$$S_I(\xi) = \int_{0.1}^{2.5} Sv\,(\xi, T)\,\mathrm{dT}. \qquad (7)$$

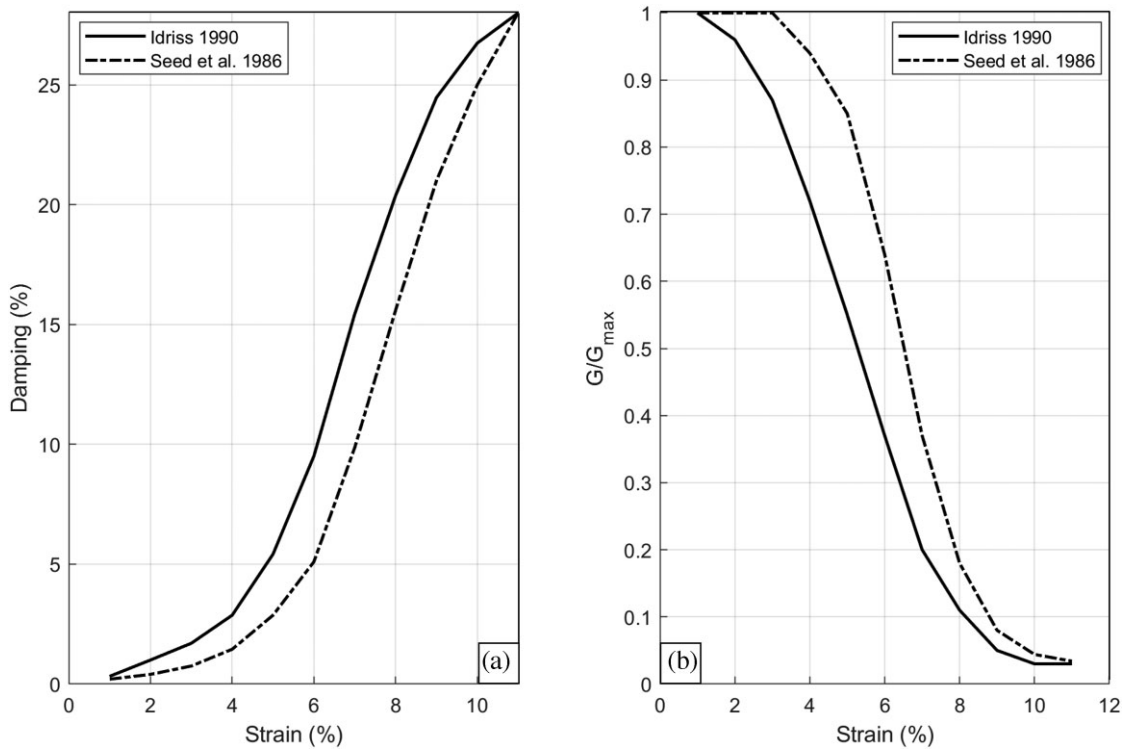

Figure 6. (a) Shear modulus and (b) damping curves adopted for 1D seismic site response of ZONE 1 (Idriss 1991) and ZONE 2 (Seed *et al.* 1986).

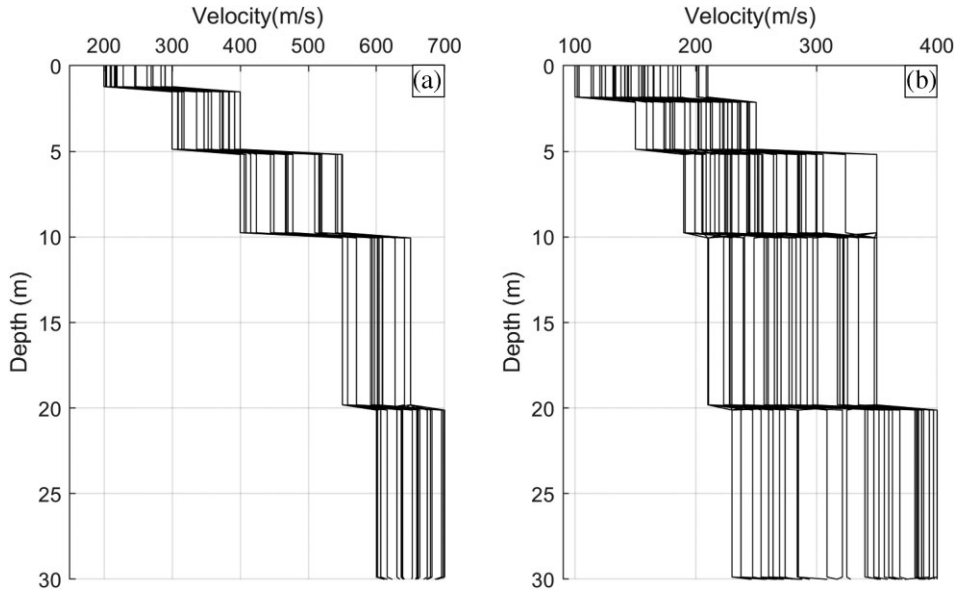

Figure 7. Example of 100 realisations of V_S profiles for (a) ZONE 1 and (b) ZONE 2.

The time integral considers the area under the pseudo-velocity response spectra S_v over the period range T between 0.1 and 2.5 s, with a damping ratio (ξ) of 5%. This is an important parameter (expressed in cm), commonly adopted to evaluate the seismic input energy and buildings damage capacity (Housner 1952).

STRATA software generates different outputs such as the acceleration time histories and the response spectra. The PGA and Housner Intensity are calculated a posteriori.

The resulting spectral acceleration curves for ZONES 1 and 2 are shown in figure 8 parts a and b, respectively. They are computed as the mean of all Monte Carlo simulations. Each curve is normalised to the common initial value of spectral acceleration, which is equal to 0.1 *g*. The response spectra obtained from the simulation of the velocity gradients of

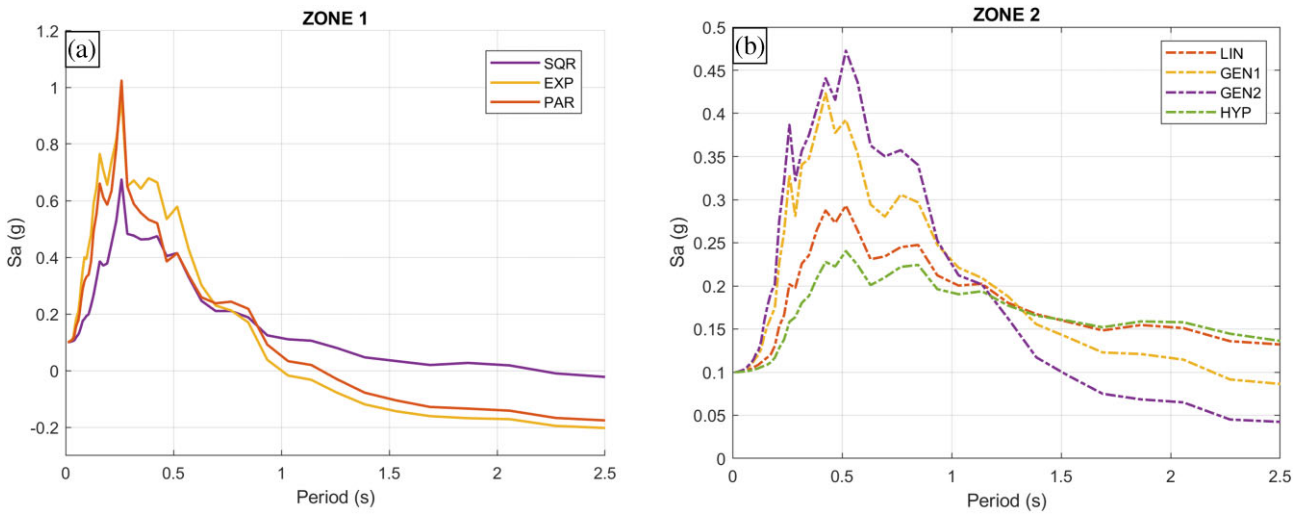

Figure 8. Mean response spectra at the ground surface for the different velocity gradients used to define the V_S profiles in (a) ZONE 1 and (b) ZONE 2.

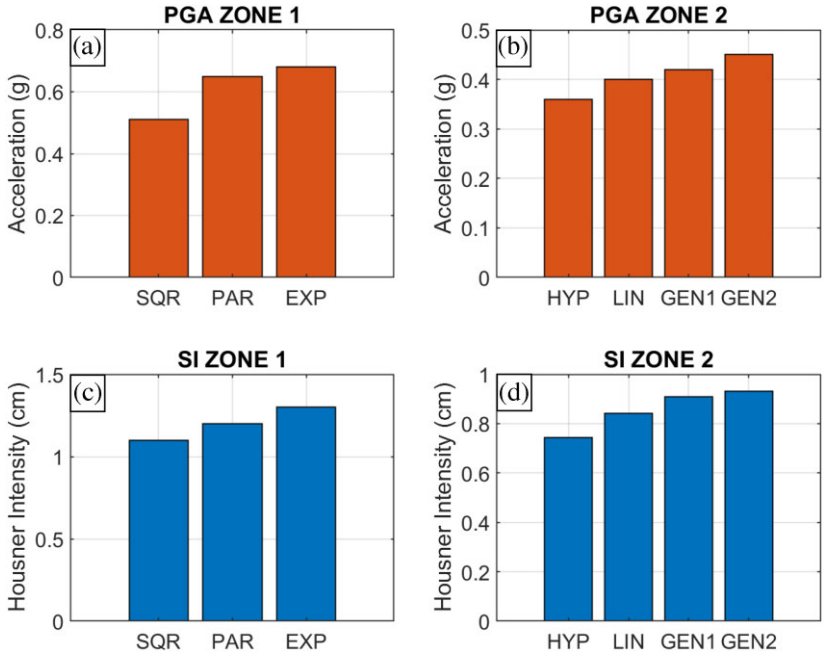

Figure 9. PGA (a, b) and Housner Spectrum Intensity SI (c, d) values, inferred from the simulations.

ZONES 1 and 2 show significant amplifications in the period range of engineering interest, with high amplifications at low periods. The peak value of spectral acceleration increases gradually from 0.64 *g* to 1.3 *g* for ZONE 1 and from 0.25 *g* to 0.48 *g* for ZONE 2**.**

It is possible to observe the same relative differences in PGA values (figure 9). In particular, the values of PGA span from 0.51 *g* to 0.68 *g* for ZONE 1 (figure 9a), and between 0.36 *g* and 0.45 *g* for ZONE 2 (figure 9b).

Figure 9 shows the Housner Spectrum Intensity values inferred from the spectra for each velocity gradient adopted in this study. The Housner Spectrum Intensities range between 1.1 and 1.3 cm for ZONE 1 (figure 9c), and between 0.74 and 0.93 cm for ZONE 2 (figure 9d).

5. Comparison with real accelerograms

In this section, we compare the results of 1D seismic site response and real data collected in Casaglia site where a borehole was available (see location in figure 2). The borehole is located in Po alluvial plain (the geological context called 'ZONE 2' in this study). The borehole reaches the Quaternary basement at 132 m deep. The sedimentary coverage is represented by Holocenic alluvial deposits, varying from clay

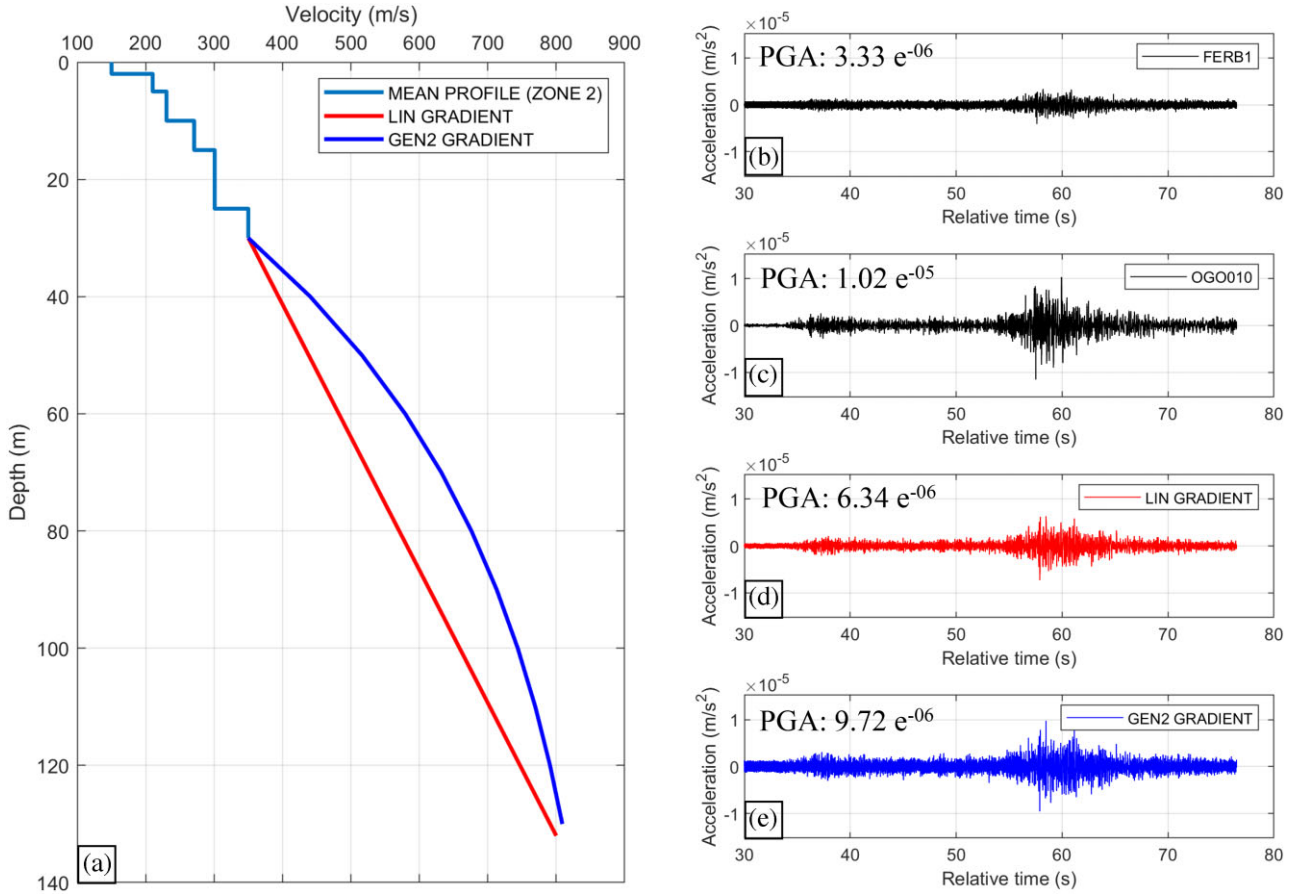

Figure 10. (a) Shear-wave velocity structures used as model for the alluvial sedimentary cover in Casaglia site (see figure 2). (b) Accelerogram of the seismic event occurred on 12 February 2013 recorded by the borehole seismic stations (FERB); (c) the same seismic event recorded by the surface station located at the top of the borehole (OG010); (d) simulated accelerogram inferred from a linear gradient LIN and (e) simulated accelerogram inferred from an exponential gradient GEN2.

to coarse loose sand poorly compacted. The site can be classified as soft soil, according to cross-hole and down-hole measurements by Pesaresi *et al.* (2014).

On the basis of this specific stratigraphic information until 132 m deep, we model the 1D shear-wave velocity structure. The first 30 m are modelled with the mean V_S profile that characterise ZONE 2 (figure 4). The engineering bedrock depth is assumed to be at 132 m, as suggested by the stratigraphic log, so the deeper velocity structures are extrapolated with LIN and GEN2 gradients (equations (4) and (6)). The V_S profiles adopted for seismic site response are shown in figure 10a.

The borehole was equipped with two broadband seismometers, one at the surface (OG010, a Lennartz velocimeter) and the other at a depth of 135 m, within the Quaternary basement (FERB, a Guralp CMG-3TB seismometer). The available recorded waveforms refer to an aseismic event that occurred on 12 February 2013, with $M_L = 3.8$ and an epicentral distance of 170 km (Pesaresi *et al.* 2014). The east-component waveforms (expressed in m s^{-1}) are converted in accelerograms and are shown in figure 10b and c, with their corresponding PGAs. It is worth noticing that the PGA recorded by the borehole station is smaller than the one recorded by the surface station, due to the soft layer amplification of motion.

To compare different *Vs* gradients, the waveform recorded by the borehole station was used as input motion for the 1D seismic site response computed with STRATA software. Figure 10c and d show the simulated accelerograms for the LIN and GEN2 gradients. The computed PGAs are also displayed. As expected, the linear gradient LIN (as suggested by the norms) underestimates the amplification effects, with a variation of the amplification effects of 43%. On the contrary, the synthetic accelerogram computed with the non-linear gradient GEN2 is characterised by a PGA value similar to the real ones recorded at the surface.

6. Discussions and conclusion

In this study, we compute the 1D seismic site response of two sectors of the Venetian Plain, where deep V_S profiles are

unknown, adopting several shear-wave velocity gradients found in literature. Our study demonstrates how the choice of the velocity gradient curves has a significant impact on the seismic site response in terms of PGAs, Spectral Accelerations and Housner Intensities. These three parameters are fundamental for strong ground motion prediction and they are the most adopted in engineering aseismic design. We consider two sectors of the Venetian Plain: ZONE 1 with gravel formations and an unknown bedrock depth and ZONE 2 with sandy-clay formations and a known bedrock depth.

In ZONE 1, where the bedrock depth is unknown, the choice of the velocity gradient determines the engineering bedrock depth, ranging between 60 and 180 m (figure 5a). In this case, the different results depend mainly on the variable thickness of the soft sedimentary layer, which is excited by the seismic input during the simulation. In particular, it is possible to observe a decrease in the amplification effects with the increase of the bedrock depth. The results related to the EXP gradient (equation (1)) present the highest amplifications, being in these terms the most conservative for the prediction of the seismic action (figures 8a and 9a,c).

In ZONE 2, where the bedrock depth is known, the soft soil column has a constant thickness of 400 m, but the shape of the velocity profiles between the 30 m and the engineering bedrock is significantly different (figure 5b). In this case, the stochastic simulation based on the use of different velocity gradients shows differences up to 20%. The smaller site response is associated to the LIN and HYP gradients (equations (4) and (7)), characterised by lower values of V_S, e.g. softer soils (figures 8b and 9b,d). The softer sites are able to accumulate larger strains and experience more damping. In particular, considering the case of a thick soil column, the damping is much more pronounced; thus, in this condition, the attenuation phenomena become dominant (Boaga *et al.* 2015).

Keeping a conservative approach for seismic design, it appears more appropriate to model the soil column with GEN1 or GEN2 gradients (equations (5) and (6)), which allow us to obtain the highest values of PGA, Spectral Acceleration and Housner Spectrum Intensity.

We evaluate the effect of the V_S gradient choice also considering real seismic data recorded at 135 m deep and at the surface in a borehole located in the Po Plain. In this way, we investigate the site amplification of the sedimentary columns between the down-hole and surface station, modelled with different types of gradients. The linear gradient method (as suggested by several seismic design norms) here again underestimates the seismic site amplification, while the non-linear gradient GEN2 reliably estimates the site amplification effect (figure 10a,d,e). This experimental study case confirms the importance of choosing an appropriate gradient in alluvial plains for an estimation of seismic effects. However, the only available accelerograms for the 1D seismic site response analysis of Casaglia site are characterised by small acceleration values, thus it could be difficult to establish the real implication for a structural aseismic design.

To avoid estimation errors induced by an arbitrary choice of the velocity gradient, the regional deep basin structure should be determined through deep geophysical investigations (e.g. seismic reflection surveys, passive surface wave techniques, etc.). When these seismic surveys are not logistically possible, it seems more appropriate to model the soil column with the V_S gradient which allows obtaining the most conservative approach, i.e. stronger seismic ground motion.

Acknowledgement

The authors thank Dr Damiano Pesaresi who provide the seismic data recorded at Casaglia site.

Author Contributions

All authors contributed to the study conception and design. Material preparation, data collection and analysis were performed by Valeria Cascone, Ilaria Barone and Jacopo Boaga. The first draft of the paper was written by Valeria Cascone and all authors commented on previous versions of the paper. All authors read and approved the final paper.

Conflict of interest statement. The authors declare no conflicts of interest.

References

Albarello, D., Cesi, C., Eulilli, V., Guerrini, F., Lunedei, E., Paolucci, E. & Puzzilli, L. M., 2011. The contribution of the ambient vibration prospecting in seismic microzoning: an example from the area damaged by the April 6, 2009 L'Aquila (Italy) earthquake, *Bollettino di Geofisica Teorica e Applicata*, **52**, 513–538.

Andreotti, G., Famà, A & Lai, C.G., 2018. Hazard-dependent soil factors for site-specific elastic acceleration response spectra of Italian and European seismic building codes, *Bulletin of Earthquake Engineering*, **16**, 5769–5800.

Barbellini, A., Morelli, A & Ferreira, A.M., 2017. Crustal structure of northern Italy from the ellipticity of Rayleigh waves, *Physics of the Earth and Planetary Interiors*, **265**, 1–14.

Boaga, J., 2013. An efficient tool for cultural heritage seismic soil classification: frequency-time analysis method in Venice historical center and its lagoon (Italy), *Geosciences Journal*, **17**, 301–311.

Boaga, J., Renzi, S., Deiana, R. & Cassiani, G., 2015. Soil damping influence on seismic ground response: a parametric analysis for weak to moderate ground motion, *Soil Dynamics and Earthquake Engineering*, **79**, 71–79.

Boaga, J., Vignoli, G. & Cassiani, G., 2012. Shear wave profile from surface wave inversion: the impact of uncertainty on seismic site response analysis, *Journal of Geophysics and Engineering*, **9**, 244–246.

Boore, D.M., Joyner, W.B. & Fumal, T. E., 1993. Estimation of response spectra and peak accelerations from western North American earthquakes. Technical report.

Borcherdt, R.D., 1994. Estimates of site-dependent response spectra for design (methodology and justification), *Earthquake spectra*, **10**, 617–653.

Budny, M., 1984: *Seismische Bestimmung der bodendynamischen Kennwerte von oberflächennahen Schichten in Erdbebengebieten der Niederrheinischen Bucht und ihre ingenieurseismologische Anwendung. PhD thesis*, Geologisches Institut der Universität zu Köln.

Building Seismic Safety Council-BSSC. 2003. NEHRP-recommended provisions for seismic regulations for new buildings and other structures, *Federal Emergency Management Agency- Fema*, **302**, 303.

Cardarelli, E., Cercato, M. & De Donno, G., 2018. Surface and borehole geophysics for the rehabilitation of a concrete dam (Penne, Central Italy), *Engineering Geology*, **241**, 1–10.

Carminati, E., Doglioni, C. & Scrocca, D., 2003. Apennines subduction-related subsidence of Venice (Italy), *Geophysical Research Letters*, **30**, 47–50**.**

Carraro, A., Fabbri, P., Giaretta, A., Peruzzo, L., Tateo, F. & Tellini, F., 2015. Effects of redox conditions on the control of arsenic mobility in shallow alluvial aquifers on the Venetian Plain (Italy), *Science of the Total Environment*, **532**, 581–594.

Cassinis, R., 2006. Reviewing pre-TRANSALP DSS models, *Tectonophysics*, **414**, 79–86.

Chong, J. & Ni, S., 2009. Near surface velocity and Q_S structure of the Quaternary sediment in Bohai basin, China, *Earthquake Science*, **22,** 451–458.

Claprood, M. & Asten, M.W, 2010. Statistical validity control on SPAC microtremor observations recorded with a restricted number of sensors, *Bulletin of the Seismological Society of America*, **100,** 776–791.

Doglioni, C., 1993. Some remarks on the origin of foredeeps, *Tectonophysics*, **228**, 1–20.

European Committee for Standardization, 2004. Eurocode 8: Design of structures for earthquake resistance, P1: General rules, seismic actions and rules for buildings, Draft 6, Doc CEN /TC250/SC8/N335.

Faccioli, E., Paolucci, R. & Vanini, M., 2015. Evaluation of probabilistic site-specific seismic-hazard methods and associated uncertainties, with applications in the Po Plain, northern Italy. *Bulletin of the Seismological Society of America*, **105**, 2787–2807.

Gibson, E., 1967. Some results concerning displacements and stresses in a non-homogeneous elastic half-space. *Geotechnique*, **17**, 58–67.

Gruppo di Lavoro, ICMS, 2018. Indirizzi e criteri per la microzonazione sismica. In *Conferenza delle Regioni e delle Provincie autonome. Dipartimento della protezione civile*, (Vol. 3) Roma.

Gruppo di Mappa di Pericolosità Sismica (GdL MPS), 2004. *Redazione della mappa di pericolosità sismica prevista dall'Ordinanza PCM 3274 del 20 marzo 2003, Rapporto conclusivo per il dipartimento di Protezione Civile*, INGV, Milano, Roma, 65 pp., available at http://zonesismiche.mi.ingv.it

Guéguen, P., Cornou, C., Garambois, S. & Banton, J., 2007. On the limitation of the H/V spectral ratio using seismic noise as an exploration tool: application to the Grenoble valley (France), a small apex ratio basin. *Pure and Applied Geophysics*, **164**, 115–134.

Housner, G.W., 1952. *Intensity of Ground Motion during Strong Earthquakes*. California Institute of Tech Pasadena Earthquake Engineering Research Laboratory.

Hunter, J.A., Benjumea, B., Harris, J.B., Miller, R.D., Pullan, S.E., Burns, R.A. & Good, R.L, 2002. Surface and downhole shear wave seismic methods for thick soil site investigations, *Soil Dynamics and Earthquake Engineering*, **22**, 931–941.

Idriss, I., 1991. Earthquake Ground Motions at Soft Soil Sites. International Conferences on Recent Advances in Geotechnical Earthquake Engineering and Soil Dynamics. 3.

Idriss, I.M. & Sun, J.I., 1992. *SHAKE91: A Computer Program for Conducting Equivalent Linear Seismic Response Analyses of Horizontally Layered Soil Deposits*. Center for Geotechnical Modeling, Department of Civil and Environmental Engineering, University of California, Davis, CA.

Iervolino, I., Galasso, C. & Cosenza, E., 2009. REXEL: computer aided record selection for code-based seismic structural analysis. *Bulletin of Earthquake Engineering*, **8**, 339–362.

Kottke, A.R. & Rathje, E.M., 2009. *Technical Manual for Strata*. PEER Report, Pacific Earthquake Engineering Research Center

Kramer, S. L., 1996. *Geotechnical Earthquake Engineering*. Prentice Hall, Upper Saddle River, N.J

Lacoss, R.T., Kelly, E.J. & Toksöz, M.N., 1969. Estimation of seismic noise structure using arrays. *Geophysics*, **34**, 21–38.

Langston, C.A., 2003. Local earthquake wave propagation through Mississippi embayment sediments, part I: body-wave phases and local site responses. *Bulletin of the Seismological Society of America*; **93**, 2664–2684.

Louie, J.N., 2001. Faster, better: shear-wave velocity to 100 meters depth from refraction microtremor arrays. *Bulletin of the Seismological Society of America*, **91**, 347–364.

Martin, G.R. & Dobry,, R., 1994. Earthquake site response and seismic code provisions, *NCEER Bulletin*, **8.4**, 1–6.

Mascandola, C., Massa, M., Barani, S., Albarello, D., Lovati, S., Martelli, L. & Poggi, V., 2019. Mapping the seismic bedrock of the Po Plain (Italy) through ambient-vibration monitoring, *Bulletin of the Seismological Society of America*, **109**, 164–177.

Nakamura, Y., 1989. A method for dynamic characteristics estimation of sub-surface using microtremor on the ground surface, *Quarterly Report of Railway Technical Research Institute*, **30**, 25–33.

Norme Tecniche per le Costruzioni, 2008. Aggiornamento delle Norme tecniche per le costruzioni. *Gazzetta Ufficiale Serie Generale*.

Park, C.B., Miller, R.D., Xia, J., Ivanov, J., Hunter, J.A., Good, R.L. & Burns, R.A., 2000. Multichannel analysis of underwater surface waves near Vancouver, BC, Canada. In *SEG Technical Program Expanded Abstracts 2000*, pp. 1303–1306.

Pesaresi, D., Romanelli, M., Barnaba, C., Bragato, P.L. & Durì, G., 2014. OGS improvements in 2012 in running the North-eastern Italy seismic network: the Ferrara VBB borehole seismic station. *Advances in Geosciences*, **36**, 61–67.

Pitilakis, K., Alexoudi, M., Argyrodius, S. & Anastasiadis, A., 2006. Seismic risk scenarios for an efficient seismic risk management: the case of Thessaloniki (Greece). In *Advances in Earthquake Engineering for Urban Risk Reduction*, 229–244. Springer, Dordrecht.

Poggi, V., Fäh, D., Burjanek, J. & Giardini, D., 2012. The use of Rayleigh-wave ellipticity for site-specific hazard assessment and microzonation: application to the city of Lucerne, Switzerland, *Geophysical Journal. International* **188**, 1154–1172.

Poli, M.E., Burrato, P., Galadini, F. & Zanferrari, A., 2008. Seismogenic sources responsible for destructive earthquakes in north-eastern Italy. *Bollettino di Geofisica Teorica e Applicata*, **49**, 301–313.

Rathje, E.M., Kottke, A.R. & Trent, W.L, 2010. Influence of input motion and site property variabilities on seismic site response analysis. *Journal of geotechnical and geoenvironmental engineering*, **136**, 607–619.

Régnier, J., Bonilla, L.F., Bard, P.Y., Bertrand, E., Hollender, F., Kawase, H. & Boldini, D., 2016. International benchmark on numerical simulations for 1D, nonlinear site response (PRENOLIN): Verification phase based on canonical cases. *Bulletin of the Seismological Society of America*, **106**, 2112–2135.

Santamarina, J.C., Klein, K.A. & Fam, M.A., 2001. *Soils and Waves–Particulate Materials Behavior, Characterization and Process Monitoring*. Wiley, Chichester

Schnabel, P.B., Lysmer, J. & Seed, H.B., 1972. *SHAKE: A computer program for earthquake response analysis of horizontally layered sites*. Report No. EERC 72-12, Earthquake Engineering Research Center, University of California, Berkeley.

Seed, H.B., Wong, R.T., Idriss, I.M. & Tokimatsu, K., 1986. Moduli and damping factors for dynamic analyses of cohesionless soils. *Journal of Geotechnical Engineering*, **112**, 1016–1032.

Strobbia, C., Andreas, L., Vermeer, P. & Glushchenko, A., 2011. Surface waves: use them then lose them. Surface-wave analysis, inversion and attenuation in land reflection seismic surveying, *Near Surface Geophysics*, **9**, 503–513.

Strobbia, C., Boaga, J. & Cassiani, G., 2015. Double-array refraction microtremors. *Journal of Applied Geophysics*, **121**, 31–41.

TRANSALP Working Group, 2002. First deep seismic reflection images of the Eastern Alps reveal giant crustal wedges and transcrustal ramps, *Geophysical Research Letters*, **29**, doi: 10.1029/2002GL014911.

Vuan, A., Klin, P., Laurenzano, G. & Priolo, E., 2011. Far-source long-period displacement response spectra in the Po and Venetian Plains (Italy) from 3D wavefield simulations. *Bulletin of the Seismological Society of America*, **101**, 1055–1072.

Appendix B

APPENDIX B: Conference Papers

B.1 GNGTS 2019: Convegno Nazionale del Gruppo Nazionale di Geofisica della Terra Solida

SEISMIC SITE RESPONSE ANALYSIS WITH DIFFERENT VELOCITY GRADIENTS

V. Cascone, J. Boaga
Dipartimento di Geoscienze, Università di Padova, Italia

The distribution of shear-wave velocities in depth is a key parameter to evaluate amplification effects in region characterized by a shallow subsurface structure with soft sediments overlying much stiffer layers. The study demonstrates that the type of velocity gradient is crucial for seismic site characterization.

In alluvial basins (or valleys), layers can cause resonance of vertically traveling shear-waves at specific frequencies.

Site response analysis of a one-dimensional soil column is usually computed using linear wave propagation with strain-dependent dynamic soil properties. This is commonly referred to as the equivalent-linear analysis method, computes by computer program such as SHAKE (Schnabel *et al*., 1972) or STRATA (Kottke and Rathje, 2008). These programs compute the response of vertically propagating, horizontally polarized shear waves propagated through a site with horizontal layers. In this contest, the soil profile consist of discrete layers that vary in thickness. Each layer is characterized by mass density, shear-wave velocity and non-linear properties.

The upper 30 meters of the subsoil, very important for strong motion related studies, have always a well defined velocity structure. However when the engineering bedrock (Vs=800m/s)

reaches depths greater than 30 meters the velocity structures are extrapolated, commonly with linear gradients.

The choice of a linear gradient represents a simplified approach, and is the most common case treated in literature. A most realistic choice could be represented by velocity gradients which follow an exponential function. (Kaufman, 1953).

One of the base equations used to obtain the distribution of shear-wave velocity (vs) in depth (z) is given by the following expression:

$$vs(z)=v_0(1+z)^x \quad (1)$$

Where:

- v_0 : surface shear-wave velocity
- x: dependence of velocity in depth. $x \in]0,1[$, which holds for each $z \geq 0$

This equation holds for granular media only, i.e., for media such as sands. In real cases, saturation level, fluid pressure and cementation (besides variations in form of sedimentation or exhumation) can significantly affect the exponent, which control the dependence of Vs on the depth.

It is possible to find a consistent number of velocity gradients in literature, which follow the equation (1).

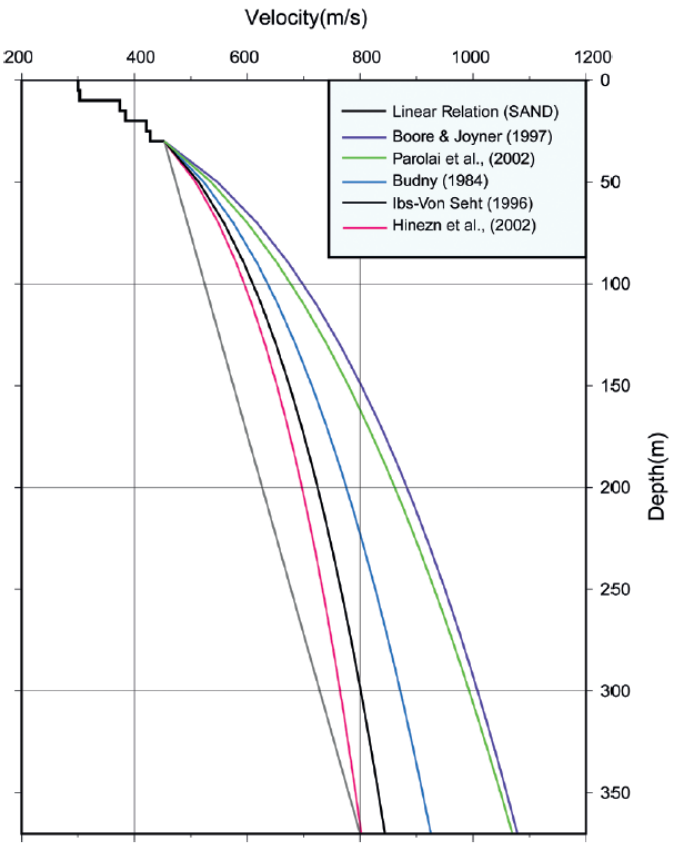

Fig.1 - Velocity Gradients which follow the linear and exponential functions.

In this study we collect the velocity gradients obtained for different alluvial basin such as the Lower Rhine Basin (Germany) (Budny, 1984; Hinzen *et al.*, 2002; Ibs-Von Seht, 1996; Parolai *et al.*, 2002) or other region characterized by widespread sedimentary cover (Boore *et al.*, 2003).

For the upper 30 meters of the subsoil we consider a mean shear-wave profile composed by seven layers with typical properties of a sand deposit. Below the 30 meters we consider different type of exponential gradients found in literature and the linear gradient. The linear gradient is built assuming a seismic bedrock reaching a depth of 370 m (Fig.1).

We perform simulations for each type of gradient using STRATA program, performing site response analysis in the frequency domain using time domain input option (the accelerogram of Friuli Earthquake, 6/5/1996, Mw: 6.5). In Fig.2 are shown the acceleration spectra obtained for each velocity gradient in Fig.1. We want to focus our attention on two points: first of all, there are differences for the maximum values for spectral acceleration. Moreover, the different bedrock depths (given by the threshold of 800 m/s) influence the spectral response.

In general, the type of velocity gradient is of paramount importance for ground response analysis and, consequently, for seismic hazard assessment.

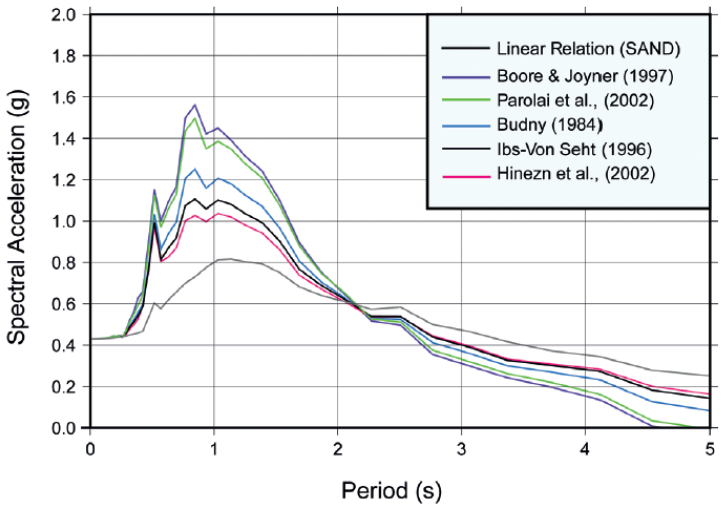

Fig. 2 - Acceleration Spectra obtained by the simulation of seismic site response considering the velocity gradients in Fig. 1.

References

Boore D.M., Joyner W.B. 1997. Site Amplifications for Generic Rock Sites. Bulletin of the Seismological Society of America, Vol. 87, No. 2, pp. 327-341.

Budny, M. 1984. Seismische Bestimmung der bodendynamischen Kenn-werte von oberfla ¨schennahen Schichten in Erdbebengebieten derNiederrheinnischen Bucht und ihre ingenieurseismologische Anwen-dung,Geol. Inst. Univ. Cologne, special issue 57.

Hinzen, K. G., Weber, B., and Scherbaum, F. 2002. On the resolution of H/V measurements to determine sediment thickness, a case study across a normal fault in the Lower Rhine Embayment, Germany. Journal of Earthquake Engineering, 8(06), 909-926.

Ibs von Seht, M. 1996. "Die seismische Bodenunruhe als Werkzeug zur Erkundung desgeologischen Untergrundes, "Aachener Geowissenschaftliche Beitr ¨age.

Kaufman, H. 1953. Velocity functions in seismic prospecting. Geophysics, 18(2), 289-297

Kottke, A. R., and Rathje, E. M. 2008. Technical manual for Strata. University of California, Berkeley.

Parolai, S., Bormann, P., and Milkereit, C. 2002. New relationships between Vs, thickness of sediments, and resonance frequency calculated by the H/V ratio of seismic noise for the Cologne area (Germany). Bulletin of the seismological society of America, 92(6), 2521-2527.

Schnabel, P. B., Lysmer, J., and Seed, H. B. 1972. SHAKE A Computer program for earthquake response analysis of horizontally layered sites, Report No. EERC72-12, EERC, 12

B.2 EGU 2020: European Geosciences Union

EGU2020-5123
https://doi.org/10.5194/egusphere-egu2020-5123
EGU General Assembly 2020

The influence of velocity gradients choice in deep alluvial basin seismic site response

Valeria Cascone and Jacopo Boaga
Department of Geosciences, University of Padova, Italy (valeria.cascone@phd.unipd.it)

The characterization of seismic site response represents one of the most important issues of seismic hazard assessment and risk mitigation planning. Characterizing the site conditions involves the measurement of several soil properties such as the shear-wave velocity (Vs), density and damping properties as a function of depth. Therefore, most of the site-effect studies in earthquake ground motions are based on the properties of the upper 30 meters and the anti-seismic building codes propose in most cases a simplified analysis based on shear wave velocity of the shallow subsoil. From a seismological perspective, the upper 30 meters would almost never represent more than 1% of the distance from the source. This should be taken into account especially for large and deep alluvial basins, representing the most inhabited geological environment of the world, where could be difficult to estimate the thickness and the velocity profile of the soft sediment overlying the rigid seismic bedrock.

The common approach adopted to characterize greater depths is then an extrapolation of shear wave velocity in depth, considering a selected linear or non-linear velocity gradients till the depth of the considered seismic bedrock (usually set to Vs ≥ 800 m/s). These gradients are generally derived from geological information or from literature, but how much the gradients choice affects the final site response analyses is often a neglected aspect.

In this work we try to investigate the generic case of deep alluvial basins. We consider the shallow subsoil as characterized by several *in-situ* tests in northern Italy. We extrapolate the deeper soil structure considering different literature velocity gradients obtained for deep basins in different geological contests: tectonic basins (Lower Rhine Basin and Po Plain) and Alpine basins (Grenoble and Lucerna Basins). We perform one-dimensional analysis of shear waves with the Linear Equivalent Method. The study demonstrates how relevant can be the role of velocity gradient choice for the ground response scenario. Starting from the same shallower Vs structures, the computed seismic motion at surface can present variation in the order of 50% varying the velocity gradients in depth. The results are of relevant interest for the analysis of seismic hazard in the deep alluvial basins environments, which host the main urban areas around the world.

How to cite: Cascone, V. and Boaga, J.: The influence of velocity gradients choice in deep alluvial basin seismic site response, EGU General Assembly 2020, Online, 4–8 May 2020, EGU2020-5123, https://doi.org/10.5194/egusphere-egu2020-5123, 2020

Display materials

Display file

Comments on the display material

AC: Author Comment | **CC**: Community Comment | Report abuse

Display material version 1 – uploaded on 30 Apr 2020

CC1: Comment on EGU2020-5123, Hans-Balder Havenith, 03 May 2020
AC1: Reply to CC1, Valeria Cascone, 04 May 2020

CC2: Comment on EGU2020-5123, Daniel Bowden, 04 May 2020

Università degli Studi di Padova
Dipartimento di Geoscienze

EGU General Assembly 2020
Online | 4–8 May 2020

The influence of velocity gradients choice in deep alluvial basin seismic site response

Valeria Cascone[1], Jacopo Boaga[1], Ilaria Barone[1]

[1] Università degli Studi di Padova
Dipartimento di Geoscienze, Via G. Gradenigo 6
Padova, Italia

valeria.cascone@phd.unipd.it

(A) INTRODUCTION

The distribution of shear-wave velocities in depth is a key parameter to evaluate amplification effects.

The shallow subsoil, very important for strong motion related studies, has often a well defined velocity structure, inferred from different geophysical surveys. However when the engineering bedrock (*Vs*=800*m/s*) reaches high depths, the velocity structures are extrapolated, commonly with linear gradients.

The choice of a linear gradient represents a simplified approach, and is the most common case treated in literature. A more realistic choice could be represented by velocity gradients which follow exponential functions. (Kaufman, 1953).

The type of velocity gradient is crucial for seismic site characterization.

(B) METHOD

In this study we collect the velocity gradients obtained for different alluvial basins (see references in Figure 1). All of these authors follow the base equations used to obtain the distribution of shear-wave velocity (*vs*) in depth (*z*):

$$vs(z)=v_0(1+z)^x$$

- v_0 : surface shear-wave velocity
- x: dependence of velocity in depth. $x \in]0,1[$, which holds for each $z \geq 0$

We perform simulations for each type of gradients (including the linear one) using STRATA program, performing site response analysis in the frequency domain using time domain input option (the accelerogram of Friuli Earthquake, 6/5/1976, Mw: 6.5).

(C) PRELIMINARY RESULTS

Figure 1

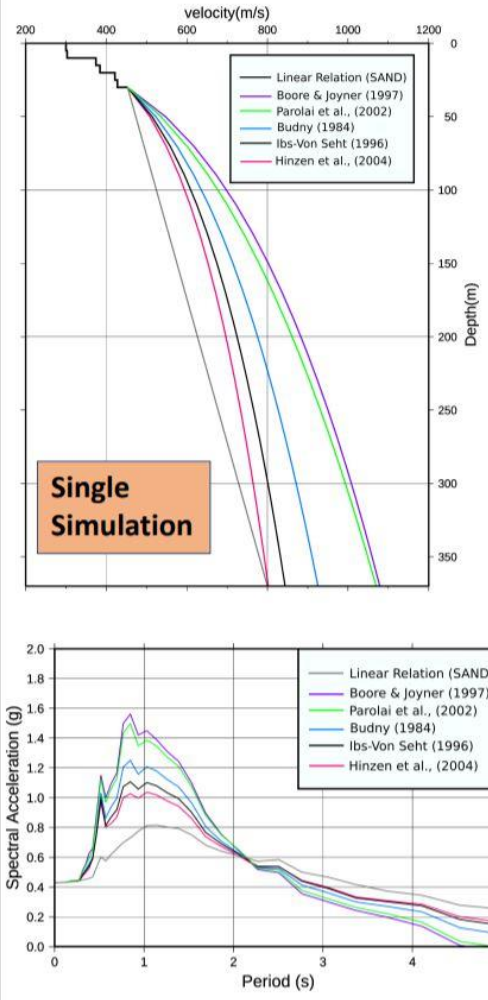

Figure 1. For the upper 30 meters of the subsoil we consider a mean shear-wave profile typical of a sand deposit. Below the 30 meters we consider different type of exponential gradients found in literature and the linear gradient. The linear gradient is built assuming a seismic bedrock reaching a depth of 370 m; the acceleration spectra obtained for each velocity gradient are also shown.

Figure 2. Probabilistic analysis with Monte Carlo method. We consider a population of 50 random velocity profiles and we plot the response spectrum of each realization.

There are differences for the maximum values of spectral acceleration (ξ=5%); in particular the simplified approach of the linear gradient underestimates the acceleration.

In general, **the choice of velocity gradient is of paramount importance for ground response analysis and, consequently, for seismic hazard assessment** (Cascone et al., 2020)

Figure 2

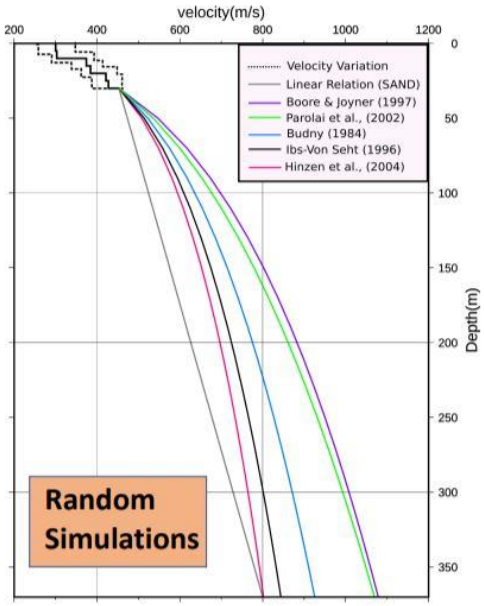

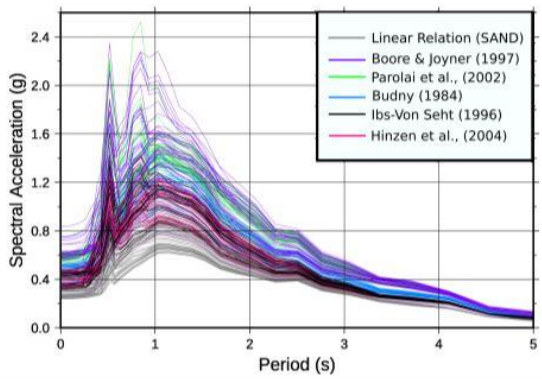

REFERENCES

- Boore D.M., Joyner W.B. 1997. Site Amplifications for Generic Rock Sites. Bulletin of the Seismological Society of America. Vol. 87, No. 2, pp. 327-341.
- Budny, M. 1984. Seismische Bestimmung der bodendynamischen Kenn-werte von oberflächennahen Schichten in Erdbebengebieten derNiederrheinnischen Bucht und ihre ingenieurseismologische Anwen-dung,Geol. Inst. Univ. Cologne, special issue 57.
- Cascone V., Barone I., Boaga J., (2020) Bedrock reference models in alluvial plain: assessing the uncertainty in seismic response estimation', to be submitted.
- Hinzen, K. G., Weber, B., & Scherbaum, F. 2002. On the resolution of H/V measurements to determine sediment thickness, a case study across a normal fault in the Lower Rhine Embayment, Germany. Journal of Earthquake Engineering, 8(06), 909-926.
- Ibs von Seht, M. 1996. "Die seismische Bodenunruhe als Werkzeug zur Erkundung desgeologischen Untergrundes, "Aachener Geowissenschaftliche Beiträge.
- Kaufman, H. 1953. Velocity functions in seismic prospecting. Geophysics, 18(2), 289-297
- Parolai, S., Bormann, P., & Milkereit, C. 2002. New relationships between Vs, thickness of sediments, and resonance frequency calculated by the H/V ratio of seismic noise for the Cologne area (Germany). Bulletin of the seismological society of America, 92(6), 2521-2527.

B.3 NSG 2021: Near Surface Geoscience

Seismic monitoring with low-cost MEMS sensor arrays in Italy

Introduction

MEMS (Micro-electro-mechanical Systems) devices are highly enabling technology with a huge commercial potential. MEMS accelerometers have dimensions on the order of microns and are made directly on a silicon substrate. In the 90's, MEMS sensors revolutionized the automotive airbag system and are today widely used in smartphones, game controllers and so on. Thanks to the great commercial success, the research and development of MEMS technology actively continues all over the world. (D'Alessandro et al., 2014, Lawrence et al., 2014). Moreover, thanks to their versatility, these accelerometers are used in a wide field of science, including the seismological one (Boaga et al., 2019, D'Alessandro et al., 2019).
The recent technological development in the field of MEMS sensors can greatly reduce the per-stations costs (two order of magnitude lower than the typical broad-band seismic stations) (Cochran et al., 2012). An efficient seismic wavefield recording is achieved if a seismic network has sufficient sensors dynamic range, frequency response and spatial resolution (Evans et al., 2005). The first two aspects can be tackled by the installation of modern seismographs with very large dynamic range (> 120 dB) and broadband response (10^{-2} to 10^{2} Hz). Although the higher resolution of modern broad-band and force-balanced seismic stations, the spatial sampling is limited by the number of sensors installed. The high costs associated with the construction and installation of traditional seismic stations don't allow the realization of dense seismic networks.
Thanks to their low cost and small size, MEMS accelerometers could allow to build seismic network constituted by high density of observation points, improving the spatial sampling of wavefield recording. Moreover, these sensors can be easily installed in urban centers and they could provide immediate alert and post-earthquake information, summarized in maps of ground motion parameters (e.g. shake maps).
Recently, moderate to strong earthquakes were collected worldwide by MEMS sensors arrays (D'Alessandro et al, 2014). The sensitivity and dynamic range of these sensors are such as to allow the recording of earthquake of moderate-to-strong magnitude events even at distances of several tens of kilometers (Evans et al., 2005). However, the potential of such technology is far to be fully explored.
This study aims to investigate the performance of new prototypes of MEMS sensor, a multirange tri-axial accelerometer, with high sensitivity and high digital resolution. Moreover, we introduce two seismic networks based on MEMS technology installed in Italy.

Method

The MEMS sensors prototypes, used in this work, integrate a three-axis digital accelerometer. They have a sampling rate of 250 Hz; a dynamic range of ±4g and a noise density of 25 μg/√Hz.
The continuous recordings are stored in a SD Memory up to 64Gbyte which is reset every 4 months. The available storage formats are miniSeed, binary 24-bit and csv.
The MEMS sensor prototype was tested in laboratory under excitation of sweeping waves for a calibration with a shake table (Figure 1a), with a frequency range between 0 and 100 Hz and a maximum and minimum amplitude of ± 0.2 m/s^2. The calibration is made with a laser sensor which allows accurate measures in a range of 400 mm and a resolution of ± 2.54 nm. The MEMS sensor prototype results in very good agreement with the laser motion reference of the shake table (Figure 1b). We made a self-noise test by placing the MEMS sensor in a laboratory far from noise sources, and recording for 30 minutes. The Power Spectrum Density of the continuous recording ranges between -80 dB and -60 dB in the frequency band of 0.1 – 10 Hz. These results suggest that the MEMS sensor prototype analyzed in this study is capable of recording local events with magnitude > 2.5 in the frequency range of 1-10 Hz (Hong, 2016)

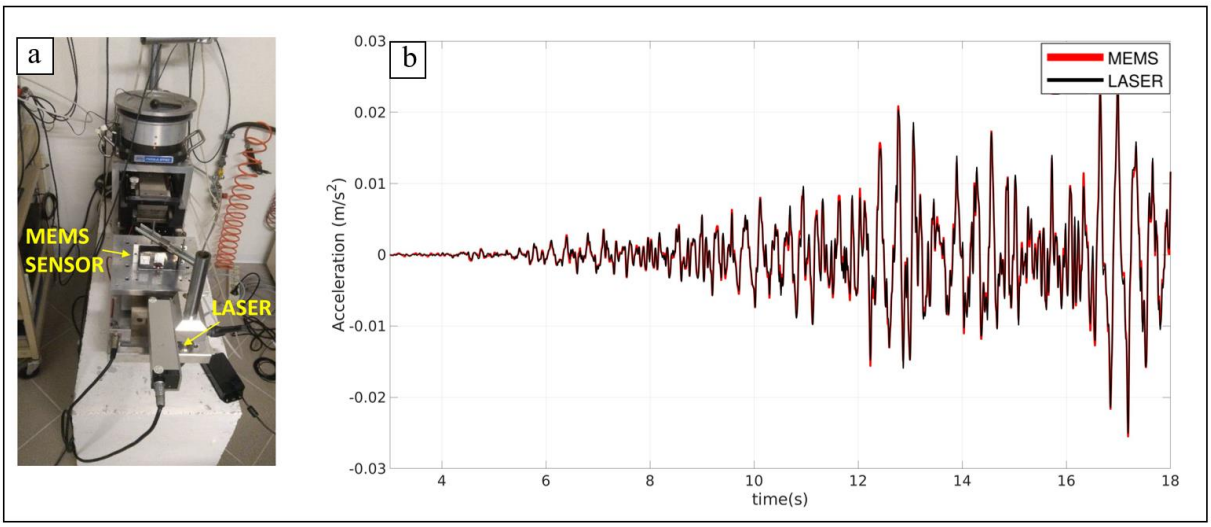

Figure 1: *a) Shake Table apparatus with the co-mounted laser and the MEMS sensor prototype analysed in this study. b) Comparison of the sweeping wave recordings by MEMS and laser (red and black signal respectively)*

Two MEMS sensors distributed arrays were installed in 2019 and cover two seismically active zones in Italy, characterized by a notable seismic risk (Figure 2). The first selected area, shown in the left panel of Figure 1, is the southern Alps front (Northern Italy). This pede-mountain area has been hit by strong historical and instrumental earthquakes, associated with the south-verging thrust faults (Rovida et al., 2011). The second MEMS sensors' array was installed in Central Italy (Right Panel in Figure 2) The main seismic events are associated to the faulting in the Umbria-Marche Apennines, affected by intense Plio-Quaternary extensional deformations. This sector was stuck by several seismic sequences in the last decades, such as the Gubbio-Colfiorito (1997-1998), and Amatrice-Visso-Norcia (2016) seismic sequences (Michele et al., 2016).

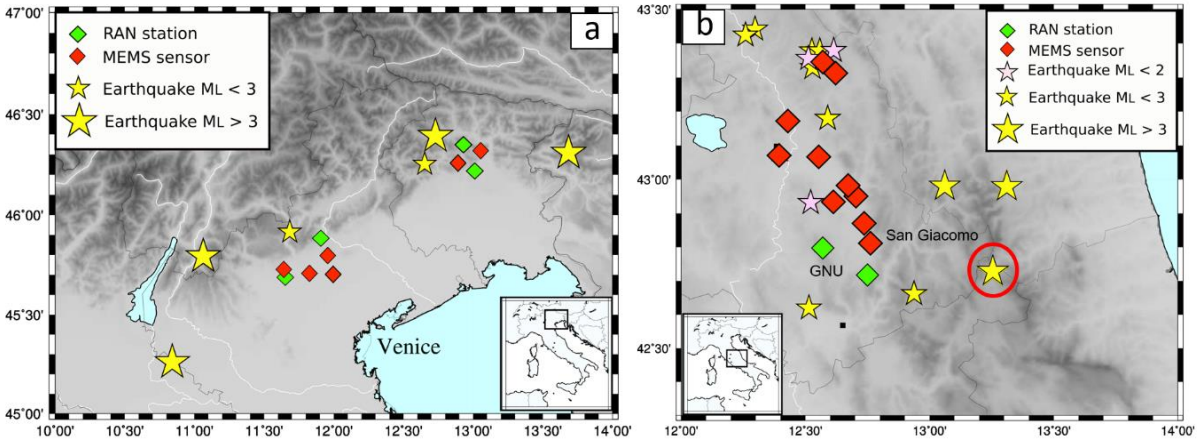

Figure 2: *a) Maps of the MEMS sensors' array in Northern Italy and b) in Central Italy (red diamonds). The broad-band stations belonging to the RAN network are indicated with green diamonds. The recorded seismic events are displayed with different symbols on the basis of their seismic energy (Pink stars: $M_L < 2.0$, small sized yellow stars: $2.0 < M_L < 3.0$, high sized yellow stars $M_L > 3.0$).*

The MEMS sensors are located inside telecommunication buildings and are fixed to the ground with screw and plugs. The continuous recorded waveforms can be downloaded and processed in real-time.

It is worth notice that several MEMS sensors are located close to broad-band seismic stations belonging to the National Accelerometric Network (RAN – Rete Accelerometrica Nazionale) managed by the Italian Civil Protection authorities (green diamonds in Figure 2).
In a period between January 2020 and March 2021 the MEMS sensors' arrays were able to record 20 local seismic events, with a $1.7 < M_L < 4.0$. Their epicentres are plotted in Figure 2 (Pink stars: $M_L <$ 2.0, small sized yellow stars: $2.0 < M_L < 3.0$, high sized yellow stars $M_L > 3.0$). The enucleations depths of the recorded seismic events range between 7 and 11 km.

For earthquakes with $M_L \geq 2.5$ it is possible to download under request the seismic data collected by RAN accelerometric network. Thus, a comparison of the ground motion parameters (PGA and Spectral Acceleration) obtained from MEMS sensors and the high-quality stations of the RAN is made. In Figure 3 we show an example of the comparison between RAN and MEMS sensors' data (blue and magenta curves, respectively). For this example, we consider a seismic event, occurred on 28th January 2020, ML= 3.3. Its epicenter is indicated in Figure 2 with a red circle (event-MEMS sensor distance equal to 56 km). The comparison was made considering the three components of the sensors.
The time series show comparable values of PGAs, and the shape of the normalized Spectral accelerations are very similar.

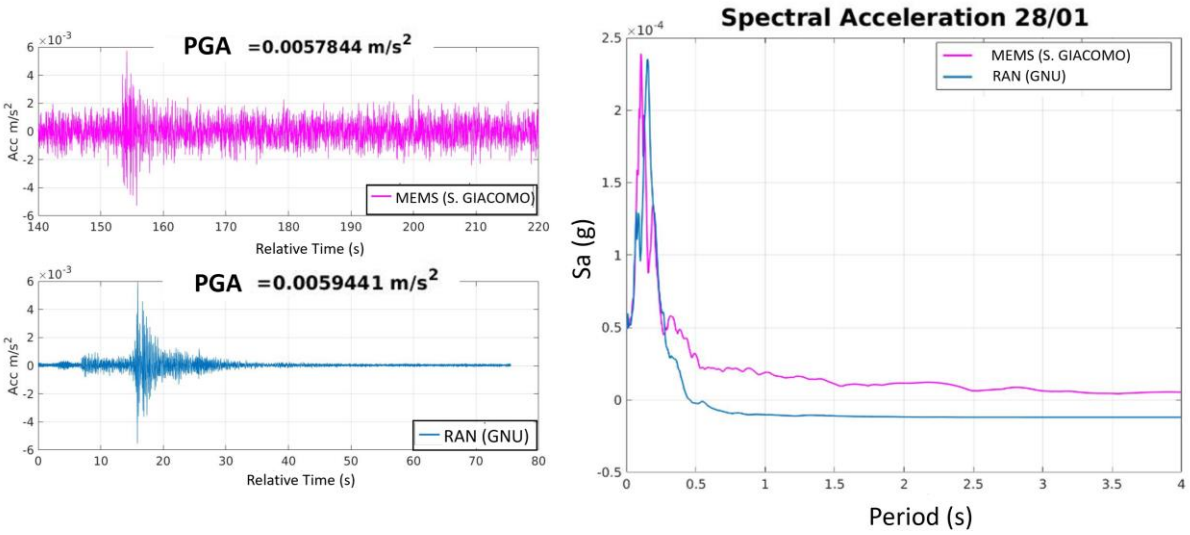

***Figure 3**: Comparison of the strong motion parameters (PGA and Spectral Acceleration) inferred from MEMS senor and broad-band stations (magenta and blue curves, respectively). The considered seismic event is indicated in Figure 2, within the red circle.*

Conclusions

In this study we evaluate the suitability of a new prototype of low-cost MEMS sensor to detect seismicity. The sensor shows a good performance on a calibration experiment on a shake table apparatus.
The two arrays of MEMS accelerometers installed in Northern and Central Italy were able to record local seismic events. In particular, these sensors were able to record small magnitude seismic events, lower than a local magnitude of 2.0. We demonstrate in fact that this new MEMS sensor prototype can reach efficient performance for the detection of local seismicity with $M_L > 1.7$ at epicentral distances lower than 10 km. These sensors are able to record also earthquakes with a M_L of 3.0 at epicentral distances in the order of 30 km.
The fundamental strong motion parameters (PGA and Spectral Acceleration) inferred from the accelerograms recorded by MEMS sensors, are comparable with the ones inferred from the broad-band seismic stations (the seismic data of the RAN network can be downloaded only for seismic events with $M_L \geq 2.5$). These parameters represent practical indexes to describe, at a particular site, the degree of shaking. They are critical also for seismic design of engineering structures. Thus, a denser seismic

network built with low-cost MEMS sensors (also installed on the urban centers), can improve the seismic wavefield recording. Moreover, it could provide immediate alert and post-earthquake information. In possible future developments, these MEMS stations will be located inside strategic and sensitive buildings (i.e. characterized by high vulnerability and exposure) such as schools, hospitals, public buildings and places of worship. The impact of a strong earthquake on an urban center can be considerably reduced by an emergency management center, through timely and targeted actions.
We remark that networks based on MEMS sensors cannot substitute the information broad-band seismometers, especially for weaker events. On the other hand, considering the quick industrial development of MEMS technology, in the next future these sensors could integrate the existing strong-motion networks.

References

Boaga, J., Casarin, F., De Marchi, G., Valluzzi, M. R., & Cassiani, G. (2019). 2016 Central Italy Earthquakes Recorded by Low-Cost MEMS-Distributed Arrays. *Seismological Research Letters*, *90*(2A), 672-682.

Chiaraluce, L., Di Stefano, R., Tinti, E., Scognamiglio, L., Michele, M., Casarotti, E., ... & Marzorati, S. (2017). The 2016 central Italy seismic sequence: A first look at the mainshocks, aftershocks, and source models. *Seismological Research Letters*, *88*(3), 757-771.

Cochran, E. S., Lawrence, J. F., Kaiser, A., Fry, B., Chung, A., & Christensen, C. (2012). Comparison between low-cost and traditional MEMS accelerometers: a case study from the M7. 1 Darfield, New Zealand, aftershock deployment. *Annals of Geophysics*, *54*(6).

D'Alessandro, A., Luzio, D., & D'Anna, G. (2014). Urban MEMS based seismic network for post-earthquakes rapid disaster assessment. *Advances in Geosciences*, *40*, 1-9.

D'Alessandro, A., Costanzo, A., Ladina, C., Buongiorno, F., Cattaneo, M., Falcone, S., ... & Doglioni, C. (2019). Urban seismic networks, structural health and cultural heritage monitoring: the national earthquakes observatory (INGV, Italy) experience. Frontiers in Built Environment, 5, 127.

Evans, J. W., Morzinski, K., Reza, L., Severson, S., Poyneer, L., Macintosh, B. A., ... & Olivier, S. (2005, September). Extreme adaptive optics testbed: high contrast measurements with a MEMS deformable mirror. In *Techniques and Instrumentation for Detection of Exoplanets II* (Vol. 5905, p. 59050Y). International Society for Optics and Photonics.

Hong, T., & Marone, C. (2005). Effects of normal stress perturbations on the frictional properties of simulated faults. *Geochemistry, Geophysics, Geosystems*, *6*(3).

Lawrence, J. F., Cochran, E. S., Chung, A., Kaiser, A., Christensen, C. M., Allen, R., ... & Taufer, M. (2014). Rapid earthquake characterization using MEMS accelerometers and volunteer hosts following the M 7.2 Darfield, New Zealand, earthquake. *Bulletin of the Seismological Society of America*, *104*(1), 184-192.

Rovida, R. Camassi, P. Gasperini, M. Stucchi CPTI11, la versione 2011 del Catalogo Parametrico dei Terremoti Italiani Milano, Bologna (2011), 10.6092/INGV.IT-CPTI1

Bibliography

K. Aki and P. G. Richards. *Quantitative seismology*. 2002.

D. Albarello, C. Cesi, V. Eulilli, F. Guerrini, E. Lunedei, E. Paolucci, D. Pileggi, and L.M. Puzzilli. The contribution of the ambient vibration prospecting in seismic microzoning: an example from the area damaged by the april 6, 2009 l'aquila (italy) earthquake. *Boll. Geof. Teor. Appl*, 52:513–538, 2011.

J. G. Anderson, J. N. Brune, R. Anooshehpoor, and S.D. Ni. New ground motion data and concepts in seismic hazard analysis. *Current Science*, pages 1278–1290, 2000.

G. Andreotti, A. Fam, and C.G. Lai. Hazard-dependent soil factors for site-specific elastic acceleration response spectra of italian and european seismic building codes. *Bulletin of Earthquake Engineering*, 16(12):5769–5800, 2018.

A. Ansal, Gökçe Tönük, and A. Kurtulucs. Microzonation for urban planning. In *Earthquakes and Tsunamis*, pages 133–152. Springer, 2009.

L. Al Atik, N. Abrahamson, J. J. Bommer, F. Scherbaum, F. Cotton, and N. Kuehn. The variability of ground motion prediction models and its components. *Seismological Research Letters*, 81(5):794–801, 2010.

G.D. Bensen, M.H. Ritzwoller, M.P. Barmin, A. Lin Levshin, Feifan Lin, M.P. Moschetti, N.M. Shapiro, and Yanyan Yang. Processing seismic ambient noise data to obtain reliable

broad-band surface wave dispersion measurements. *Geophysical Journal International*, 169 (3):1239–1260, 2007.

A. Berbellini, A. Morelli, and A. M.G. Ferreira. Crustal structure of northern italy from the ellipticity of rayleigh waves. *Physics of the Earth and Planetary Interiors*, 265:1–14, 2017.

C. Bignami, P. Burrato, V. Cannelli, M. Chini, E. Falcucci, A. Ferretti, S. Gori, C. Kyriakopoulos, D. Melini, M. Moro, et al. Coseismic deformation pattern of the emilia 2012 seismic sequence imaged by radarsat-1 interferometry. *Annals of Geophysics*, 55(4), 2012.

J. Boaga, V. Iliceto, F. Vaccari, and G.F. Panza. Shear-wave structural model of venetian plane (italy), from seismic noise measurements. In *American Geophysical Union, Fall Meeting 2007, abstract NS11D-0797*, 2007.

J. Boaga, G. Vignoli, and G. Cassiani. Reply to comment on 'shear wave profile from surface wave inversion: the impact of uncertainty on seismic site response analysis'. *Journal of Geophysics and Engineering*, 9(2):244–246, 2012.

J. Boaga, F. Casarin, G. De Marchi, M.R. Valluzzi, and G. Cassiani. 2016 central italy earthquakes recorded by low-cost mems-distributed arrays. *Seismological Research Letters*, 90(2A):672–682, 2019.

D.M. Boore, W.B. Joyner, and T.E. Fumal. Estimation of response spectra and peak accelerations from western north american earthquakes: an interim report. 1993.

R. D. Borcherdt. Estimates of site-dependent response spectra for design (methodology and justification). *Earthquake spectra*, 10(4):617–653, 1994.

L. Boschi and Weemstra K. Stationary-phase integrals in the cross correlation of ambient noise. *Reviews of Geophysics*, 53(2):411–451, 2015.

L. Boschi, E. D. Kästle, R. Soomro, K. Weemstra, and T. Meier. Cross-validation of ambient-noise and earthquake-based observations of love-and rayleigh-wave dispersion. In *AGU fall meeting 2016*, 2016.

L. Boschi, F. Magrini, F. Cammarano, and M. Van der Meijde. On seismic ambient noise cross-correlation and surface-wave attenuation. *Geophysical journal international*, 219(3): 1568–1589, 2019.

M. Budny. Seismische bestimmung der bodendynamischen kennwerte von oberflächennahen schichten in erdbebengebieten der niederrheinischen bucht. In *Ingenieurgeologische Probleme im Grenzbereich zwischen Locker-und Festgesteinen*, pages 560–582. Springer, 1985.

H. Bungum, S. Mykkeltveit, and T. Kvaerna. Seismic noise in fennoscandia, with emphasis on high frequencies. *Bulletin of the Seismological Society of America*, 75(6):1489–1513, 1985.

S. Bussat and S. Kugler. Recording noise-estimating shear-wave velocities: Feasibility of offshore ambient-noise surface-wave tomography (answt) on a reservoir scale. In *SEG Technical Program Expanded Abstracts 2009*, pages 1627–1631. Society of Exploration Geophysicists, 2009.

M. Campillo and A. Paul. Long-range correlations in the diffuse seismic coda. *Science*, 299 (5606):547–549, 2003.

E. Cardarelli, M. Cercato, and G. De Donno. Surface and borehole geophysics for the rehabilitation of a concrete dam (penne, central italy). *Engineering Geology*, 241:1–10, 2018.

E. Carminati, C. Doglioni, and D. Scrocca. Apennines subduction-related subsidence of venice (italy). *Geophysical Research Letters*, 30(13), 2003.

A. Carraro, P. Fabbri, A. Giaretta, L. Peruzzo, F. Tateo, and F. Tellini. Effects of redox conditions on the control of arsenic mobility in shallow alluvial aquifers on the venetian plain (italy). *Science of the Total Environment*, 532:581–594, 2015.

V. Cascone, J. Boaga, and G. Cassiani. Small local earthquake detection using low-cost mems accelerometers: Examples in northern and central italy. *The Seismic Record*, 1(1):20–26, 2021.

V. Cascone, I. Barone, and J. Boaga. Velocity gradients choice affecting seismic site response in deep alluvial basins: Application to the venetian plain (northern italy). *Journal of Geophysics and Engineering*, 19(1):1–13, 2022.

R. Cassinis. Reviewing pre-transalp dss models. *Tectonophysics*, 414(1-4):79–86, 2006.

N. Cenni, J. Boaga, Filippo Casarin, G. De Marchi, M. R. Valluzzi, and G. Cassiani. 2016 central italy earthquakes: comparison between gps signals and low-cost distributed mems arrays. *Advances in Geosciences*, 51:1–14, 2019.

L. Chiaraluce, C. Collettini, M. Cattaneo, and G. Monachesi. The shallow boreholes at the altotiberina near fault observatory (taboo; northern apennines of italy). *Scientific Drilling*, 17:31–35, 2014.

R. Clayton, T. Heaton, M. Chandy, A. Krause, M. Kohler, J. Bunn, R. Guy, M. Olson, M. Faulkner, M. Cheng, et al. Community seismic network. *Annals of Geophysics*, 54(6): 738–747, 2011.

E. S Cochran, J. F. Lawrence, C. Christensen, and R. S. Jakka. The quake-catcher network: Citizen science expanding seismic horizons. *Seismological Research Letters*, 80(1):26–30, 2009.

E. S Cochran, J.F. Lawrence, A. Kaiser, B. Fry, A. Chung, and C. Christensen. Comparison between low-cost and traditional mems accelerometers: a case study from the m7. 1 darfield, new zealand, aftershock deployment. *Annals of Geophysics*, 54(6), 2011.

W.C. Crone and W.N. Sharpe. A brief introduction to mems and nems. In *Springer handbook of experimental solid mechanics*, pages 203–228. Springer New York, 2008.

A. D'Alessandro, D. Luzio, and G. D'Anna. Urban mems based seismic network for post-earthquakes rapid disaster assessment. *Advances in Geosciences*, 40:1–9, 2014.

A. D'Alessandro, S. Scudero, and G. Vitale. A review of the capacitive mems for seismology. *Sensors*, 19(14):3093, 2019.

A. Deschamps, F. Courboulex, Stéphane Gaffet, A. Lomax, J. Virieux, A. Amato, A. Azzara, B. Castello, C. Chiarabba, G.B. Cimini, et al. Spatio-temporal distribution of seismic activity during the umbria-marche crisis, 1997. *Journal of Seismology*, 4(4):377–386, 2000.

C. Doglioni. Some remarks on the origin of foredeeps. *Tectonophysics*, 228(1-2):1–20, 1993.

J.R. Evans, R. M. Allen, A.I. Chung, E. Cochran, R. Guy, M. Hellweg, and J.F. Lawrence. Performance of several low-cost accelerometers. *Seismological Research Letters*, 85(1):147–158, 2014.

R.E. Gibson. Some results concerning displacements and stresses in a non-homogeneous elastic half-space. *Geotechnique*, 17(1):58–67, 1967.

P. Guéguen, C. Cornou, S. Garambois, and J. Banton. On the limitation of the h/v spectral ratio using seismic noise as an exploration tool: application to the grenoble valley (france), a small apex ratio basin. *Pure and applied geophysics*, 164(1):115–134, 2007.

E. Guidoboni, A. Comastri, and E. Boschi. The "exceptional" earthquake of 3 january 1117 in the verona area (northern italy): A critical time review and detection of two lost

earthquakes (lower germany and tuscany). *Journal of Geophysical Research: Solid Earth*, 110(B12), 2005.

W.D. Halliday, S.J. Insley, R. C. Hilliard, T. de Jong, and M.K. Pine. Potential impacts of shipping noise on marine mammals in the western canadian arctic. *Marine Pollution Bulletin*, 123(1-2):73–82, 2017.

George.W. Housner. Intensity of ground motion during strong earthquakes. 1952.

I.M. Idriss. Earthquake ground motions at soft soil sites. 1990.

I. Iervolino, C. Galasso, and E. Cosenza. Rexel: computer aided record selection for code-based seismic structural analysis. *Bulletin of Earthquake Engineering*, 8(2):339–362, 2010.

Q. Kong, R.M. Allen, L. Schreier, and Y. Kwon. Myshake: A smartphone seismic network for earthquake early warning and beyond. *Science advances*, 2(2):e1501055, 2016.

A. R. Kottke and E.M. Rathje. *Technical manual for Strata.* Pacific Earthquake Engineering Research Center Berkeley, California, 2009.

J.F. Lawrence, E.S. Cochran, A. Chung, A. Kaiser, Carl M. Christensen, R. Allen, J.W. Baker, B. Fry, T. Heaton, et al. Rapid earthquake characterization using mems accelerometers and volunteer hosts following the m 7.2 darfield, new zealand, earthquake. *Bulletin of the Seismological Society of America*, 104(1):184–192, 2014.

M.S. Longuet-Higgins. A theory of the origin of microseisms. *Philosophical Transactions of the Royal Society of London. Series A, Mathematical and Physical Sciences*, 243(857): 1–35, 1950.

J. N. Louie. Faster, better: shear-wave velocity to 100 meters depth from refraction microtremor arrays. *Bulletin of the Seismological Society of America*, 91(2):347–364, 2001.

F. Lucente, P. De Gori, L. Margheriti, D. Piccinini, M. Di Bona, C. Chiarabba, and N. Piana Agostinetti. Temporal variation of seismic velocity and anisotropy before the 2009 mw 6.3 l'aquila earthquake, italy. *Geology*, 38(11):1015–1018, 2010.

P. M. Mai. *Ground Motion: Complexity and Scaling in the Near Field of Earthquake Ruptures*, pages 4435–4474. Springer New York, New York, NY, 2009. ISBN 978-0-387-30440-3. doi: 10.1007/978-0-387-30440-3_263. URL https://doi.org/10.1007/978-0-387-30440-3_263.

G.R. Martin, R. Dobry, et al. Earthquake site response and seismic code provisions. *NCEER Bulletin*, 8(4):1–6, 1994.

C. Mascandola, M. Massa, S. Barani, D. Albarello, S. Lovati, L. Martelli, and V. Poggi. Mapping the seismic bedrock of the po plain (italy) through ambient-vibration monitoring. *Bulletin of the Seismological Society of America*, 109(1):164–177, 2019.

M. Michele, R. Di Stefano, L. Chiaraluce, M. Cattaneo, P. De Gori, G. Monachesi, D. Latorre, S. Marzorati, L. Valoroso, C. Ladina, et al. The amatrice 2016 seismic sequence: a preliminary look at the mainshock and aftershocks distribution. *Annals of Geophysics*, 59, 2016.

Y. Nakamura. A method for dynamic characteristics estimation of subsurface using microtremor on the ground surface. *Railway Technical Research Institute, Quarterly Reports*, 30(1), 1989.

G. F Panza, L. Alvarez, and A. Aoudia. Realistic modeling of seismic input for megacities and large urban areas. 2002.

G.F. Panza, F. Romanelli, et al. Seismic ground motion modelling and damage earthquake scenarios: A bridge between seismologists and seismic engineers. 2003.

D. Pesaresi, M. Romanelli, C. Barnaba, P.L. Bragato, and G. Durì. Ogs improvements in 2012 in running the north-eastern italy seismic network: the ferrara vbb borehole seismic station. *Advances in Geosciences*, 36:61–67, 2014.

Kyriazis Pitilakis, M. Alexoudi, S. Argyroudis, and Anastasios Anastasiadis. Seismic risk scenarios for an efficient seismic risk management: the case of thessaloniki (greece). In *Advances in earthquake engineering for urban risk reduction*, pages 229–244. Springer, 2006.

V. Poggi, D. Fäh, J. Burjanek, and D. Giardini. The use of rayleigh-wave ellipticity for site-specific hazard assessment and microzonation: application to the city of lucerne, switzerland. *Geophysical Journal International*, 188(3):1154–1172, 2012.

M.E. Poli, P. Burrato, F. Galadini, A. Zanferrari, et al. Seismogenic sources responsible for destructive earthquakes in ne italy. *Bollettino di Geofisica Teorica e Applicata*, 2008.

P. Poli, J. Boaga, I. Molinari, V. Cascone, and L. Boschi. The 2020 coronavirus lockdown and seismic monitoring of anthropic activities in northern italy. *Scientific reports*, 10(1): 1–8, 2020.

E. M Rathje, A.R. Kottke, and W.L. Trent. Influence of input motion and site property variabilities on seismic site response analysis. *Journal of geotechnical and geoenvironmental engineering*, 136(4):607–619, 2010.

F. Romanelli and F. Vaccari. Site response estimation and ground motion spectrum scenario in the catania area. *Journal of Seismology*, 3(3):311–326, 1999.

F. Romanelli, A. Peresan, F. Vaccari, and G.F. Panza. Scenarios based earthquake hazard assessment. In *Urban Habitat Constructions Under Catastrophic Events: Proceedings of the COST C26 Action Final Conference*, page 105. CRC Press, 2010.

P. Roux, K. G. Sabra, W.A. Kuperman, and A. Roux. Ambient noise cross correlation in free space: Theoretical approach. *The Journal of the Acoustical Society of America*, 117 (1):79–84, 2005.

A. Rozenberg and M. Ritter. Laboratory study of the fine structure of short surface waves due to breaking: Two-directional wave propagation. *Journal of Geophysical Research: Oceans*, 110(C2), 2005.

J. C. Santamarina, K.A. Klein, and M.A. Fam. *Soils and waves*. J. Wiley & Sons New York, 2001.

F. Scherbaum, K. Hinzen, and M. Ohrnberger. Determination of shallow shear wave velocity profiles in the cologne, germany area using ambient vibrations. *Geophysical Journal International*, 152(3):597–612, 2003.

S. Scudero, A. D'Alessandro, L. Greco, and G. Vitale. Mems technology in seismology: A short review. In *2018 IEEE International Conference on Environmental Engineering (EE)*, pages 1–5. IEEE, 2018.

D.K. Shaeffer. Mems inertial sensors: A tutorial overview. *IEEE Communications Magazine*, 51(4):100–109, 2013.

N. M Shapiro, M. Campillo, L. Stehly, and M.H. Ritzwoller. High-resolution surface-wave tomography from ambient seismic noise. *Science*, 307(5715):1615–1618, 2005.

N.M. Shapiro and M. Campillo. Emergence of broadband rayleigh waves from correlations of the ambient seismic noise. *Geophysical Research Letters*, 31(7), 2004.

P.M. Shearer. *Introduction to seismology*. Cambridge university press, 2019.

C. Strobbia, L. Andreas, P. Vermeer, and A. Glushchenko. Surface waves: use them then lose them. surface-wave analysis, inversion and attenuation in land reflection seismic surveying. *Near Surface Geophysics*, 9(6):503–513, 2011.

C. Strobbia, J. Boaga, and G. Cassiani. Double-array refraction microtremors. *Journal of Applied Geophysics*, 121:31–41, 2015.

A. Vuan, P. Klin, G. Laurenzano, and E. Priolo. Far-source long-period displacement response spectra in the po and venetian plains (italy) from 3d wavefield simulations. *Bulletin of the Seismological Society of America*, 101(3):1055–1072, 2011.

K. Wapenaar and J. Fokkema. Green's function representations for seismic interferometry. *Geophysics*, 71(4):SI33–SI46, 2006.

R.L. Weaver and .I. Lobkis. Ultrasonics without a source: Thermal fluctuation correlations at mhz frequencies. *Physical Review Letters*, 87(13):134301, 2001.

K. Weemstra, D. Draganov, E. N. Ruigrok, J. Hunziker, M. Gomez, and K. Wapenaar. Application of seismic interferometry by multidimensional deconvolution to ambient seismic noise recorded in malargüe, argentina. *Geophysical Journal International*, page ggw425, 2016.

K. Weemstra, K. Wapenaar, and K. N. Van Dalen. Reflecting boundary conditions for interferometry by multidimensional deconvolution. *The Journal of the Acoustical Society of America*, 142(4):2242–2257, 2017.

J. Zhang, P. Gerstoft, and P.M. Shearer. High-frequency p-wave seismic noise driven by ocean winds. *Geophysical Research Letters*, 36(9), 2009.

E. Zuccolo, F. Vaccari, A. Peresan, A. Dusi, A. Martelli, and G.F. Panza. Neo-deterministic

definition of seismic input for residential seismically isolated buildings. *Engineering Geology*, 101(3-4):89–95, 2008.